Concentratable Entanglement: Determining the entanglement of multipartite states with parallelized operations

STEPHANIE CLAIRE FOULDS

Concentratable Entanglement

Determining the entanglement of multipartite states with parallelized operations

Steph Foulds

A thesis presented for the degree of

Doctor of Philosophy

Quantum Light and Matter

The University of Durham

United Kingdom

Monday 20th November, 2023

Concentratable Entanglement

Steph Foulds

Abstract

Entanglement is a vital resource in quantum computation and information. In general, the amount of entanglement in a state determines its usefulness. The standard methods for detecting and characterising quantum entanglement are either resource intensive or require prior knowledge of the state in question. We extend the two-qubit pure state entanglement measure concurrence to the multipartite entanglement measure Concentratable Entanglement (CE) and provide two efficient methods of experimentally estimating it, the Bell-basis test and the controlled SWAP test, the output probabilities of which are related to the CE and purity of the input ensemble state. We show these results are robust to small variations in the input states and are therefore suitable for experimental estimation. The Bell-basis test can be achieved experimentally on multipartite states with current hardware with number of trials at maximum according to Hoeffding's inequality, and is particularly suited to larger ($n > 3$) multipartite states. Unlike many other multipartite measures, Concentratable Entanglement (CE) has a simple form, can be directly estimated from experiment, and can be used for mixed states; therefore, we present CE as a standard entanglement measure for multipartite states.

Supervisors: Dr Nicholas Chancellor, Professor Stuart Adams, and Professor Viv Kendon

Contents

Declaration

The work in this thesis is based on research carried out at Quantum Light and Matter, Department of Physics, University of Durham, England. The initial research was conducted at the University of York, York, England, which is specified in the Introduction.

Some of the work presented in this thesis has been published in journals and conference proceedings – the relevant publications are listed below. These works were collaborative; credit is indicated throughout the thesis.

Publications

- MPhys dissertation 'The controlled SWAP test: a shortcut to determining quantum entanglement' supervised by Tim Spiller at University of York (2019)
- Steph Foulds, Viv Kendon, and Tim Spiller. The controlled swap test for determining quantum entanglement. *Quantum Science and Technology*, 6(3):035002, 2021.
- Jacob L. Beckey, Gerard Pelegrí, Steph Foulds, and Natalie J. Pearson. Multipartite entanglement measures via Bell-basis measurements. *Phys. Rev. A* 107:062425, 2023.
- Oliver Prove, Steph Foulds, and Viv Kendon. Generalizing the controlled swap test for entanglement for practical applications: qudit, optical, and slightly mixed states. *arXiv preprint*, 2022. arXiv:2112.04333.

Acknowledgements

Viv Kendon has been the most encouraging, supportive, and inspiring supervisor and it has been a joy to work with her for the last four years. I thank her so much for all her help and for introducing me to the world of academia!

I thank Tim Spiller for being an excellent MPhys supervisor and beyond, for introducing me to the c-SWAP test and encouraging my love of analytics.

A huge thank you to the whole of QLM for such a joyous and welcoming environment. I will always remember our lunchtimes filled with wheels vs doors, sandwich topology, and orange peel debates. Shout out to Puya, Bethan, Tom, Matt, Fraser, Mitch, and Ali among many others for fascinating conversations and memorable nights out. Thank you specifically to Maple for their friendship, calming energy, and sanity-saving coffee breaks.

Thank you to Antonio, Ruairidh, Asher, and Elk for being constant sources of joy in my life. Thank you for your extraordinary emotional, mental, and financial support from near and far. I hope you all know how much you mean to me.

I thank my parents for encouraging my education all throughout my life, from giving me simultaneous equations for fun, to attempting to understand my publications and practice talks, to encouraging my creative talents. I am so lucky to have such a special and supportive family.

And finally my eternal love and gratitude to my endlessly supportive fiancé for being the perfect person to come home to. Your grace and strength has been my rock during the stress of university and adulthood. Thank you for being my partner in everything, Seven, I don't know how I would have done this without you.

Chapter 1

Introduction

Quantum entanglement is a phenomenon in quantum physics where measurements on two or more quantum objects yield highly correlated results, regardless of separation or lack of communication between the objects. Called "spooky action at a distance" and derided by Einstein, today entanglement is considered essential in quantum fundamental theory. Since 1972, it has been used in Bell's experiment [1, 2, 3] to disprove local hidden variable theory and in 2021, an experiment was proposed using entanglement to test quantum gravity [4].

There are innumerable applications for entanglement; it is present in almost all quantum computation [5, 6, 7, 8] and is a requirement for quantum advantage in some quantum algorithms [9]. In quantum information science – the study of communication, storage, and learnability of quantum information – entanglement is an integral resource [10, 11, 12, 13]. For example, quantum teleportation [14] uses pre-shared entanglement to transfer an unknown quantum state from one location to another using only classical channels. It provides a fundamental primitive for quantum information processing. Teleportation has been realised optically [15, 16] and with ion traps [17] as approaches towards distributed quantum computation [18].

In general, the amount of entanglement in a state determines its usefulness. For example, information can only be teleported perfectly by maximally entangled states [19]. The standard methods for detecting and characterising quantum entanglement

are either resource intensive (such as quantum state tomography [20]) or require prior knowledge of the state in question (such as entanglement witnesses [21]).

The controlled SWAP (c-SWAP) test for entanglement is an alternative test for quantum entanglement, first proposed by Tim Spiller *et al.* in [22] for the two-qubit pure state case. It is a quantum gate circuit which when applied iteratively to a (potentially unknown) ensemble of states can evidence entanglement. It was then used in [23] to prove a series of computational complexity results. In my MPhys dissertation (supervised by Tim Spiller) 'The controlled SWAP test: a shortcut to determining quantum entanglement' (2019) we show that the c-SWAP test can estimate the two-qubit measure of entanglement 'concurrence', extended the c-SWAP test to three-qubit pure states, and investigated various state error cases for two- and three-qubit states. During my PhD, I published Foulds *et al.* [24] with Tim Spiller and Viv Kendon which among other results extends this analysis to n-qubit states and proposes a multipartite measure of entanglement, based on concurrence, related to the c-SWAP test's probability results. Jacob Beckey *et al.* [25] then used this to define a family of entanglement measures called Concentratable Entanglements (CEs) which can be directly estimated from c-SWAP test results. This in turn led to collaborations on the extension of the c-SWAP test to higher dimensional states [26], to mixed states [26, 27], and a proposal for experimentally estimating CEs via a Bell-basis test [27].

In this thesis, I aim to determine the practical usefulness of the new multipartite entanglement measure *concentratable entanglement* (CE). CE is a experimentally motivated multipartite entanglement measure. It is derived directly from the controlled-SWAP (c-SWAP) test for entanglement and therefore has both a physical meaning and can be directly estimated from experiment. The c-SWAP test for entanglement, or its equivalent for two-level states the Bell-basis measurement test, is particularly suited to highly entangled near-pure states, for which the greater the system size the fewer resources required to estimate the CE.

I begin with the necessary background on various multipartite states: namely qubit, qudit, and optical states. I then explain entanglement in terms of its mathematical

formalism, previously introduced measures of entanglement, and known methods experimental detection and measurement of entanglement. To conclude the background section I explain in full the c-SWAP test for equivalence and the c-SWAP test for entanglement as presented in the previous work [22]. This leads to my original work on the behaviour of the CE of bipartite and multipartite qubit states under various state variations and errors, with the view to bound experimental results outputted by the c-SWAP test. Further, this chapter discusses the information contained in the c-SWAP test's results on the entanglement structure of the input qubit states. Next, I present work obtained in collaboration with Oliver Prove during his Level 4 project at Durham whereby we extend the c-SWAP test, and therefore CE, to higher dimensional states. In the final original work chapter, I present work completed in collaboration with Jacob Beckey (PhD student at the Univeristy of Colorado), Gerard Pelegri, and Natalie Pearson (postdocs at the University of Strathclyde). In this chapter, we propose the Bell-basis test as a more experimentally viable method of obtaining the results of the c-SWAP test on qubit states, and detail how this test might be performed on the neutral atom platform via Rydberg excitations. Finally, I conclude with an argument for Concentratable Entanglement to be adopted as a the standard, all-encompassing measure of entanglement, able to be efficiently estimated by experiment.

Chapter 2

Background

First, I will provide the required background to understand the work presented in this thesis. The first section establishes the mathematical framework used to represent the relevant quantum states and their operators. The second section introduces entanglement, entanglement classes, and previously defined measures of entanglement; the third section reviews established methods of evidencing and characterising entanglement. The fourth section describes the controlled SWAP (c-SWAP) test for equivalence, a method for distinguishing states and the precursor to the c-SWAP test for entanglement, which is covered in the fifth section.

2.1 Qubit and qudit states

A quantum superposition state, prior to measurement, is in a superposition of D possible states, where D is the dimensionality of the available state space [28]. These states are discrete and quantised, such as nuclear spin, spatial paths, and atomic energy levels [28]. A pure quantum state is a linear superposition of D basis states, represented in

Dirac notation with state vector [28]

$$|\psi\rangle = \sum_{k \in K_D} A_k |k\rangle \tag{2.1}$$

$$= \begin{bmatrix} A_{k_0} \\ A_{k_1} \\ \vdots \\ A_{k_{D-1}} \end{bmatrix} \tag{2.2}$$

where $K_D = \{k_0, k_1, \ldots, k_{D-1}\}$ is the set of all possible states the superposition state ψ could be in. The linear functional conjugate transpose of $|k\rangle$ is denoted $\langle k|$. The probability of obtaining $|k\rangle$ when measuring $|\psi\rangle$ is $P(|k\rangle) = |\langle k|\psi\rangle|^2 = |A_k|^2$, and the state vector is normalised such that $\langle\psi|\psi\rangle = \sum_k |A_k|^2 = \sum_k P(|k\rangle) = 1$.

Much of this thesis uses the computational basis, where the basis states are denoted with $K_D = \{k \in \mathbb{Z}, 0 \leq k < D\}$ and form an orthogonal basis (for a D-dimensional complex vector Hilbert space) such that $\langle k'|k\rangle = \delta_{kk'}$ [28]. There are exceptions to this notation to signify intermediary states outside the input state's basis; for example, Rydberg states $|r\rangle$ are highly excited electronic states of an atom or molecule that therefore exhibit highly tunable long-range interactions with electromagnetic fields [29].

'Qubit' denotes a state with two computational basis states whereas 'qudit' is an umbrella term for states with $D > 2$ computational basis states [30, 31]. A pure 'n-qubit(qudit) state' is the combined state of n pure qubit(qudit) substates in one system, with state vector [28, 30, 31]

$$|\psi\rangle = \sum_{q \in Q_n} A_q |q\rangle \tag{2.3}$$

where $Q_n = \{0, 1, \ldots, D-1\}^n$ is the set of all possible bit/dit strings of length n, with k denoting the qubit(qudit) label in the set $S = \{1, 2, ..., n\}$. The probability of measuring $|q\rangle$ is $P(|q\rangle) = |A_q|^2$. Again the state vector is normalised such that $\langle\psi|\psi\rangle = \sum_{q \in Q_n} |A_q|^2 = 1$. For example, a two-qubit (pure) state has a state vector of

the form

$$|\psi\rangle = A_{00}\,|00\rangle + A_{01}\,|01\rangle + A_{10}\,|10\rangle + A_{11}\,|11\rangle \tag{2.4}$$

$$= \begin{bmatrix} A_{00} \\ A_{01} \\ A_{10} \\ A_{11} \end{bmatrix} \tag{2.5}$$

where $|jj'\rangle \equiv |j\rangle \otimes |j'\rangle$.

These states are called 'pure' states as they can be represented by state vectors, however they are actually special cases. Most states are in fact 'mixed', meaning they are a probabilistic mixture of pure states. Instead of a state vector these states must be represented by density matrices of the form: [28]

$$\rho = \sum_k p_k\,|\psi_k\rangle\langle\psi_k| \tag{2.6}$$

$$= \sum_k p_k \begin{bmatrix} A^*_{0^{\otimes n}} & A^*_{0^{\otimes n-1}1} & \cdots & A^*_{1^{\otimes n-1}0} & A^*_{1^{\otimes n}} \end{bmatrix}_k \begin{bmatrix} A_{0^{\otimes n}} \\ A_{0^{\otimes n-1}1} \\ \vdots \\ A_{1^{\otimes n-1}0} \\ A_{1^{\otimes n}} \end{bmatrix}_k \tag{2.7}$$

where p_k is the probability of the pure state $|\psi_k\rangle$ in the ensemble ρ, $\sum_k p_k = 1$, and therefore the matrix trace $\mathrm{tr}[\rho] = 1$. A pure state is the special case $\rho = |\psi\rangle\langle\psi|$ where $|\psi\rangle$ is its state vector.

The 'purity', the opposite of mixedness, of any state is given by [32]

$$\gamma = \mathrm{tr}[\rho^2]. \tag{2.8}$$

For pure states, $\rho^2 = |\psi\rangle\,\langle\psi|\psi\rangle\,\langle\psi| = |\psi\rangle\langle\psi| = \rho$ and therefore $\gamma = \mathrm{tr}[\rho^2] = \mathrm{tr}[\rho] = 1$. A maximally mixed state of the form $\rho = I_d/d$, where I_d is an identity matrix of size $d = D^n$, has purity $\gamma = \frac{1}{d}$. The purity of a state characterises the available information about the quantum system [33]. Werner states [19] are of the form

$$\rho = (1-p)\,|\Psi\rangle\langle\Psi| + p\frac{I_d}{d} \tag{2.9}$$

and therefore the purity of ρ is dependant on p, where ρ is pure when $p = 0$ and maximally mixed when $p = 1$.

It is useful to be able to extract the density matrix of a substate or substates from a larger composite state. The reduced density matrix of the n_a-qubit/qudit state A within composite n_t-qubit/qudit state AB is given by the partial trace [28]

$$\rho_A = \mathrm{tr}_B(\rho_{AB}) = \sum_{s \in Q_B} {}_B\langle s| \rho_{AB} |s\rangle_B \tag{2.10}$$

where Q_B is the set of all possible bit/dit strings of length $n_t - n_a$.

In this thesis, computation on quantum states is modelled with circuits of quantum logic gates. An operator A representing a quantum logic gate acts on a state vector $|\psi\rangle$ with $A|\psi\rangle = |\psi'\rangle$ and on a density matrix ρ with $A\rho A^\dagger = \rho'$ [28]. The gates used in this thesis are the Hadamard gate, C$_n$NOT gates, and C$_n$Z gates.

The Hadamard gate is a one qubit gate with matrix [28]

$$H = \frac{1}{\sqrt{2}} \begin{bmatrix} 1 & 1 \\ 1 & -1 \end{bmatrix} \tag{2.11}$$

and therefore operates on qubit computational basis states such that $H|0\rangle = \frac{1}{\sqrt{2}}(|0\rangle + |1\rangle)$ and $H|1\rangle = \frac{1}{\sqrt{2}}(|0\rangle - |1\rangle)$.

The two-qubit controlled-NOT gate, or $CNOT$ gate, flips the target qubit if and only if the control qubit is in state $|1\rangle$ [34]. It is represented by the matrix

$$CNOT = \begin{bmatrix} 1 & 0 & 0 & 0 \\ 0 & 1 & 0 & 0 \\ 0 & 0 & 0 & 1 \\ 0 & 0 & 1 & 0 \end{bmatrix} \tag{2.12}$$

where the first qubit is the control and the second is the target.

The Toffoli gate, otherwise known as the $CCNOT$ gate, is a three-qubit gate that flips the target qubit if and only if the two control qubits are both in state $|1\rangle$. It has matrix

[28]

$$CCNOT = \begin{bmatrix} 1 & 0 & 0 & 0 & 0 & 0 & 0 & 0 \\ 0 & 1 & 0 & 0 & 0 & 0 & 0 & 0 \\ 0 & 0 & 1 & 0 & 0 & 0 & 0 & 0 \\ 0 & 0 & 0 & 1 & 0 & 0 & 0 & 0 \\ 0 & 0 & 0 & 0 & 1 & 0 & 0 & 0 \\ 0 & 0 & 0 & 0 & 0 & 1 & 0 & 0 \\ 0 & 0 & 0 & 0 & 0 & 0 & 0 & 1 \\ 0 & 0 & 0 & 0 & 0 & 0 & 1 & 0 \end{bmatrix} \tag{2.13}$$

where the first two qubits are the control and the third is the target.

The controlled-Z gate or CZ gate is a two-qubit gate that flips the phase ($|0\rangle \rightarrow |0\rangle$, $|1\rangle \rightarrow -|1\rangle$) of the target qubit if the control qubit is in the $|1\rangle$ state with matrix [28]

$$CZ = \begin{bmatrix} 1 & 0 & 0 & 0 \\ 0 & 1 & 0 & 0 \\ 0 & 0 & 1 & 0 \\ 0 & 0 & 0 & -1 \end{bmatrix} \tag{2.14}$$

where the first qubit is the control.

The CCZ gate is then

$$CCZ = \begin{bmatrix} 1 & 0 & 0 & 0 & 0 & 0 & 0 & 0 \\ 0 & 1 & 0 & 0 & 0 & 0 & 0 & 0 \\ 0 & 0 & 1 & 0 & 0 & 0 & 0 & 0 \\ 0 & 0 & 0 & 1 & 0 & 0 & 0 & 0 \\ 0 & 0 & 0 & 0 & 1 & 0 & 0 & 0 \\ 0 & 0 & 0 & 0 & 0 & 1 & 0 & 0 \\ 0 & 0 & 0 & 0 & 0 & 0 & 1 & 0 \\ 0 & 0 & 0 & 0 & 0 & 0 & 0 & -1 \end{bmatrix} \tag{2.15}$$

flipping the phase of the third target qubit if the first two control qubits are both $|1\rangle$.

2.2 Coherent states

The quantum harmonic oscillator is a model of quantised energy levels in an oscillating quantum system such as modes of vibration in molecules, or spatial modes in elecromagnetic waves [28]. Coherent states are minimum uncertainty states of the quantum harmonic oscillator [28]. In this thesis we refer to optical coherent states, which describe laser light: electromagnetic radiation produced such that there is a high probability the light is emitted into the coherent resonant mode [35].

We define the coherent state $|\alpha\rangle$ as the unique eigenstate of the annihilation operator $\hat{a}$ in a quantum harmonic oscillator [35]:

$$\hat{a}\,|\alpha\rangle = \alpha\,|\alpha\rangle\,. \tag{2.16}$$

where α is the coherent state amplitude [35]. Therefore coherent states minimise the quadrature uncertainty principle such that [35]

$$\langle(\Delta\hat{X}_1)^2\rangle\,\langle(\Delta\hat{X}_2)^2\rangle = \frac{1}{16}. \tag{2.17}$$

where $\hat{X}_1 = \frac{1}{2}(\hat{a}^\dagger+\hat{a})$, $\hat{X}_2 = \frac{i}{2}(\hat{a}^\dagger-\hat{a})$, and $\langle x\rangle$ is the average over the momentum/position basis states.

Photon number states, or Fock states, are states of a well-defined number of photons such that $|n\rangle$ are energy eigenstates of the Hamiltonian $H = \hbar\omega\left(\hat{a}^\dagger\hat{a} + \frac{1}{2}\right)$ where n is the number of photons (one quantum of energy) in this state, $\hat{a}\,|n\rangle = \sqrt{n}\,|n-1\rangle$, and $\hat{a}^\dagger\,|n\rangle = \sqrt{n+1}\,|n+1\rangle$[35]. When represented in this basis, coherent states follow a Poisson number distribution: [35]

$$|\alpha\rangle = e^{-\frac{|\alpha|^2}{2}}\sum_{n=0}^{\infty}\frac{\alpha^n}{\sqrt{n!}}\,|n\rangle \tag{2.18}$$

where $|\alpha|^2 = \mu$ is the average number of photons. It follows that the probability of measuring m photons is $P(m|\mu) = \langle m|\,\alpha^*\alpha\,|m\rangle = \mu^m e^{-\mu}/m!$.

A coherent state can also be thought of as the vacuum state $|0\rangle$ displaced to a location α in phase space, due to the action of a displacement operator $\hat{D}(\alpha)$ such that [35]

$$|\alpha\rangle = e^{\alpha\hat{a}^\dagger - \alpha^*\hat{a}}\,|0\rangle = \hat{D}(\alpha)\,|0\rangle\,. \tag{2.19}$$

In contrast to the photon number states, these states are not orthogonal, and form an overcomplete basis. The inner product between coherent states $|\alpha\rangle$ and $|\beta\rangle$ is given by [35]

$$\langle\alpha|\beta\rangle = e^{-\frac{1}{2}|\alpha|^2 - \frac{1}{2}|\beta|^2 + \beta^*\alpha}. \tag{2.20}$$

A squeezed coherent state is one that 'squeezes' the quadrature uncertainty principle in equation (2.17) such that $\langle(\Delta\hat{X}_1)^2\rangle < \frac{1}{4}$ or $\langle(\Delta\hat{X}_2)^2\rangle < \frac{1}{4}$ [35]. A single mode squeezed state is of the form [35]

$$|\alpha,\xi\rangle = \hat{D}(\alpha)\hat{S}(\xi)\,|0\rangle \tag{2.21}$$

$$= \hat{S}(\xi)\hat{D}(\alpha)\,|0\rangle \tag{2.22}$$

where

$$\hat{S}(\xi) = \exp\left[\frac{1}{2}(\xi^*\hat{a}^2 - \xi\hat{a}^{\dagger 2})\right] \tag{2.23}$$

and $\xi = re^{i\theta}$, where r is the squeeze parameter, squeezing in direction θ. The two mode squeezing operator is [35]

$$\hat{S}_2(\xi) = \exp(\xi^*\hat{a}\hat{b} - \xi\hat{a}^\dagger\hat{b}^\dagger). \tag{2.24}$$

where $\hat{b}\,|\beta\rangle = \beta\,|\beta\rangle$. $\hat{S}_2(\xi) \neq \hat{S}(\xi)_{\hat{a}}\hat{S}(\xi)_{\hat{b}}$ and therefore entangles (see section 2.3) the two modes $|\alpha\rangle$ and $|\beta\rangle$. The entropy of entanglement (defined in section 2.3) increases with the squeeze parameter r [35, 36].

Cat states are linear superpositions of coherent states with phase differences. Their name reflects the fact that one can macroscopically distinguish the states in the superposition, similar to the states of the cat in Schrödinger's thought experiment [37]. Cat states are of particular interest due to their applicability in quantum computing [38]

and as the building blocks for entangled coherent states [39, 38]. A general cat state is of the form [35]

$$|\psi_{cat}\rangle = \mathcal{N}(|\alpha\rangle + e^{i\phi}\,|-\alpha\rangle) \tag{2.25}$$

where $\mathcal{N}$ is a normalisation factor given by $\mathcal{N} = [2+2\exp(-2\alpha^2)\cos(\phi)]^{-1/2}$ for relative phase angle $0 \leq \phi \leq 2\pi$. Coherent states $|\alpha\rangle$ and $|-\alpha\rangle$ are the macroscopically distinguishable states: the greater the value of α the smaller the overlap $\langle\alpha|-\alpha\rangle = e^{-2|\alpha|^2}$. Small valued α cat states can be produced with photon subtraction from a squeezed vacuum state [40].

Entangled coherent states (ECS) exhibit entanglement between modes of the electromagnetic field and have applications across a range of fields such as quantum optics [38], quantum information processing [39], and quantum metrology [41]. They can be realised [39] by combining and operating on cat states of the form given in equation (2.25). ECS are also fundamentally interesting as entangled macroscopic states with minimised uncertainty. We will consider two-mode entangled coherent states of the form

$$\begin{aligned}|ECS_2^{\alpha}\rangle = \mathcal{N}_2^{\alpha}(A_{++}\,|\alpha\rangle\,|\alpha\rangle + A_{+-}\,|\alpha\rangle\,|-\alpha\rangle + \\ A_{-+}\,|-\alpha\rangle\,|\alpha\rangle + A_{--}\,|-\alpha\rangle\,|-\alpha\rangle).\end{aligned} \tag{2.26}$$

2.3 Entanglement and its measures

Quantum entanglement is the quantum phenomenon where two or more quantum objects cannot be considered as separate systems, but must be thought of as one system. Therefore, any measurement outcomes on these objects will be strongly correlated in a way not explained by local classical descriptions [28].

For example, a general two-qubit pure state has state vector $|\psi_2\rangle = A_{00}\,|00\rangle + A_{01}\,|01\rangle + A_{10}\,|10\rangle + A_{11}\,|11\rangle$. However, two separate one-qubit pure states have combined state

vector

$$|\psi_1\rangle \otimes |\phi_1\rangle = (A_0 |0\rangle + A_1 |1\rangle) \otimes (A'_0 |0\rangle + A'_1 |1\rangle) \tag{2.27}$$

$$= A_0 A'_0 |00\rangle + A_0 A'_1 |01\rangle + A_1 A'_0 |10\rangle + A_1 A'_1 |11\rangle \tag{2.28}$$

which since it can be written as its composite substates product together, is a 'product' or 'separable' state. Any state $|\psi_2\rangle$ such that $|\psi_2\rangle \neq |\psi_1\rangle \otimes |\phi_1\rangle$ is an entangled state.

'Bell states' are a class of maximally entangled two-qubit states. If one qubit is traced out of a Bell state (see Equation 2.10), the remaining qubit will be a maximally mixed state. The four Bell states are [28]

$$\begin{aligned} |\Phi^{\pm}\rangle &= \frac{1}{\sqrt{2}}(|00\rangle \pm |11\rangle) \\ |\Psi^{\pm}\rangle &= \frac{1}{\sqrt{2}}(|01\rangle \pm |10\rangle). \end{aligned} \tag{2.29}$$

Under reversible LOCC – local operations and classical communication – Bell states can be transformed into one another, but cannot be transformed into a state with less than maximal entanglement. They are therefore considered one class of equivalent states.

Note that the basis used in this thesis so far are the state vectors $|k \in \mathbb{Z}, 0 \leq k < D\rangle$, however any state vectors $|k_i\rangle$ can be chosen as a basis such that

$$|\psi\rangle = \sum_i c_i |k_i\rangle \tag{2.30}$$

for pure states where $\langle\psi|\psi\rangle = 1$. Relevant to this thesis is the Bell basis, a two-qubit basis where $|k_i, 0 \leq i \leq 3\rangle$ are the four Bell states described in equation (2.29). This basis is related to the $\{|0\rangle, |1\rangle\} \otimes \{|0\rangle, |1\rangle\}$ basis with

$$(H \otimes \mathbb{I}) CNOT \{\left|\Phi^+\right\rangle, \left|\Psi^+\right\rangle, |\Phi^-\rangle, |\Psi^-\rangle\} = \{|00\rangle, |01\rangle, |10\rangle, |11\rangle\}. \tag{2.31}$$

Therefore, if a state cannot be measured in the Bell basis directly, one can simply apply a Hadamard gate and a CNOT gate and measure each qubit in the $\{|0\rangle, |1\rangle\}$ basis to

recover the Bell basis. The Bell basis states are in fact eigenstates of the SWAP gate:

$$SWAP\left|\Phi^{+}\right\rangle = \left|\Phi^{+}\right\rangle \tag{2.32}$$

$$SWAP\left|\Phi^{-}\right\rangle = \left|\Phi^{-}\right\rangle \tag{2.33}$$

$$SWAP\left|\Psi^{+}\right\rangle = \left|\Psi^{+}\right\rangle \tag{2.34}$$

$$SWAP\left|\Psi^{-}\right\rangle = -\left|\Psi^{-}\right\rangle. \tag{2.35}$$

and therefore the $|\Psi^{-}\rangle$ state is called the singlet state, as opposed to a triplet state, as it is the only Bell state with a negative eigenvalue.

The more entangled the composite state, the stronger the correlations in the measurement outcomes, and the more mixed the individual qubits are when traced out. There is a well-defined measure of entanglement for bipartite states called 'concurrence'. For pure states it is defined as [42, 43, 44]

$$c_2(|\psi_2\rangle) = \sqrt{2\left(1 - \mathrm{tr}\left[\rho_1^2\right]\right)} \tag{2.36}$$

where $\rho_1 = \mathrm{Tr}_2[|\psi_2\rangle\langle\psi_2|_{12}]$. If $|\psi\rangle$ is a product state then $c_2 = 0$; if it is a maximally entangled state $c_2 = 1$ [42]. In the case of two-qubit states of the form equation (2.4) a more simple equation for concurrence is

$$c_2(A_{00}\,|00\rangle + A_{01}\,|01\rangle + A_{10}\,|10\rangle + A_{11}\,|11\rangle) = 2|A_{00}A_{11} - A_{01}A_{10}|. \tag{2.37}$$

There is also a convex roof extension to bound concurrence for mixed states: [45]

$$c_2(\rho) \geq \sqrt{2\,\mathrm{tr}\left[\rho^2\right] - \mathrm{tr}\left[\rho_1^2\right] - \mathrm{tr}\left[\rho_2^2\right]} = c_2^l(\rho) \tag{2.38}$$

If ρ is a pure state, $\mathrm{tr}\left[\rho^2\right] = 1$ and $\mathrm{tr}\left[\rho_1^2\right] = \mathrm{tr}\left[\rho_2^2\right]$, therefore $c_2^l(|\psi\rangle\langle\psi|) = c_2(|\psi\rangle)$. If ρ is a maximally mixed state $c_2^l(\rho) = \frac{1}{2}$ – this measure therefore includes both entanglement and mixedness. In fact, the two are inextricably linked.

In general, an entangled pure state is any $|\psi_n\rangle$ that satisfies

$$|\psi_n\rangle \neq \bigotimes_{k=1}^{n} |\phi_1\rangle_k. \tag{2.39}$$

The entangled classes used in this thesis are W states, GHZ states, and Line states.

True n-qubit W states have state vector [46, 47]

$$|\mathrm{W}_n\rangle = \frac{1}{\sqrt{n}} \sum_{k=1}^{n} |0...1_k...0\rangle_n \tag{2.40}$$

where $|0...1_k...0\rangle_n$ denotes a string of length n with a single qubit k in state $|1\rangle$ in each state in the superposition, e.g. $|0...1_2...0\rangle_4 = |0010\rangle$. A strength of $n > 2$-qubit W states is that if a qubit is lost, an $n-1$-qubit W state remains. An n-qubit W-like state has form

$$|\psi_n\rangle = \sum_{k=1}^{n} A_k |0...1_k...0\rangle_n \tag{2.41}$$

which exhibits the same properties of true W states with less total entanglement. Each qubit in this state has purity $\gamma_k = A_k^4 + \left(\sum_{j=1,j\neq k}^{n} A_j^2\right)^2$, which equals $\gamma = \frac{1}{n^2}((n-1)^2+1)$ for true W states.

True n-qubit GHZ states are defined as [48, 47]

$$|\mathrm{GHZ}_n\rangle = \frac{1}{\sqrt{2}}(|0\rangle^n + |1\rangle^n) \tag{2.42}$$

where $|0\rangle^n \equiv \bigotimes_{k=1}^{n} |0\rangle_k$. Each qubit in this state is a maximally mixed one-qubit state. This class of state is often considered a stronger form of entanglement than W states, however it is less robust as the measurement or other of one qubit will destroy all entanglement in the state. We define an n-qubit GHZ-like state as $|\psi_n\rangle = \alpha_0 |0\rangle^n + \alpha_1 |1\rangle^n)$; each qubit has purity $\alpha_0^4 + \alpha_1^4$.

When $n = 2$, both W states and GHZ states reduce to Bell states. However, for $n \geq 3$, W states and GHZ states are two inequivalent classes of entangled states. Frequently in this thesis Bell states are included in the analysis of GHZ and W states as the $n = 2$ case.

The final class discussed are line cluster states, with state vector [49]

$$|\mathrm{L}_n\rangle = \prod_{\text{adjacent } i,j} CZ_{ij} H^n |0\rangle^n \tag{2.43}$$

where CZ is a controlled-Z gate from equation (2.14) and H is a Hadamard gate from equation (2.11). This creates a line of n qubits each entangled with their two nearest

neighbours. They are equivalent to a Bell state for $n = 2$ and equivalent to a GHZ state for $n = 3$.

Measures for the entanglement of a multipartite ($n > 2$) state are plentiful and varied. An entanglement measure has to satisfy certain properties, such as not increasing on average under local operations and classical communication (LOCC) [28]. In essence, it must be true that [50, 51]

$$\varepsilon(\rho) \geq \sum_{m=1}^{M} p_m \, \varepsilon(\rho^{(m)}) \tag{2.44}$$

where ε is an entanglement measure, $\rho^{(m)}$ is the outcome of a local measurement on ρ, and p_m the probability of the outcome $\rho^{(m)}$. This equality must be true for any value of M. Prominent examples of multipartite entanglement measures include the n-tangle, which characterises the n-way entanglement in a state [52, 53]. Therefore W states, which have only 2-way entanglement, have an n-tangle of zero and GHZ states for which all entanglement is n-way have an n-tangle of one. In terms of the concurrence the n-tangle is defined as

$$\tau_{12\ldots n} = c^2_{1(2\ldots n)} - (c^2_{12} + \cdots + c^2_{1n}). \tag{2.45}$$

The two-qubit entanglement measure concurrence has been extended to the n-partite generalised concurrence [43]. Label each qubit in the n-partite state with $S = \{1, 2, ..., n\}$. Then let the concurrence of any bipartition $\mathcal{M}|\bar{\mathcal{M}}$ (where $\bar{\mathcal{M}}$ is the complementary set of $\mathcal{M}$) of set S be defined as

$$E_{\mathcal{M}} = \sqrt{2(1 - \mathrm{tr}[\rho^2_{\mathcal{M}}])}. \tag{2.46}$$

The generalised concurrence of the n-partite state is then

$$E = \sum_{\mathcal{M}|\bar{\mathcal{M}} \in \mathcal{P}} E_{\mathcal{M}} \tag{2.47}$$

where $\mathcal{P}$ is the set of possible bipartitions in S. For example, a four-partite state has general concurrence $E = E_1 + E_2 + E_3 + E_4 + E_{1,2} + E_{1,3} + E_{1,4}$, which for a true W state corresponds to $E = 2\sqrt{5} + 3$.

Additionally there is the 'entropy of entanglement' which is the von Neumann entropy of a subsystem defined as [51]

$$S_A(\rho_A) = -\mathrm{tr}\left[\rho_A \log(\rho_A)\right] \tag{2.48}$$

where $\rho_A = \mathrm{Tr}_B\left[\rho_{AB}\right]$. This measure is therefore related to the mixedness of a subsystem A, and therefore the entanglement between A and B for pure states.

2.4 Experimental detection of entanglement

The most general method for experimentally determining entanglement is quantum state tomography (QST). QST involves performing a large number of measurements on an ensemble of identical quantum states, using the results to reconstruct the system's density matrix entry by entry [21, 54]. The entanglement of the system can then be quantified using a given entanglement measure. For n qudits, standard QST requires at least D^{2n} (the number of basis states $|y\rangle\langle x|$) measurements and as many copies of the state [21], an exponential scaling in n which renders the method impractical for large numbers of qubits. There are many improvements to this method, among them Haeffner *et al.* [55] which characterises the entanglement of the trapped ion W state qubits with $100 \cdot 3^n$ measurements and Cramer *et al.* [56] for which QST on a 1-D chain of pure qudits requires a linear number of measurements with system size n.

An alternative method uses entanglement witnesses. An entanglement witness $\mathcal{W}$ is an observable such that $\mathrm{Tr}\left(\mathcal{W}\rho_s\right) \geq 0$ for all separable ρ_s and $\mathrm{Tr}\left(\mathcal{W}\rho_e\right) < 0$ for selected entangled state ρ_e. It can be shown that for any pure state there exists a witness that requires only $2n - 1$ measurements, far fewer than the number needed for QST [21]. Nevertheless, as suggested by the definition, entanglement witnesses must be optimised for the state considered and are therefore not a general method.

2.5 The controlled SWAP test for state comparison

The SWAP test is a widely used procedure for state comparison [57], first experimentally demonstrated in [58]. The name derives from the controlled SWAP (c-SWAP) gate used to perform the test, which has input systems A and B controlled on a control qubit C. If the control qubit is in state $|1\rangle_C$, the c-SWAP gate swaps the states of systems A and B, and if in state $|0\rangle_C$, states A and B are unchanged.

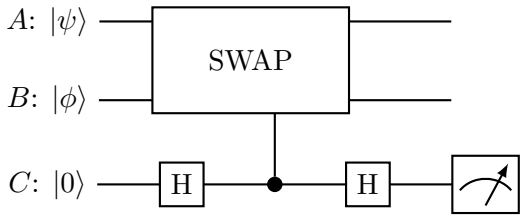

Figure 2.1: One round of the controlled SWAP test for comparison of states $|\psi\rangle$ and $|\phi\rangle$. H is a Hadamard gate. The SWAP gate performs the operation $|\psi\rangle_A |\phi\rangle_B |1\rangle_C \rightarrow |\phi\rangle_A |\psi\rangle_B |1\rangle_C$.

Three states are prepared in the initial composite state $|\Psi\rangle = |\psi\rangle_A |\phi\rangle_B |0\rangle_C$ where $|\psi\rangle$ and $|\phi\rangle$ are pure qubit states to be compared [57]. First, a Hadamard gate (equation (2.11)) is applied to the control qubit. A c-SWAP gate is then performed on $|\psi\rangle_A$ and $|\phi\rangle_B$ controlled on C, followed by a second Hadamard gate applied to the control qubit, giving the composite state [59]

$$|\Psi\rangle = \frac{1}{2}[(|\psi\rangle_A |\phi\rangle_B + |\phi\rangle_A |\psi\rangle_B) |0\rangle_C + (|\psi\rangle_A |\phi\rangle_B - |\phi\rangle_A |\psi\rangle_B) |1\rangle_C]. \tag{2.49}$$

This sequence of gates is shown in Figure 2.1. From the above expression it can be seen that the probability of measuring state $|1\rangle$ in the control is zero if the two states $|\psi\rangle_A$ and $|\phi\rangle_B$ are identical. A measurement of $|1\rangle_C$ therefore proves the two states are different, while multiple measurements of $|0\rangle_C$ are required to achieve confidence of equivalence. It can be shown that in general the probability of measuring $|1\rangle_C$ is given by

$$P(|1\rangle_C) = \frac{1}{2} - \frac{1}{2} |\langle\psi|\phi\rangle|^2 \tag{2.50}$$

giving a maximum probability of $\frac{1}{2}$ for orthogonal states. Further, the overlap can be calculated from estimating the probability from repeat measurements on an ensemble of $|\psi\rangle_A$ and $|\phi\rangle_B$ [57].

Note that if systems A and/or B are mixed, the test will have a non-zero probability of measuring $|1\rangle_C$ regardless of whether the inputs are equivalent, i.e., $\rho_A = \rho_B$. Non-unity purity implies some uncertainty in the actual state, allowing the two copies to be different up to the limit allowed by the mixedness.

2.6 The controlled SWAP test for entanglement

The controlled SWAP test for entanglement is a modified version of the controlled SWAP test for state comparison. The following is the test as as proposed in [22].

Two-qubit pure input states $\rho = |\psi\rangle\langle\psi|$ and $\rho' = |\phi\rangle\langle\phi|$ and a two-qubit control ancilla are subject to two controlled SWAP tests in parallel such that the first qubits in $|\psi\rangle$ and $|\phi\rangle$, $\rho_1 \equiv \mathrm{Tr}_2(\rho)$ and $\rho'_1 \equiv \mathrm{Tr}_2(\rho')$ respectively, are compared using the c-SWAP test for state comparison and the second qubits in $|\psi\rangle$ and $|\phi\rangle$, $\rho_2 \equiv \mathrm{Tr}_1(\rho)$ and $\rho'_2 =\equiv \mathrm{Tr}_1(\rho')$ respectively, are also compared, using one control qubit each. This and the universal gate breakdown are shown in Figure 2.2.

The input to each round of the test is therefore $|\Psi_{\text{in}}\rangle = |\psi\rangle_A \otimes |\phi\rangle_B \otimes |00\rangle_C$ where the subscript C denotes the control qubits. The final composite state before measurement is then: [22]

$$|\Psi_{\text{out}}\rangle = H_{C_1} H_{C_2} CSWAP_{C_1 A_1 B_1} CSWAP_{C_2 A_2 B_2} H_{C_1} H_{C_2} |\psi\rangle_A |\phi\rangle_B |00\rangle_C \tag{2.51}$$

$$\begin{aligned} = \frac{1}{4} \sum_{ijrs} |ij\rangle_A |rs\rangle_B \, & (A_{ij}B_{rs} + A_{is}B_{rj} + A_{rj}B_{is} + A_{rs}B_{ij}) |00\rangle_C \\ & + (A_{ij}B_{rs} - A_{is}B_{rj} + A_{rj}B_{is} - A_{rs}B_{ij}) |01\rangle_C \\ & + (A_{ij}B_{rs} + A_{is}B_{rj} - A_{rj}B_{is} - A_{rs}B_{ij}) |10\rangle_C \\ & + (A_{ij}B_{rs} - A_{is}B_{rj} - A_{rj}B_{is} + A_{rs}B_{ij}) |11\rangle_C] \end{aligned} \tag{2.52}$$

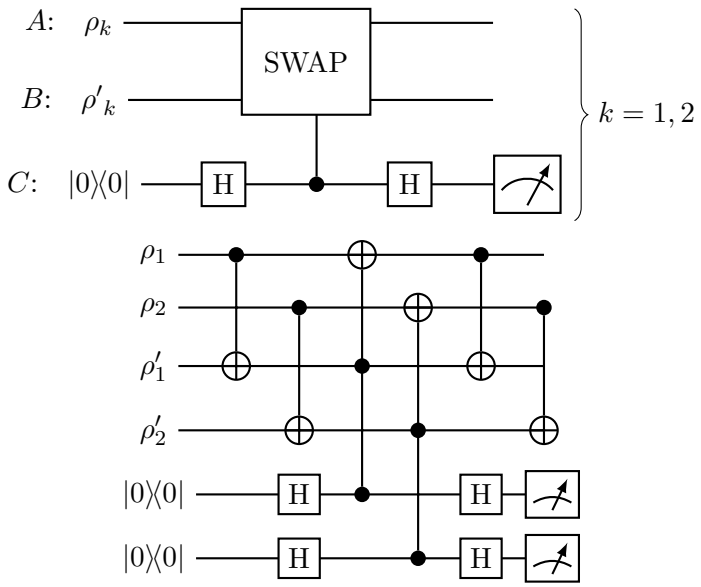

Figure 2.2: One round of the c-SWAP test for entanglement on two-qubit states $\rho \approx \rho'$ where the one-qubit states $\rho_1 \equiv \mathrm{Tr}_2(\rho)$ and so on. The lower plot shows the gate decomposition for the SWAP gate where the two-qubit gates represent $CNOT$ gates from Equation (2.12) and the three-qubit gates represent Toffoli gates from Equation (2.13).

If the two input states are identical such that $|\phi\rangle = |\psi\rangle$ this reduces to

$$|\Psi_{\text{out}}\rangle = \frac{1}{2}\sum_{ijrs} |ij\rangle_A |rs\rangle_B \left[(A_{ij}A_{rs} + A_{is}A_{rj})|00\rangle_C + (A_{ij}A_{rs} - A_{is}A_{rj})|11\rangle_C\right] \quad (2.53)$$

$$= \frac{1}{2}\sum_{ijrs} |ij\rangle_A |rs\rangle_B (A_{ij}A_{rs} + A_{is}A_{rj})|00\rangle_C \quad (2.54)$$

$$+ \frac{1}{2}(|00\rangle|11\rangle - |01\rangle|10\rangle - |10\rangle|01\rangle + |11\rangle|00\rangle)_{AB}(A_{00}A_{11} - A_{01}A_{10})|11\rangle_C .$$

Recall the equation for concurrence from Equation (2.37), $c_2 = 2|A_{00}A_{11} - A_{01}A_{10}|$, therefore:

$$\langle 11|_C |\Psi_{\text{out}}\rangle = \frac{1}{4}(|00\rangle|11\rangle - |01\rangle|10\rangle - |10\rangle|01\rangle + |11\rangle|00\rangle)_{AB}\, c_2. \quad (2.55)$$

Given a resource of many copies of $|\psi\rangle$, which we will refer to as the resource ensemble, the test can be be repeated many times and the control state measured to estimate the probability

$$P(|11\rangle_C) = \frac{1}{4}c_2^2 \quad (2.56)$$

and therefore the concurrence of $|\psi\rangle$ can be obtained.

The c-SWAP test for entanglement can be extended to pure or mixed n-party states, the performance of which is the subject of this thesis. The test requires a resource ensemble of $2M$ near copies of an n-party test state ρ and Mn control qubits. For each round of the test $m \in \{1, 2, \ldots, M\}$, two states are selected from the resource ensemble and denoted ρ and ρ' respectively such that the intital composite state is $\rho_{\text{initial}} = \rho_A \rho'_B \, |0\rangle\langle 0|_C^{\otimes n}$. The c-SWAP test for equivalence is applied to $\rho_k \otimes \rho'_k \otimes |0\rangle\langle 0|$ for each $k \in \{1, 2, \ldots, n\}$ in parallel such that

$$\rho_{\text{out}} = U \rho_A \rho'_B \, |0\rangle\langle 0|_C^{\otimes n} \, U^\dagger \tag{2.57}$$

where $U = \prod_{k=1}^{n} H_{C_k} CSWAP_{C_k A_k B_k} H_{C_k}$ which is shown in Figure 2.3. The control state is then measured. After M rounds of the test the probability distribution of the n-qubit control state is estimated. In this thesis the exact probability results are obtained with $P(|q\rangle_C) = \langle q|_C \, \rho_{\text{out}} \, |q\rangle_C$ for $q \in \{0, 1, \ldots, D-1\}^n$.

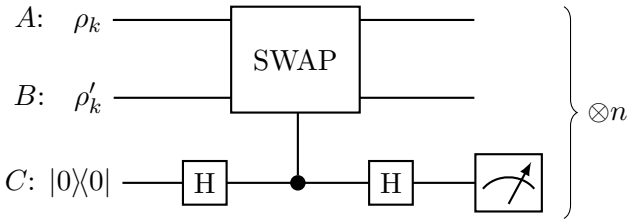

Figure 2.3: One round m of the c-SWAP test for entanglement on state ρ. H is a Hadamard gate from Equation (2.11) and the SWAP gate performs $(\rho_k)_A(\rho'_k)_B \rightarrow (\rho'_k)_A(\rho_k)_B$ controlled on C.

2.7 Measurement statistics

Hoeffding's inequality [60] states that an experimentally calculated value $\hat{X} = \frac{1}{M} \sum_{m=1}^{M} X_m$ where $X_1 ... X_M$ are independent random variables such that $0 \leq X_m \leq 1$, is ϵ-close to $X = \lim_{M \to \infty} \hat{X}$ with probability

$$P(|\hat{X} - X| < \epsilon) \geq 1 - \delta \tag{2.58}$$

when the total number of measurements M is of the order

$$M = \Theta\left(\frac{\ln(1/\delta)}{\epsilon^2}\right) \tag{2.59}$$

where $\Theta(g(\delta, \epsilon))$ is the set bounded both above and below by g asymptotically.

Similarly let there be M measurements with outcomes $X_1...X_M$ where $X \in \{0, 1\}$ such that the probability of measuring $X = 1$ K times is the binomial distribution

$$P(\{X = 1\} \otimes K) = \binom{M}{K} p^K (1-p)^{M-K} \tag{2.60}$$

where $p = P(X = 1)$. If p is unknown it can be estimated from $X_1...X_M$ by the Maximum Likelihood Estimation (MLE) with

$$\hat{p} = \frac{K}{M}. \tag{2.61}$$

The Clopper-Pearson confidence intervals provide bounds for the accuracy of $\hat{p}$ with upper and lower bounds p_U and p_L: [61]

$$\sum_{j=0}^{K} \binom{M}{K} p_U^j (1-p_U)^{M-j} = \frac{\delta}{2} \tag{2.62}$$

$$\sum_{j=K}^{M} \binom{M}{j} p_L^j (1-p_L)^{M-j} = \frac{\delta}{2} \tag{2.63}$$

with a confidence interval of $100(1-\delta)\%$, where $\binom{n}{k} = \frac{n!}{k!(n-k)!}$ is are the binomial coefficients.

2.8 Neutral atom platform

Neutral atoms are a versatile experimental platform, supporting analogue and digital operation [62] and combinations of atomic species [63]. It is the only quantum platform with a programmable qubit layout [62, 64, 65], allowing for arbitrary 1-3D arrays using holographic traps [65, 66], optical addressing [67], and atom shuttling [68]. The

technique is highly scalable, with current hardware demonstrating <1000 qubits [69]. Neutral atoms exhibit all-to-all connectivity [70], with high-fidelity multi-qubit gate operations using strong Rydberg atom interactions [67].

Recent experiments have realised a Toffoli gate with 87.0(4)% fidelity [71], programmable generation of entangled graph states such as cluster states [67], two-qubit entangling gates with 99.5% fidelity on up to 60 atoms in parallel [70], controlling quantum many-body scars [68], maximum independent set optimization [65], and non-destructive, state-selective fluorescence detection, demonstrated with $\leq$5 qubits and 99% detection fidelity [72].

Chapter 3

The concentratable entanglement for qubit states

In this chapter, I will investigate the entanglement measure 'concentratable entanglement' (CE) for multipartite qubit states and how it relates to the outputs of the c-SWAP test for entanglement (from now on referred to as simply the c-SWAP test) described in Section 2.6. This includes the pure state definition from Equation (3.1), a mixed state extension, and a modified version taking into account variations in the resource ensemble. Results for $n = 2$ and $n = 3$ were calculated analytically and results where $n > 3$ were calculated numerically. The full probability results for pure states of varying number of qubits n can be found in the Appendix.

Higher dimensional states will be similarly explored in Chapter 4. I have focused on the suitability of CE as a measure able to be calculated from experimental results and so I have also detailed the effect of input state errors on CE. Further sources of error are considered in Chapter 5. All results are my own unless otherwise stated.

3.1 Identical pure states

In this section we consider the given ensemble of states to be identical pure n-qubit states: therefore the input states are described by $\rho = \rho' = |\psi\rangle \langle\psi|$.

Following the publication of Foulds *et al.* [73], the paper Beckey *et al.* [25] introduces the family of entanglement measures 'concentratable entanglements' which extends concurrence, and therefore the formalism of the c-SWAP test results, to n-qubit pure states. For input state $|\psi\rangle$, denote the set of labels for each qubit as $S = \{1, 2, ..., n\}$ with $\mathcal{P}(S)$ as its power set. For any set of qubit labels $s \in \mathcal{P}(S)\backslash\{\emptyset\}$, the concentratable entanglement (CE) is [25]

$$\mathcal{C}_{|\psi\rangle}(s) = 1 - \frac{1}{2^{c(s)}} \sum_{\alpha \in \mathcal{P}(s)} \mathrm{tr}\left[\rho_\alpha^2\right] \tag{3.1}$$

where $c(s)$ is the cardinality (the number of elements) of the set s and ρ_α is the joint reduced state of the subsystems labeled by the elements in α where $\mathrm{tr}\left[\rho_\emptyset^2\right] = 1$.

Local purities $\mathrm{tr}[\rho_\alpha^2]$ (in any possible partition) cannot decrease, on average, under local or separable operations [25]. Therefore pure state concentratable entanglement in equation (3.1) is also non-increasing, on average, under LOCC, since LOCC operations are a subset of separable operations. Therefore the requirement of equation (2.44) for CE to be a valid entanglement measure is satisfied.

The concentratable entanglement is related to the outputs of the c-SWAP test as described in Section 2.6 by

$$\mathcal{C}_{|\psi\rangle}(s) = 1 - P(|0\rangle_C \text{ on all in } s) \tag{3.2}$$

$$= P(\text{non-zero even no. of } |1\rangle_C \text{s on } s). \tag{3.3}$$

This is true for all pure n-qubit input states $\rho = \rho' = |\psi\rangle\langle\psi|$, the proof of which is as follows [25]: The operation of the c-SWAP test U_{CSWAP} is

$$U_{\mathrm{CSWAP}} |0^n\rangle_C |\psi\rangle |\psi\rangle = H^n CSWAP^n H^n |0^n\rangle_C |\psi\rangle |\psi\rangle \tag{3.4}$$

$$= \frac{1}{2^n} \prod_{k=1}^{n} \sum_{z=0}^{1} |z_k\rangle_C \left(I_k + (-1)^{z_k} SWAP_k\right) |\psi\rangle |\psi\rangle \tag{3.5}$$

where $SWAP\,|k\rangle\,|k'\rangle = |k'\rangle\,|k\rangle$. Tracing out the test states we find

$$P(|\mathbf{z}\rangle_C) = \langle\psi|\langle\psi| \frac{1}{2^n} \prod_{k=1}^{n} \left(I_k + (-1)^{z_k} SWAP_k\right) |\psi\rangle |\psi\rangle \tag{3.6}$$

where $\mathbf{z} = \prod_{k=1}^{n} z_k$. Therefore

$$1 - P(|0\rangle_C \text{ on all in } s) = 1 - \sum_{\mathbf{z}\in\mathcal{Z}_0(s)} \langle\psi| \langle\psi| \frac{1}{2^n} \prod_{k=1}^{n} (I_k + (-1)^{z_k} SWAP_k) |\psi\rangle |\psi\rangle$$

$$= 1 - \frac{1}{2^{c(s)}} \mathrm{Tr}\left[\rho_s \otimes \rho_s \prod_{k=1}^{n} (I_k + SWAP_k)\right] \tag{3.7}$$

$$= 1 - \frac{1}{2^{c(s)}} \sum_{\alpha\in\mathcal{P}(s)} \mathrm{tr}\left[\rho_\alpha^2\right] \tag{3.8}$$

$$= \mathcal{C}_{|\psi\rangle}(s) \tag{3.9}$$

as required, where $\mathcal{Z}_0(s)$ is the set of all n bits with $|0\rangle_C$ on all in s, and we have used $\mathrm{Tr}[SWAP(\rho \otimes \rho)] \equiv \mathrm{Tr}[\rho^2]$.

Therefore any instance of an non-zero even no. of $|1\rangle_C$ s, where even in any round m of the c-SWAP test evidences entanglement, and the probability estimated over M rounds gives the CE. Note that in this case $P(\text{odd no. of } |1\rangle_C \text{ s}) = 0$. In the rest of this thesis, 'even' refers to 'non-zero even' numbers, such that $P(|0\rangle^n) + P(\text{odd no. of } |1\rangle_C \text{ s}) + P(\text{even no. of } |1\rangle_C \text{ s}) = 1$. In Sections 3.1-3.4 we refer exclusively to the *total* CE, $\mathcal{C}_\rho(s = S)$, which we write as $\mathcal{C}_\rho$ for easy of notation.

Any Bell state $|\psi\rangle$ from Equation (2.29) gives $\mathcal{C}_{|\psi\rangle} = \frac{1}{4}$. This is therefore the upper bound for pure two-qubit states. For a general two-qubit pure state $|\psi\rangle = A_{00}|00\rangle + A_{01}|01\rangle + A_{10}|10\rangle + A_{11}|11\rangle$:

$$\mathcal{C}_{|\psi\rangle} = P(|11\rangle_C) \tag{3.10}$$

$$= (A_{00}A_{11} - A_{01}A_{10})^2 \tag{3.11}$$

$$= \frac{c_2^2}{4} \tag{3.12}$$

where c_2 is the concurrence from equation 2.36. Therefore the well established two-qubit entanglement measure concurrence is recovered from two-qubit concentratable entanglement.

A similarly general three-qubit state $|\psi\rangle = \sum_{ijk} A_{ijk}|ijk\rangle$ results in non-zero probab-

ilities

$$P(|011\rangle_C) = \frac{1}{2}[2(A_{000}A_{011} - A_{001}A_{010})^2 + 2(A_{100}A_{111} - A_{101}A_{110})^2 + (A_{000}A_{111} - A_{001}A_{110} - A_{010}A_{101} + A_{011}A_{100})^2], \quad (3.13)$$

$$P(|101\rangle_C) = \frac{1}{2}[2(A_{000}A_{101} - A_{001}A_{100})^2 + 2(A_{010}A_{111} - A_{011}A_{110})^2 + (A_{000}A_{111} - A_{001}A_{110} + A_{010}A_{101} - A_{011}A_{100})^2], \quad (3.14)$$

$$P(|110\rangle_C) = \frac{1}{2}[2(A_{000}A_{110} - A_{010}A_{100})^2 + 2(A_{001}A_{111} - A_{011}A_{101})^2 + (A_{000}A_{111} + A_{001}A_{110} - A_{010}A_{101} - A_{011}A_{100})^2], \quad (3.15)$$

$$P(|000\rangle_C) = 1 - P(|011\rangle_C) - P(|101\rangle_C) - P(|110\rangle_C) \quad (3.16)$$

From this CE of $|\psi\rangle$ can be calculated as $\mathcal{C}_{|\psi\rangle} = P(|011\rangle_C) + P(|101\rangle_C) + P(|110\rangle_C)$. Further, which qubits are entangled with one another can be identified. In the partially separable case $|\psi\rangle = (\alpha_0 |0\rangle + \alpha_1 |1\rangle)_1 \otimes (A_{00} |00\rangle + A_{01} |01\rangle + A_{10} |10\rangle + A_{11} |11\rangle)_{23}$ these probabilities become

$$P(|011\rangle_C) = (A_{00}A_{11} - A_{01}A_{10})^2 \quad (3.17)$$

$$= \frac{c_2^2}{4} \quad (3.18)$$

$$P(|101\rangle_C) = 0, \quad (3.19)$$

$$P(|110\rangle_C) = 0, \quad (3.20)$$

$$P(|000\rangle_C) = 1 - P(|011\rangle_C) \quad (3.21)$$

where c_2 is the concurrence of qubits 2 and 3. If the separable qubit was instead qubits 2 or 3, then the non-zero probability becomes $P(|101\rangle_C)$ and $P(|110\rangle_C)$ respectively. We can see therefore that $P(|1_j 1_k\rangle_C)$ is non-zero iff qubits j and k are entangled, and so it follows that a non-zero $P(|1_j 1_k\rangle_C)$ evidences entanglement between qubits j and k.

Three-qubit states have two distinct ways of being entangled, GHZ state entanglement and W state entanglement [47]. These are the classes of states I will focus on.

A maximally entangled n-qubit true GHZ state $|\mathrm{GHZ}_n\rangle = \frac{1}{\sqrt{2}}(|0\rangle^n + |1\rangle^n)$ has CE $\mathcal{C}_{|\mathrm{GHZ}\rangle} = \frac{1}{2} - \frac{1}{2^n}$, whereas a true W state $|\mathrm{W}_n\rangle = \frac{1}{\sqrt{n}} \sum_k |0...1_k...0\rangle$ has CE $\mathcal{C}_{|\mathrm{W}\rangle} = \frac{1}{2} - \frac{1}{2n}$.

Both are shown in Figure 3.1 for comparison. The CE of each tends to $\frac{1}{2}$ as n increases, however for all $n > 2$, $\mathcal{C}_{|\mathrm{GHZ}\rangle} > \mathcal{C}_{|\mathrm{W}\rangle}$.

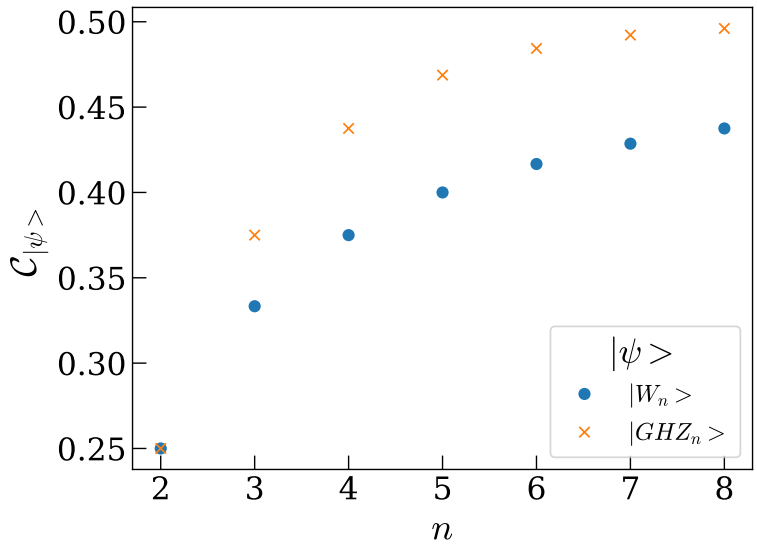

Figure 3.1: The CE of true GHZ and W states for various numbers of qubits n.

For n-qubit W-like states which are defined by $|\psi\rangle = |\mathrm{W}_n\rangle = \sum_{i=1}^{n} a_i |0...1_i...0\rangle$, the non-zero probabilities given by the c-SWAP test are

$$P(|0\rangle_C^n) = \sum_{i=1}^{n} \left(a_i^4 + \sum_{j>i}^{n} a_i^2 a_j^2 \right) \tag{3.22}$$

$$P(|0...1_i...1_j...0\rangle_C) = a_i^2 a_j^2 \tag{3.23}$$

and therefore its CE is

$$\mathcal{C}_{|\mathrm{W}_n\rangle} = P(\text{exactly two } |1\rangle_C \text{s}) \tag{3.24}$$

$$= \sum_{i}^{n} \sum_{j>i}^{n} a_i^2 a_j^2 \tag{3.25}$$

$$= \sum_{\text{all pairs}} \mathcal{C}_{|\mathrm{W}_2\rangle} \tag{3.26}$$

Provided each a_i and a_j are both non-zero, entanglement is present between every pair. However, strings with greater than two $|1\rangle_C$s have a probability of zero; therefore in the W state case, no more than one pair of qubits are evidenced as entangled simultaneously (i.e. during one round m). This is equivalent to the fact that W states have an n-tangle of zero.

Alternatively, n-qubit GHZ-like states defined as $|\psi\rangle = |\text{GHZ}_n\rangle = \alpha_0 |0\rangle^n + \alpha_1 |1\rangle^n$ give:

$$P(|0\rangle_C^n) = \alpha_0^4 + \alpha_1^4 + \frac{4}{2^n}\alpha_0^2\alpha_1^2 \tag{3.27}$$

$$P(\text{each string with even no.}\,|1\rangle_C\,\text{s}) = \frac{4}{2^n}\alpha_0^2\alpha_1^2 \tag{3.28}$$

This tells us that there is entanglement between any given pair of qubits in the input state, so long as both amplitudes are non-zero. Further, GHZ states with $n \geq 4$ result in a non-zero probability of measuring even numbers of $|1\rangle_C$s greater than two, meaning that more than two qubits can be identified as entangled simultaneously.

Note that the c-SWAP test cannot identify odd-way entanglement during one round m, therefore odd-way entanglement is not explicitly represented in the total CE.

The CEs of GHZ states are

$$\mathcal{C}_{|\text{GHZ}_n\rangle} = P(\text{even no.}\,|1\rangle_C\,\text{s}) \tag{3.29}$$

$$= \left(2^{n-1} - 1\right)\frac{4}{2^n}\alpha_0^2\alpha_1^2 \tag{3.30}$$

$$= \frac{2^{n+1} - 4}{2^n}\alpha_0^2\alpha_1^2 \tag{3.31}$$

shown in Figure 3.2. Compare this with its n-tangle calculated equation (2.45), $\tau(|\text{GHZ}_n\rangle) = 4\alpha_0^2\alpha_1^2$, which has the same form, but a coefficient independent of n [52]. Further consider generalised concurrence (Equation 2.47) of the same states, $E_{|\text{GHZ}_n\rangle} = (2^n - 2)\alpha_0\alpha_1$; therefore for GHZ-like states

$$\mathcal{C}_{|\text{GHZ}_n\rangle} = \frac{2E_{|\text{GHZ}_n\rangle}{}^2}{2^n(2^n - 2)}. \tag{3.32}$$

Note that if these values are treated as fractions of 'maximal' entanglement they relate more straight-fowardly with

$$\left[\frac{E_{|\text{GHZ}_n\rangle}}{\max(E_{|\text{GHZ}_n\rangle})}\right]^2 = \frac{\mathcal{C}_{|\text{GHZ}_n\rangle}}{\max(\mathcal{C}_{|\text{GHZ}_n\rangle})}. \tag{3.33}$$

This relation suggests that the lack of odd-way entanglement directly represented in the total CE does not result in an underestimation of the degree of entanglement in GHZ states, as the n-tangle explicitly includes odd-way entanglement.

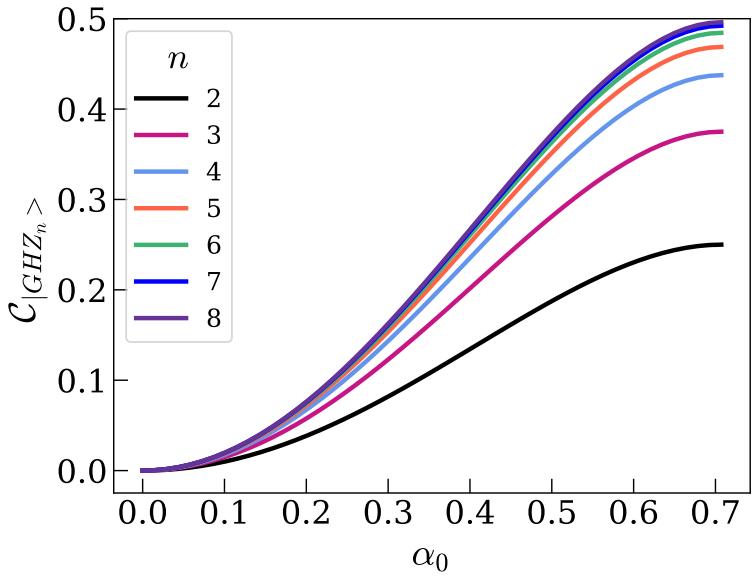

Figure 3.2: The CE of GHZ-like states $|\text{GHZ}_n\rangle = \alpha_0 |0\rangle^n + \sqrt{1-\alpha_0^2}\,|1\rangle^n$ for various numbers of qubits n.

The above formalism tells us more about the structure of GHZ and W states respectively. For W states, the total CE is merely the sum of the CE of each possible pair in the state. However, the CE of GHZ-like states is that of each possible pair and any possible pairs of pairs. While W state entanglement can be thought of as a connected graph, GHZ state entanglement is a more like a single vertex of size n (see Figure 3.3).

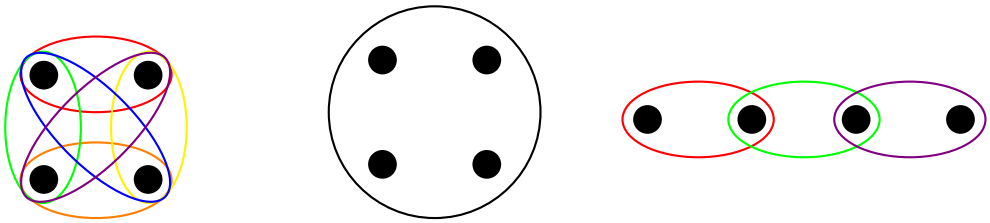

(a) W state (b) GHZ state (c) Line cluster state

Figure 3.3: Pictographic representations of a four-partite system entangled in different ways. The dots represent a single partite states and the circles/ellipses represent entanglement between the states within them. If each of these entangled states are maximally entangled with respect to their entanglement class, then the CEs are $\mathcal{C}_{|\text{W}\rangle} = \frac{3}{8}$, $\mathcal{C}_{|\text{GHZ}\rangle} = \frac{7}{16}$, $\mathcal{C}_{|\text{Line}\rangle} = \frac{1}{2}$.

The above states are n-entangled, as in all qubits are entangled with all other qubits.

Consider instead a partially separable four-qubit state

$$|\psi\rangle = |\chi_4\rangle = (\cos\theta\,|00\rangle + \sin\theta\,|11\rangle)_{12} \otimes (\cos\phi\,|00\rangle + \sin\phi\,|11\rangle)_{34}\,. \tag{3.34}$$

which has the c-SWAP results

$$P(|0000\rangle_C) = (1 - \frac{1}{4}\sin^2(2\theta))(1 - \frac{1}{4}\sin^2(2\phi)) \tag{3.35}$$

$$P(|0011\rangle_C) = \frac{1}{4}\sin^2(2\phi)(1 - \frac{1}{4}\sin^2(2\theta)) \tag{3.36}$$

$$P(|1100\rangle_C) = \frac{1}{4}\sin^2(2\theta)(1 - \frac{1}{4}\sin^2(2\phi)) \tag{3.37}$$

$$P(|1111\rangle_C) = \frac{1}{16}\sin^2(2\theta)\sin^2(2\phi). \tag{3.38}$$

It is straightforward to see that there is no entanglement between qubits 1 and 2, and between qubits 3 and 4, since $P(|0101\rangle_C) = P(|0110\rangle_C) = P(|1001\rangle_C) = P(|1010\rangle_C) = 0$. However, as long as each pair is entangled, $P(1111)$ is non-zero; therefore even numbers of $|1\rangle_C$s greater than two do not necessarily evidence GHZ-like entanglement. n qubit GHZ-like states are n-entangled, evidenced by $P(|\ldots k \ldots k' \ldots\rangle_c) > 0$ for all $k \in S$ and $k' \in S$ where $k \neq k'$ and $S = \{1, 2, ..., n\}$.

A final class to consider are line cluster states, as they demonstrate that $\mathcal{C}_{|\psi\rangle} = \frac{1}{2}$ is not a global maximum. If $|\psi\rangle = |\mathrm{L}_n\rangle$ from Equation (2.43) then

$$\mathcal{C}_{|\psi\rangle} = 1 - \frac{1}{2^n}\mathrm{Fib}_{n+2} \tag{3.39}$$

where Fib is the Fibonarchi series, calculated by Jacob Beckey [27]. This suggests that unity is the upper bound of CE. For $n > 3$ the CE of n-qubit line cluster states is greater than that of n-qubit GHZ states. We currently do not have intuition on why the CE of line states is so much greater and leave this to further work.

The next investigation is the robustness of pure state CE to variations in the inputs states. I first look at maximally entangled states with their amplitudes offset. Consider a GHZ-like state with the variable δ to parameterise its amplitudes: $|\psi(\delta)\rangle = \sin\left(\frac{\pi}{4} + \delta\right)|0\rangle^n + \cos\left(\frac{\pi}{4} + \delta\right)|1\rangle^n$, therefore $|\psi(\delta = 0)\rangle$ is a true n-qubit GHZ state and $|\psi(\delta = \frac{\pi}{4})\rangle$ is a product state. This state's fidelity with a true GHZ state is

$F = |\langle\psi(\delta=0)|\,|\psi(\delta)\rangle|^2 = \cos^2\delta$. The CE of $|\psi(\delta)\rangle$ is

$$\mathcal{C}_{|\psi(\delta)\rangle} = \left(\frac{1}{2} - \frac{1}{2^n}\right)\cos^2(2\delta) \tag{3.40}$$

$$= \frac{1}{2} - \frac{1}{2^n} - 4\left(\frac{1}{2} - \frac{1}{2^n}\right)F(1-F) \tag{3.41}$$

This is simply a reparameterisation of Equation (3.29) and Figure 3.2. Denote the effect of δ on the CE as $\Delta = \mathcal{C}_{|\psi(\delta)\rangle} - \mathcal{C}_{|\psi(\delta=0)\rangle}$. Let δ be small such that the small angle approximation is valid. In this case, $\Delta = (\frac{4}{2^n} - 2)\delta^2$.

Similarly for the W case, let

$$|\psi(\delta)\rangle = \sqrt{\frac{1}{n}}\cos\delta\,|00...01\rangle + \sqrt{\frac{1}{n-1} - \frac{1}{n(n-1)}\cos^2\delta}\sum_{j=2}^{n}|0...1_j...0\rangle \tag{3.42}$$

such that $|\psi(\delta=0)\rangle$ is a true n-qubit W state and $|\psi(\delta=\frac{\pi}{2})\rangle$ is a true $(n-1)$-qubit W state. Therefore

$$\mathcal{C}_{|\psi(\delta)\rangle} = \frac{1}{2} - \frac{1}{2n} - \frac{1}{2n^2(n-1)}\sin^2\delta\,(4(n-1) + (n-2)\sin^2\delta) \tag{3.43}$$

in Figure 3.4. When δ is small, $F = |\langle\psi(\delta=0)|\,|\psi(\delta)\rangle|^2 = 1 - \delta^2/n$, and therefore $\Delta = \frac{2}{n^2}\delta^2 = \frac{2}{n}(1-F)$. Like the GHZ case, an amplitude offset gives a second order error, meaning that a small error in the input state gives an even smaller error in the CE.

A second error to consider is an additional non-zero amplitude. Let $|\psi(\delta)\rangle = \cos\delta\,|\mathrm{GHZ}_n\rangle + \sin\delta\,|0...1\rangle$ with fidelity $F = |\langle\psi(\delta=0)|\,|\psi(\delta)\rangle|^2 = \cos^2\delta$:

$$\mathcal{C}_{|\psi(\delta)\rangle} = \frac{1}{2} - \frac{1}{2^n} - \sin^2\delta\,\left(\frac{2}{2^n} + \left(\frac{1}{2} - \frac{3}{2^n}\right)\sin^2\delta\right) \tag{3.44}$$

$$= \frac{1}{2} - \frac{1}{2^n} - (1-F)\,\left(\frac{1}{2} - \frac{1}{2^n} - \left(\frac{1}{2} - \frac{3}{2^n}\right)F\right) \tag{3.45}$$

shown in Figure 3.5. For small δ, $\Delta = -\frac{2}{2^n}\delta^2$. Similarly if $|\psi\rangle = \cos\delta\,|\mathrm{W}_n\rangle + \sin\delta\,|0\rangle^n$, $F = |\langle\psi(\delta=0)|\,|\psi(\delta)\rangle|^2 = n\cos^2\delta$, and

$$\mathcal{C}_{|\psi(\delta)\rangle} = \frac{1}{2} - \frac{1}{2n} - \frac{n-1}{2n}\sin^2\delta\,(2 - \sin^2\delta) \tag{3.46}$$

$$= \frac{1}{2} - \frac{1}{2n} - \frac{n-1}{2n}\left(1 - \frac{F^2}{n^2}\right) \tag{3.47}$$

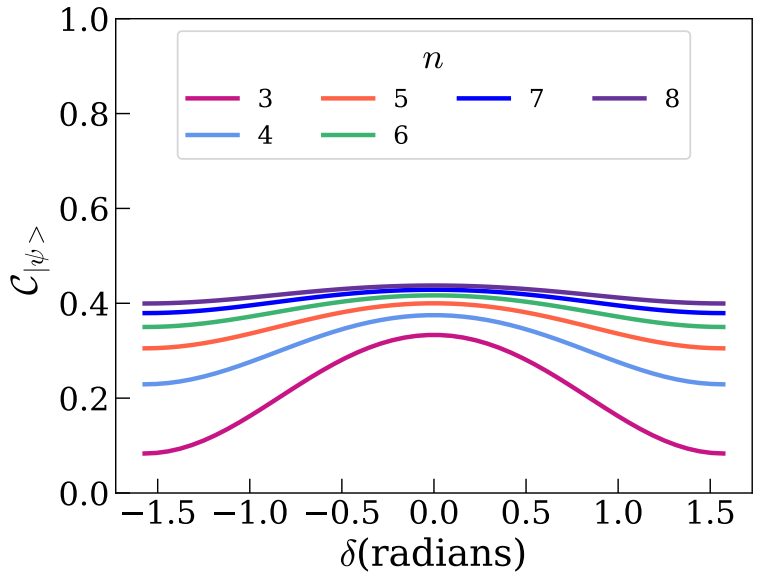

Figure 3.4: The CE of a W-like state equation (3.42) for various numbers of qubits n. δ denotes difference from a true W state such that fidelity $F \approx 1 - \delta^2/n$.

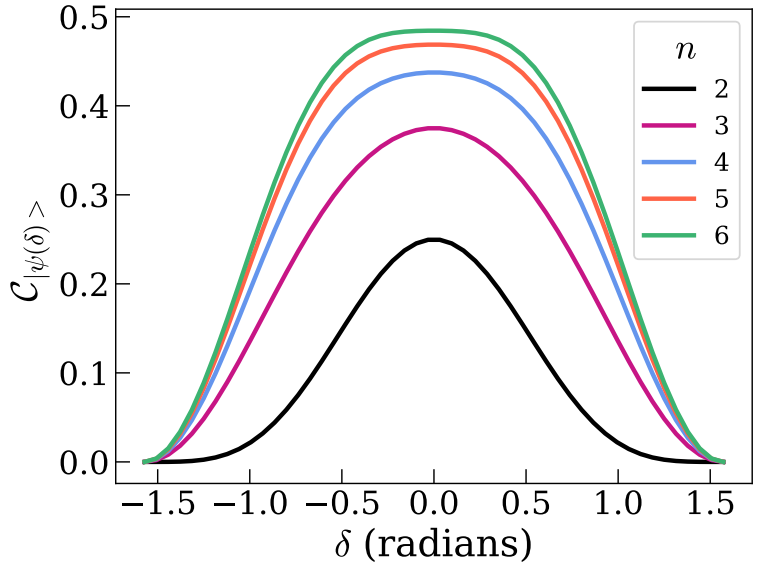

Figure 3.5: The CE of a GHZ state with error proportional to δ such that $|\psi(\delta)\rangle = \cos\delta\,|\mathrm{GHZ}_n\rangle + \sin\delta\,|0...1\rangle$ for various number of qubits n.

shown in Figure 3.6. For small δ, $\Delta = (1 - \frac{1}{n})\delta^2$. The W state case has a much sharper peak and a quicker drop-off than the GHZ state case, suggesting that the GHZ state case is more robust to this kind of error.

The continuation of the second order error for amplitude errors in both GHZ and W

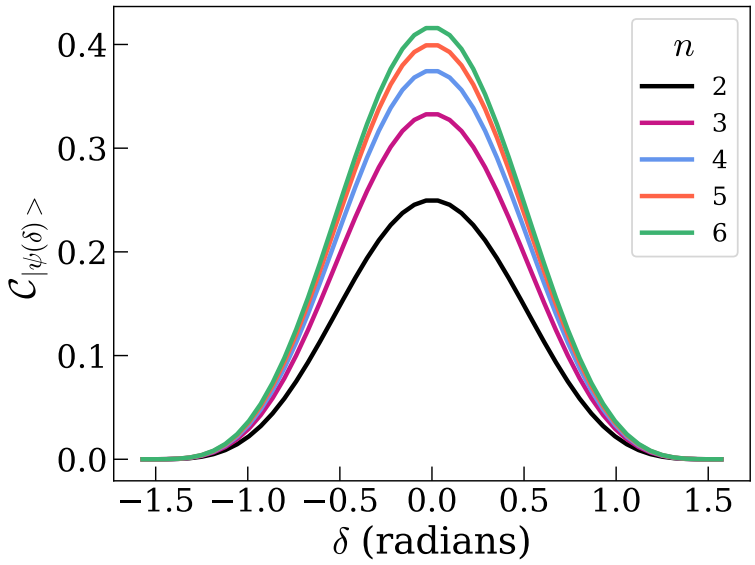

Figure 3.6: The CE of a W state with error proportional to δ such that $|\psi\rangle = \cos\delta\,|\mathrm{W}_n\rangle + \sin\delta\,|0\rangle^n$ for various number of qubits n.

states suggests that this is true for all input state amplitude errors. This suggest that errors, even ones present prior to gates being applied, are squared by the calculation of the CE. This can be seen as a positive of a negative: the relative error on the estimation of the CE will be reduced but any errors in the test state will be obscured.

3.2 Identical mixed states

Now that the pure state case has been characterised, I now move on to mixed states, starting with an identical ensemble such that $\rho = \rho'$.

Total concentratable entanglement (CE) as defined in [25] is

$$\mathcal{C} = 1 - \frac{1}{2^n} \sum_{\alpha \in \mathcal{P}(S)} \mathrm{tr}\left[\rho_\alpha^2\right] \tag{3.48}$$

$$= 1 - P(|0\rangle_C^n) \tag{3.49}$$

which in the case of a mixed ρ equals

$$\mathcal{C} = P(\text{even no. of } |1\rangle_C \text{ s}) + P(\text{odd no. of } |1\rangle_C \text{ s}). \tag{3.50}$$

To investigate how this value behaves when the input state is mixed, consider the 2-qubit Werner state $\rho = \rho' = (1-p)\left|\psi_2\right\rangle\left\langle\psi_2\right| + p\frac{I_4}{4}$ where $\left|\psi_2\right\rangle = \alpha\left|00\right\rangle + \beta\left|11\right\rangle$. Therefore ρ has purity $\gamma = 1 - \frac{3}{4}p(2-p)$ and the resulting probabilities from the c-SWAP test I have calculated are

$$P(\left|00\right\rangle_C) = 1 - \alpha^2\beta^2 - \left(\frac{7}{16} - \alpha^2\beta^2\right)p(2-p) \tag{3.51}$$

$$= \frac{1}{3}\left(\frac{5}{4} + \alpha^2\beta^2\right) + \frac{4}{3}\left(\frac{7}{16} - \alpha^2\beta^2\right)\gamma \tag{3.52}$$

$$P(\left|01\right\rangle_C) = P(\left|01\right\rangle_C) = \frac{3}{16}p(2-p) \tag{3.53}$$

$$= \frac{1}{4}(1-\gamma) \tag{3.54}$$

$$P(\left|11\right\rangle_C) = \alpha^2\beta^2 - \left(\alpha^2\beta^2 - \frac{1}{16}\right)p(2-p) \tag{3.55}$$

$$= \frac{1}{3}\left(\frac{1}{4} - \alpha^2\beta^2\right) + \frac{4}{3}\left(\alpha^2\beta^2 - \frac{1}{16}\right)\gamma. \tag{3.56}$$

It can be seen therefore that as p increases and the purity of ρ decreases, $P(\left|\text{even no. of s}\right\rangle_C)$ increases, and that a non-zero $P(\left|\text{even no. of 1s}\right\rangle_C)$ evidences non-unity purity. Further, as p increases/γ decreases, $P(\left|00\right\rangle_C)$ decreases, and so it follows that $1 - P(\left|00\right\rangle_C)$ increases. However, an ideal entanglement measure would correlate with the level of useful entanglement associated with ρ, and so we would expect said measure to *decrease* with decreased purity. Note that $P(\text{even no. of } \left|1\right\rangle_C \text{ s})$ itself fulfills this requirement.

We obtain a lower bound on concentratable entanglement for mixed states by combining the mixed state extension for the 2-qubit concurrence in Equation 2.38 with the fact that the pure state CE can be written as a sum over all pairs in S:

$$\mathcal{C}_{\left|\psi\right\rangle} = \frac{1}{2^{n+1}}\sum_{\alpha} c_\alpha^2(\left|\psi\right\rangle) \tag{3.57}$$

which gives

$$\mathcal{C}_\rho^l = \frac{1}{2^n} + \left(1 - \frac{1}{2^n}\right)\text{tr}\left[\rho^2\right] - \frac{1}{2^n}\sum_{\alpha\in\mathcal{P}(S)}\text{tr}\left[\rho_\alpha^2\right] \tag{3.58}$$

which I have calculated to equal

$$\mathcal{C}_\rho^l = P(\text{even no. of } \left|1\right\rangle_C \text{ s}) - \left(1 - \frac{2}{2^n}\right)P(\text{odd no. of } \left|1\right\rangle_C \text{ s}). \tag{3.59}$$

I will now explore this value, the original CE value $1 - P(|0\rangle_C^n)$, and the even and odd probabilties to attempt to construct bounds for the mixed state case.

An n-qubit maximally mixed state $\rho = \rho' = \frac{I_{2^n}}{2^n}$ gives results

$$P(|\text{odd no. of 1s}\rangle_C) = \frac{1}{2} - \frac{1}{2^{n+1}} \tag{3.60}$$

$$P(|\text{even no. of 1s}\rangle_C) = \frac{4^n + 2^n - 2 \cdot 3^n}{2^{2n+1}} \tag{3.61}$$

$$1 - P(|0\rangle_C^n) = 1 - \frac{3^n}{2^{2n}} \tag{3.62}$$

$$\mathcal{C}_\rho^l = -\frac{1 - 2^{n+1} + 3^n}{2^{2n}}. \tag{3.63}$$

shown in Figure 3.7. A negative CE we take to be zero. We would expect an entanglement measure to give zero for a maximally mixed state; zero is bounded by $P(|\text{even no. of 1s}\rangle_C)$ and $\mathcal{C}_\rho^l$.

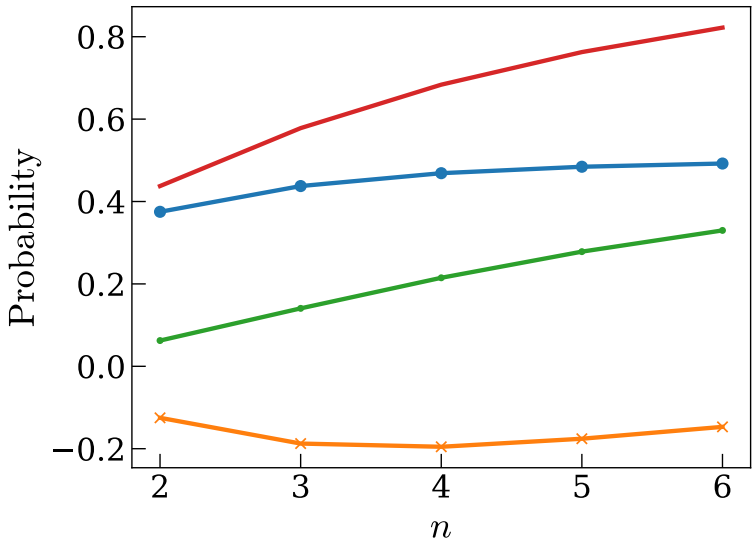

Figure 3.7: Probability results for a maximally mixed state of n qubits. The red line is $1 - P(|0\rangle_C^n)$, the blue circles are $P(|\text{odd no. of 1s}\rangle_C)$, the green dots represent $P(|\text{even no. of 1s}\rangle_C)$, and the yellow crosses are $\mathcal{C}_\rho^l$.

The relevant expressions (with regards to entanglement) for the above state $\rho = \rho' =$

$(1-p)\left|\psi_2\right\rangle\left\langle\psi_2\right| + p\frac{I_4}{4}$, $\left|\psi_2\right\rangle = \alpha\left|00\right\rangle + \beta\left|11\right\rangle$, therefore are

$$1 - P(|00\rangle_C) = \alpha^2\beta^2 + \frac{1}{16}\left(7 - \alpha^2\beta^2\right)p(2-p) \tag{3.64}$$

$$P(|11\rangle_C) = \alpha^2\beta^2 - \left(\alpha^2\beta^2 - \frac{1}{16}\right)p(2-p) \tag{3.65}$$

$$\mathcal{C}^l_\rho = \alpha^2\beta^2 - \left(\alpha^2\beta^2 + \frac{1}{8}\right)p(2-p) \tag{3.66}$$

$$\mathcal{C}_{|\psi_2\rangle} = \alpha^2\beta^2 \tag{3.67}$$

shown in Figure 3.8. The last expression would be an obvious candidate for an upper bound for $\mathcal{C}_\rho$ but, at least for all examples found in this thesis and related papers, is not calculable from c-SWAP test results.

We now have a conundrum: $P(|\text{even no. of 1s}\rangle_C)$ feels like a good candidate for the upper bound of $(c)_\rho$ since it is > 0 for a maximally mixed state. However, for $P(|\text{even no. of 1s}\rangle_C)(p) \leq P(|\text{even no. of 1s}\rangle_C)(p=0)$, where the right hand side is a natural upper bound. We cannot know for certain whether $P(|\text{even no. of 1s}\rangle_C)(p)$ is a faithful entanglement measure for mixed states.

However, the value $1 - P(|0\rangle^n_C)(p) \geq 1 - P(|0\rangle^n_C)(p=0)$ for all p, and therefore we can be assured that this is strict upper bound, even though it is not a very tight one. Therefore let

$$\mathcal{C}^u_\rho = P(\text{even no. of } |1\rangle_C \text{ s}) + P(\text{odd no. of } |1\rangle_C \text{ s}) \tag{3.68}$$

$$\mathcal{C}^l_\rho = P(\text{even no. of } |1\rangle_C \text{ s}) - \left(1 - \frac{2}{2^n}\right)P(\text{odd no. of } |1\rangle_C \text{ s}) \tag{3.69}$$

with $P(\text{even no. of } |1\rangle_C \text{ s})$ as a good estimator for ρ, which may be useful for states that result in a large range $\mathcal{C}^u_\rho - \mathcal{C}^l_\rho$.

Now I investigate these values for various n-qubit mixed states.

Let $\rho = \rho' = (1-p)\left|\psi_n\right\rangle\left\langle\psi_n\right| + p\frac{I_N}{N}$ where $\left|\psi_n\right\rangle = \alpha\left|0\right\rangle^n + \beta\left|1\right\rangle^n$ is a GHZ-like state.

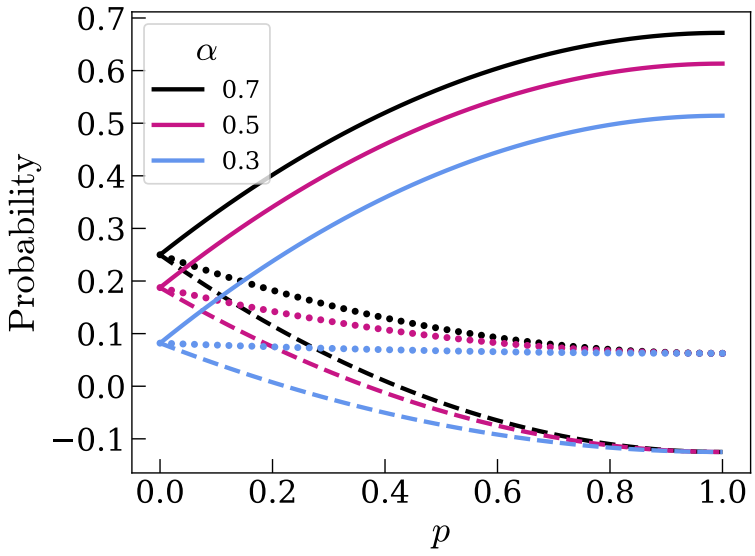

Figure 3.8: Probability results for input state $\rho = \rho' = (1-p)\left|\psi_2\right\rangle\left\langle\psi_2\right| + p\frac{I_4}{4}$ where $\left|\psi_2\right\rangle = \alpha\left|00\right\rangle + \beta\left|11\right\rangle$. Unbroken lines represent $1 - P(\left|0\right\rangle_C^n)$, dotted lines $P(\text{even } \left|1\right\rangle_C \text{s})$, and dashed lines $\mathcal{C}_\rho^l$.

The purity of ρ is $\gamma = 1 - \frac{2^n-1}{2^n}p(2-p)$. This state results in

$$P(\text{odd no. } \left|1\right\rangle_C \text{s}) = \frac{2^n-1}{2^{n+1}}p(2-p) \tag{3.70}$$

$$P(\text{even no. } \left|1\right\rangle_C \text{s}) = \frac{2(2^n-2)}{2^n}\left[\alpha^2\beta^2 - \left(\alpha^2\beta^2 - \frac{4^n+2^n-2\cdot 3^n}{2^{n+2}(2^n-2)}\right)p(2-p)\right] \tag{3.71}$$

$$\mathcal{C}_\rho^u = \frac{2(2^n-2)}{2^n}\left[\alpha^2\beta^2 + \left(\frac{16^n-2\cdot 3^n}{2^{n+2}(2^n-2)} - \alpha^2\beta^2\right)p(2-p)\right] \tag{3.72}$$

$$\mathcal{C}_\rho^l = \frac{2(2^n-2)}{2^n}\left[\alpha^2\beta^2 - \left(\frac{2^n(2\cdot 3^n+4-5\cdot 2^n)}{2(2^n-2)(2^n-1)} + \alpha^2\beta^2\right)p(2-p)\right] \tag{3.73}$$

shown in Figure 3.9 for $\alpha = \frac{1}{\sqrt{2}}$. Similarly construct a mixed W state $\rho = \rho' = (1-p)\left|W_n\right\rangle\left\langle W_n\right| + p\frac{I_N}{N}$, where $\left|W_n\right\rangle = \sum_{k=1}^n \left|0...1_k...0\right\rangle$. Therefore the purity of ρ is $\gamma = 1 - \frac{2^n-1}{2^n}p(2-p)$, giving:

$$P(\text{odd no. } \left|1\right\rangle_C \text{s}) = \frac{2^n-1}{2^{n+1}}p(2-p) \tag{3.74}$$

$$P(\text{even no. } \left|1\right\rangle_C \text{s}) = \frac{1}{2} - \frac{1}{2n} - \left(\frac{2^n-1}{2^{n+1}} - \frac{1}{2} - \frac{1}{2n} + \left(\frac{3}{4}\right)^n\right)p(2-p) \tag{3.75}$$

$$\mathcal{C}_\rho^u = \frac{1}{2} - \frac{1}{2n} + \left(\frac{1}{2} + \frac{1}{2n} - \left(\frac{3}{4}\right)^n\right)p(2-p) \tag{3.76}$$

$$\mathcal{C}_\rho^l = \frac{1}{2} - \frac{1}{2n} - \left(\frac{(2^n-1)^2}{2^{2n}} - \frac{1}{2} - \frac{1}{2n} + \left(\frac{3}{4}\right)^n\right)p(2-p) \tag{3.77}$$

shown in Figure 3.10. Although for $p \approx 0$, $\mathcal{C}_{\rho_W} < \mathcal{C}_{\rho_{GHZ}}$, for large p the two are practically identical.

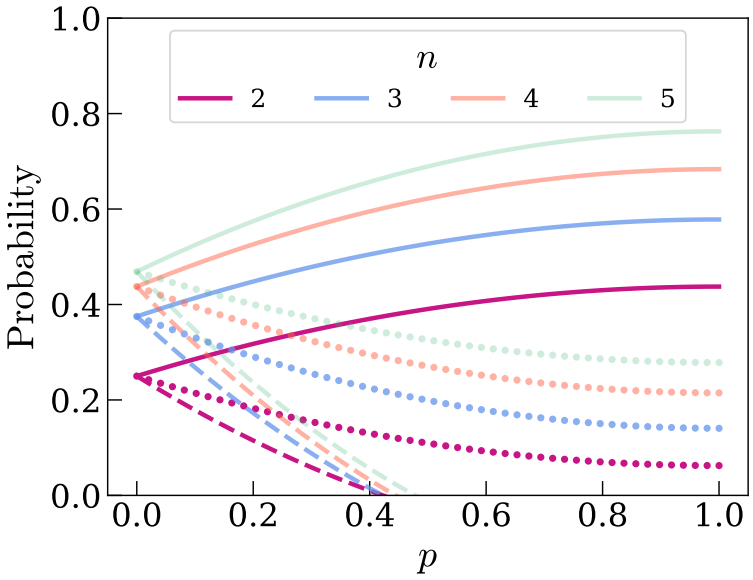

Figure 3.9: Probability results for input state $\rho = \rho' = (1-p)\left|\psi_n\right\rangle\left\langle\psi_n\right| + p\frac{I_N}{N}$ where $\left|\psi_n\right\rangle = \frac{1}{\sqrt{2}}(\left|0\right\rangle^n + \left|1\right\rangle^n)$. Unbroken lines represent $1 - P(\left|0\right\rangle_C^n)$, dotted lines $P(\text{even } \left|1\right\rangle_C \text{s})$, and dashed lines $\mathcal{C}_\rho^l$.

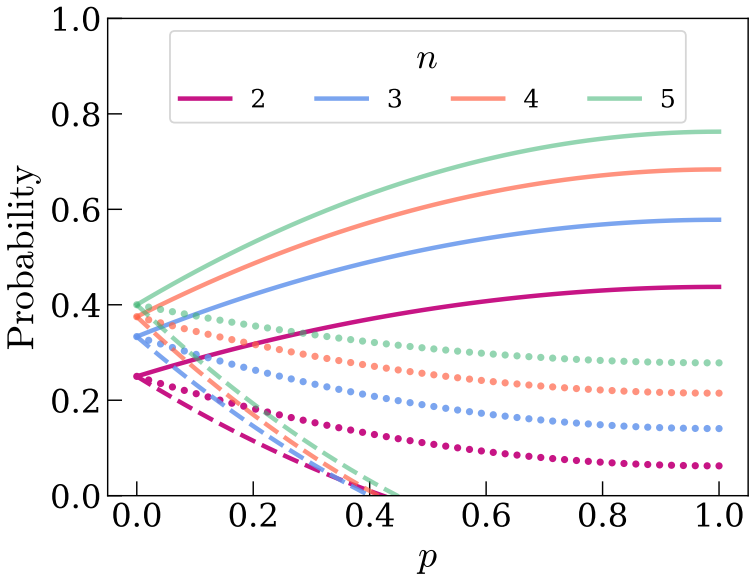

Figure 3.10: Probability results for input state $\rho = \rho' = (1-p)\left|W_n\right\rangle\left\langle W_n\right| + p\frac{I_N}{N}$, where $\left|W_n\right\rangle = \sum_{k=1}^{n}\left|0...1_k...0\right\rangle$. Unbroken lines represent $1 - P(\left|0\right\rangle_C^n)$, dotted lines $P(\text{even } \left|1\right\rangle_C \text{s})$, and dashed lines $\mathcal{C}_\rho^l$.

As with the errors/variations explored in Chapter 3, all examples have second order

error: any p gives $p^2 - 2p$ scaled error/effect in the results. Further, mixedness is evidenced with non-zero $P(\text{odd no. } |1\rangle_C \text{ s})$ which also scales quadratically with p. For all the Werner states described above, purity $\gamma = 1 - \frac{2^n-1}{2^n}p(2-p)$ and $P(\text{odd no. } |1\rangle_C \text{ s}) = \frac{2^n-1}{2^{n+1}}p(2-p) = \frac{1}{2}(1-\gamma)$. For all input states $\rho' = \rho$ in fact, $P(\text{odd no. } |1\rangle_C \text{ s}) = \frac{1}{2}(1-\gamma)$.

In conclusion, we have defined upper and lower bounds of CE for the identical mixed state case. However, these bounds, although strict, are not tight and for low purities have a large range. However, the value $P((\text{even no. of } |1\rangle_C \text{ s})$ behaves as expected for a entanglement measure and so can be regarded as a rough estimate of the CE.

3.3 Non-identical pure states

Now we consider the case where the twin input states ρ and ρ' are not identical. This is expected in an ensemble which we denote $\rho^M = \{\rho^{(m)} : m \in 1, 2, \ldots, M\}$. I model this with M copies of state ρ and M copies of states ρ' such that each round of the experiment has one input ρ and its twin input ρ', i.e. $\rho^M_{model} = \{\rho, \rho'\}^M$. This therefore models an ensemble with variations around ρ and ρ' – let $U(\rho^{(k)}) = U(\rho) + \delta_k$, therefore $\frac{1}{M}\sum_{k=1}^{M} U(\rho^{(k)}) \approx U(\rho)$ if $\frac{1}{M}\sum_{k=1}^{M} \delta_k \approx 0$.

First we stick to pure states, therefore for this section let $\rho = |\psi\rangle\langle\psi|$ and $\rho' = |\phi\rangle\langle\phi|$.

If $|\psi\rangle = |\text{GHZ}_n\rangle$ and

$$|\phi\rangle = \sin\left(\frac{\pi}{4} + \delta\right)|0\rangle^n + \cos\left(\frac{\pi}{4} + \delta\right)|1\rangle^n, \tag{3.78}$$

then the fidelity of the two is $F = |\langle\psi|\phi\rangle|^2 = \cos^2\delta$. The c-SWAP test probability results are then

$$P(|\text{odd no. of 1s}\rangle_C) = \frac{1}{2}(1 - F), \tag{3.79}$$

$$P(|\text{even no. of 1s}\rangle_C) = \frac{1}{2} - \frac{1}{2^n} - \left(\frac{1}{2} - \frac{1}{2^n}\right)(1 - F). \tag{3.80}$$

Despite the input state being pure, if the fidelity is non-unity then $P(|\text{odd no. of 1s}\rangle_C)$ is non-zero. Therefore a measurement of $|\text{odd no. of 1s}\rangle_C$ evidences *either* a mixed input state and/or non-identical states in the ensemble.

Therefore, I define the CE upper and lower bounds as:

$$\mathcal{C}^u_{|\psi\rangle,|\phi\rangle} = P(\text{even no. of } |1\rangle_C \text{ s}) + P(\text{odd no. of } |1\rangle_C \text{ s}) \tag{3.81}$$

$$\mathcal{C}^l_{|\psi\rangle,|\phi\rangle} = P(\text{even no. of } |1\rangle_C \text{ s}) - \left(1 - \frac{2}{2^n}\right) P(\text{odd no. of } |1\rangle_C \text{ s}) \tag{3.82}$$

from the definitions in section 3.2. These are the (calculable) upper and lower bounds for the identical mixed state case and therefore are not rigorously derived bounds for the non-identical case. However, these expressions only require measurable probabilities from the CE test and so we will investigate their relevance to the non-identical case. The following are my own results.

If the two input states are different GHZ-like state such that

$$|\psi\rangle = \sin\left(\frac{\pi}{4} + \theta\right)|0\rangle^n + \cos\left(\frac{\pi}{4} + \theta\right)|1\rangle^n \tag{3.83}$$

$$\text{and} \quad |\phi\rangle = \sin\left(\frac{\pi}{4} + \theta + \delta\right)|0\rangle^n + \cos\left(\frac{\pi}{4} + \theta + \delta\right)|1\rangle^n \tag{3.84}$$

then $F = \cos^2\delta$ and

$$P(|\text{odd no. of 1s}\rangle_C) = \frac{1}{2}\sin^2(\delta), \tag{3.85}$$

$$= \frac{1}{2}(1 - F) \tag{3.86}$$

$$P(|\text{even no. of 1s}\rangle_C) = \frac{1}{2} - \frac{1}{2^n} - \left(\frac{1}{2} + \frac{1}{2^n}\right)\sin^2(2\theta + \delta), \tag{3.87}$$

$$= \frac{1}{2} - \frac{1}{2^n} - \left(\frac{1}{2} + \frac{1}{2^n}\right)\left(\sqrt{F}\sin(2\theta) + \sqrt{1-F}\cos(2\theta)\right)^2, \tag{3.88}$$

$$\mathcal{C}^u_{|\psi\rangle,|\phi\rangle} = \frac{1}{2} - \frac{1}{2^n} - \left(\frac{1}{2} + \frac{1}{2^n}\right)\sin^2(2\theta + \delta) + \frac{1}{2}\sin^2\delta, \tag{3.89}$$

$$\mathcal{C}^l_{|\psi\rangle,|\phi\rangle} = \frac{1}{2} - \frac{1}{2^n} - \left(\frac{1}{2} + \frac{1}{2^n}\right)\sin^2(2\theta + \delta) - \left(\frac{1}{2} - \frac{1}{2^n}\right)\sin^2\delta. \tag{3.90}$$

Shown in Figure 3.11. For small δ, $\Delta_{odd} = \frac{1}{2}\delta^2$, $\Delta_{even} = (\frac{1}{2} - \frac{1}{2^n})\delta^2$. Similarly for W states, if $|\psi\rangle = |\mathrm{W}_n\rangle = \frac{1}{\sqrt{n}}\sum|0...1_k...0\rangle$ and

$$|\phi\rangle = \sqrt{\frac{1}{n}}\cos\delta\,|00...01\rangle + \sqrt{\frac{1}{n-1} - \frac{1}{n(n-1)}\cos^2\delta}\sum_{j=2}^{n}|0...1_j...0\rangle \tag{3.91}$$

then $F = \frac{1}{n^2}\left(\cos\delta + \sqrt{n-1}\sqrt{n-\cos^2\delta}\right)^2$ and

$$P(|\text{exactly one 1s}\rangle_C) = \frac{1}{2}(1-F) \tag{3.92}$$

$$P(|\text{exactly two 1s}\rangle_C) = \frac{1}{2} - \frac{1}{2n} - \frac{1}{4}(1-F) \tag{3.93}$$

$$\mathcal{C}^u_{|\psi\rangle,|\phi\rangle} = \frac{1}{2} - \frac{1}{2n} + \frac{1}{4}(1-F) \tag{3.94}$$

$$\mathcal{C}^l_{|\psi\rangle,|\phi\rangle} = \frac{1}{2} - \frac{1}{2n} - \left(\frac{3}{4} - \frac{1}{2^n}\right)(1-F) \tag{3.95}$$

shown in Figure 3.12. For small δ, $1-F = \frac{1}{4(n-1)}\delta^4$.The coefficients of $1-F$ for $P(|\text{even no. of 1s}\rangle_C)$ and $\mathcal{C}^u_{|\psi\rangle,|\phi\rangle}$ are n-independent, which is not true of the GHZ-like case. Therefore GHZ-like states are more robust to this kind of error than W-like states.

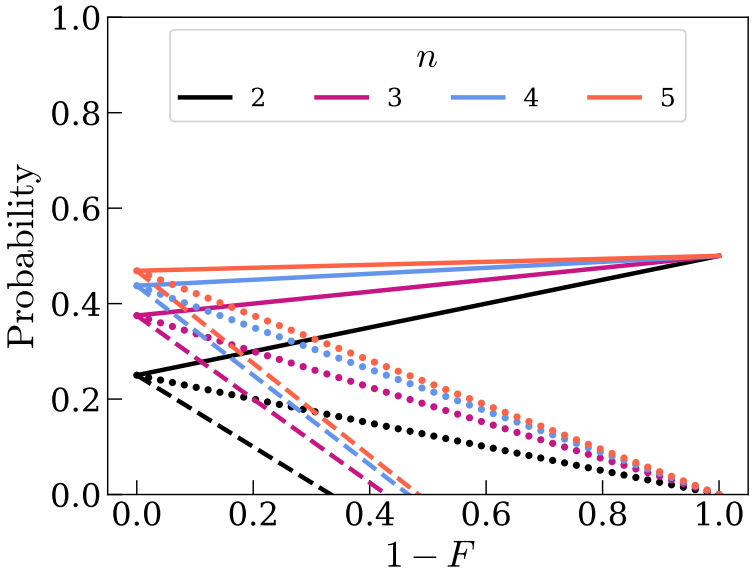

Figure 3.11: Probability results for two different GHZ-like input state in terms of fidelity F. The continuous line is $\mathcal{C}^u_\rho = 1 - P(|0\rangle_C^{\otimes n})$, the dotted line $P(\text{even } |1\rangle_C \text{ s})$, and the dashed line $\mathcal{C}^l_\rho$.

The c-SWAP test results in terms of fidelity when purity is one is of the same form in terms of purity when fidelity is one, with $P(\text{odd no. } |1\rangle_C \text{ s}) = \frac{1}{2}(1-F)$ and $P(\text{odd no. } |1\rangle_C \text{ s}) = \frac{1}{2}(1-\gamma)$ respectively. In the next section, I look at how mixedness and non-unity fidelity combine.

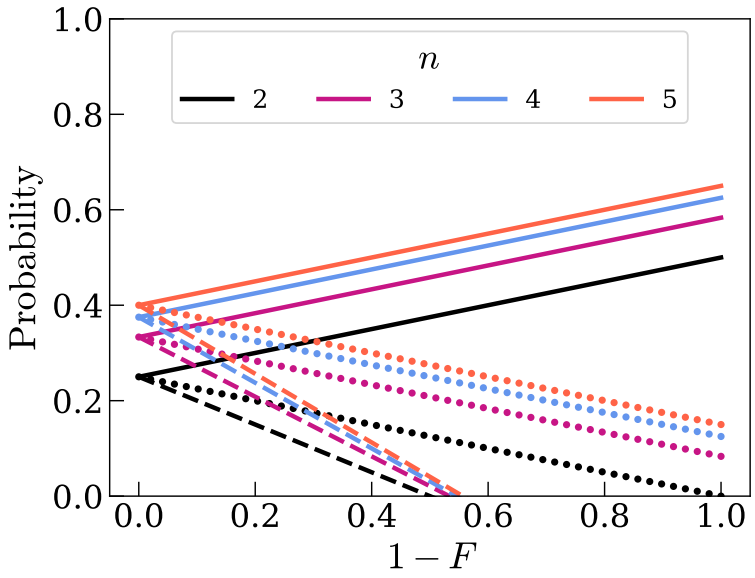

Figure 3.12: Probability results for two different W-like input state in terms of fidelity F. The continuous line is $\mathcal{C}^u_\rho = 1 - P(|0\rangle_C^{\otimes n})$, the dotted line $P(\text{even } |1\rangle_C \text{ s})$, and the dashed line $\mathcal{C}^l_\rho$.

3.4 Non-identical mixed states

We combine the previous two sections to now consider non-identical mixed states, the experimental reality undoubtedly. We assume the twin input states are similar, and model this with commuting density matrices.

Let the two input states be two different mixed GHZ-like states such that $\rho = (1-p)\,|GHZ_n\rangle\langle GHZ_n| + p\frac{I_{2^n}}{2^n}$ and $\rho' = (1-q)\,|GHZ_n\rangle\langle GHZ_n| + q\frac{I_{2^n}}{2^n}$. Using the definitions in Section 3.2, these states give results:

$$P(\text{odd no. } |1\rangle_C \text{ s}) = \frac{2^n - 1}{2^{n+1}}(p + q - pq) \tag{3.96}$$

$$P(\text{even no. } |1\rangle_C \text{ s}) = \frac{1}{2} - \frac{1}{2^n} - \left[\left(\frac{3}{4}\right)^n - \frac{3}{2^{n+1}}\right](p + q - pq) \tag{3.97}$$

$$\mathcal{C}^u_{\rho,\rho'} = \frac{1}{2} - \frac{1}{2^n} + \left[\frac{1}{2} + \frac{1}{2^n} - \left(\frac{3}{4}\right)^n\right](p + q - pq) \tag{3.98}$$

$$\mathcal{C}^l_{\rho,\rho'} = \frac{1}{2} - \frac{1}{2^n} - \left[\frac{1}{2} + \frac{1}{4^n} - \frac{3}{2^n} + \left(\frac{3}{4}\right)^n\right](p + q - pq) \tag{3.99}$$

where the purity of ρ is $\gamma = 1 - \frac{2^n-1}{2^n}p(2-p)$ and the purity of ρ' is $\gamma' = 1 - \frac{2^n-1}{2^n}q(2-q)$,

and the fidelity of the two is $F = [\mathrm{tr}\sqrt{\rho\rho'}]^2 = (\sqrt{1-p}\sqrt{1-q} + \sqrt{pq})^2$. The $n = 2$ case is shown in Figure 3.13. As expected, the range $\mathcal{C}^u_{\rho,\rho'} - \mathcal{C}^l_{\rho,\rho'}$ increases with p, q, *and* $|p - q|$.

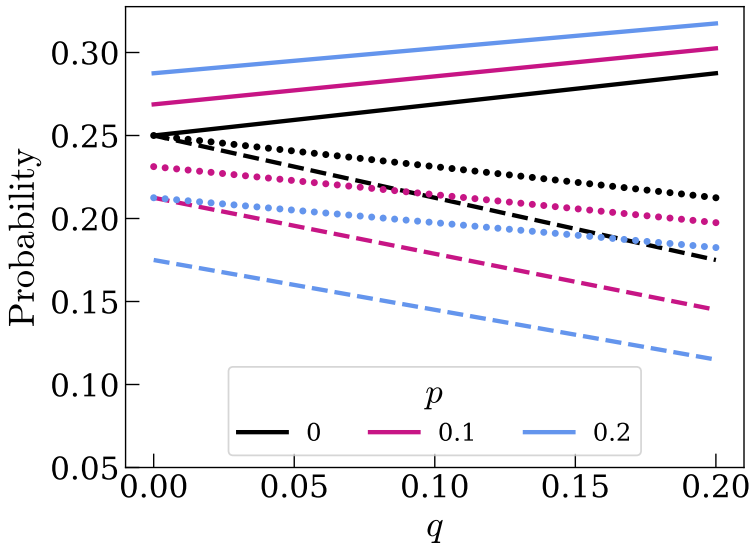

Figure 3.13: Probability results for two different GHZ-like mixed input states in terms of Werner parameters p and q respectively. The continuous line is $\mathcal{C}^u_\rho = \mathcal{C}_\rho = 1 - P(|0\rangle_C^{\otimes n})$, the dotted line $P(\text{even } |1\rangle_C \text{ s})$, and the dashed line $\mathcal{C}^l_\rho$.

In terms of purities, the p- and q-dependant expression is

$$p + q - pq \equiv \frac{1}{2}[p(2-q) + q(2-p)] \tag{3.100}$$

$$= \frac{2^n}{2^n - 1}\left(1 - \frac{1}{2}(\gamma + \gamma')\right) - \frac{1}{2}(p-q)^2 \tag{3.101}$$

i.e. the mean of the two purities minus some ideally small value. Therefore

$$P(\text{odd no. } |1\rangle_C \text{ s}) = \frac{1}{2}\left(1 - \frac{1}{2}(\gamma + \gamma')\right) - \frac{1}{4}\frac{2^n - 1}{2^n}(p-q)^2 \tag{3.102}$$

which is reminiscent of the identical mixed state case $P(\text{odd no. } |1\rangle_C \text{ s}) = \frac{1}{2}(1-\gamma)$. Let us assume that p and q are close, such that $\delta = |p - q|$. Therefore $p + q - pq = p(2-p) \mp (1-p)\delta$ and

$$P(\text{odd no. } |1\rangle_C \text{ s}) = \frac{1}{2}(1-\gamma) \mp \frac{1}{2}\frac{2^n - 1}{2^n}(1-p)\delta. \tag{3.103}$$

Let us then define an estimated value of the purity of the input state as

$$\gamma_{\text{estimated}} = 1 - 2P(\text{odd no. } |1\rangle_C \text{ s}) \tag{3.104}$$

which in the above case is

$$\gamma_{\text{estimated}} = \gamma \pm \frac{2^n - 1}{2^n}(1-p)\delta \tag{3.105}$$

$$= \gamma' \pm \frac{2^n - 1}{2^n}(1-q)\delta \tag{3.106}$$

overestimating/underestimating γ and γ' by a value proportional to $\delta = |p - q|$. I conjecture that this is true for W-like states as well due to the equivalence of equation (3.70) and equation (3.70).

In conclusion, mixed non-identical input states – the norm for experimental setups – are signified by non-zero $P(\text{odd no. } |1\rangle_C \text{ s})$. The purity of the input states can be estimated with $\gamma_{\text{estimated}} = 1 - 2P(\text{odd no. } |1\rangle_C \text{ s})$ which is $\epsilon \approx (1-p)|p-q|$ close to the actual purity γ. The more mixed and the less identical the input states the greater the range $\mathcal{C}^u_{\rho,\rho'} - \mathcal{C}^l_{\rho,\rho'}$, which is proportional to $X = \frac{2^n}{2^n-1}\left(1 - \frac{1}{2}(\gamma + \gamma')\right) - \frac{1}{2}(p - q)^2$. $P(\text{even no. } |1\rangle_C \text{ s})$ is a good estimate of $\mathcal{C}_{\rho,\rho'}$ as it decreases from the maximally entangled value proportional to X.

3.5 Sub-system concentratable entanglement

A further investigation of entanglement structure can be made with sub-system concentratable entanglement, defined in [25]. For any subset $s \in S$ where $S = \{1, 2, ..., n\}$ is the set of labels for each qubit in $|\psi\rangle$, the sub-system CE is

$$\mathcal{C}_{|\psi\rangle}(s) = 1 - \frac{1}{2^{|s|}} \sum_{\alpha \in \mathcal{P}(s)} \text{tr}\left[\rho_\alpha^2\right] \tag{3.107}$$

$$= 1 - P(|0\rangle \text{ on all in } s) \tag{3.108}$$

defined as 'the average of the entanglement between the subsets of qubits with labels in s and the rest of the system'. This can of course be calculated from a complete n-qubit control c-SWAP test applied to the full state or an $|s|$-qubit control c-SWAP test applied to just the qubits in s. Note that that when $|\psi\rangle = |\phi\rangle$, $1 - P(|0\rangle \text{ on all in } s) = P(|1\rangle_C \text{ on at least one in } s)$, and that the CE used in previous chapters is more specifically the total concentratable entanglement $\mathcal{C}_\rho(S)$. The following are my own results.

W-like input states, $|\mathrm{W}_n\rangle = \sum a_k |0...1_k...0\rangle$, have sub-system CEs:

$$\mathcal{C}_{|\mathrm{W}_n\rangle}(s) = \sum_{i\in s} a_i^2 \left(\sum_{(j>i)\in s} a_j^2 + \sum_{k\in S\setminus s} a_k^2 \right) \tag{3.109}$$

$$= \mathcal{C}_{|\mathrm{W}_{|s|}\rangle}(s) + \sum_{i\in s} \sum_{k\in S\setminus s} \mathcal{C}_{|\mathrm{W}_2\rangle}(\{i,k\}) \tag{3.110}$$

which is the total CE of the qubits in s on their own, plus the bipartite entanglement between each qubit in s and each qubit not in s.

Compare this with GHZ-like input states $|\mathrm{GHZ}_n\rangle = \alpha |0\rangle^n + \beta |1\rangle^n$. Any s with cardinality $|s| < n-1$ has CE

$$\mathcal{C}_{|\mathrm{GHZ}_n\rangle}(s) = \frac{2^{|s|+1}-1}{2^{|s|}} \alpha_0^2 \alpha_1^2 \tag{3.111}$$

$$= \mathcal{C}_{|\mathrm{GHZ}_{|s|}\rangle}(s) \tag{3.112}$$

and when $|s| = n-1$, $\mathcal{C}_{|\mathrm{GHZ}_n\rangle}(s) = \mathcal{C}_{|\mathrm{GHZ}_n\rangle}(S)$. Since GHZ states have equally distributed entanglement among each qubit, the CE is not dependant on which qubits are included in the set s. This also means that the CE of a subset with cardinality $|s| = m$ is equivalent to the total CE of an m-qubit GHZ-like state. Imagining again that GHZ-like entanglement is a single vertex of size n, an m sized cutout of an n sized circle is indistinguishable from an m sized circle.

If the qubit set being subject to the entanglement test is part of a larger entangled state, however, this will be reflected in the probabilities $P(\text{odd no. } |1\rangle_C \text{ s})$, since the sub-state will be mixed.

These GHZ-like and W-like states (in general) are n-entangled, as in all qubits are entangled with all other qubits. Consider instead a partially separable four-qubit state

$$|\psi\rangle = |\chi_4\rangle = (\cos\theta |00\rangle + \sin\theta |11\rangle)_{12} \otimes (\cos\phi |00\rangle + \sin\phi |11\rangle)_{34} . \tag{3.113}$$

with CEs

$$\mathcal{C}_{|\chi_4\rangle}(\{1,2\}) = \frac{1}{4}\sin^2(2\theta) \tag{3.114}$$

$$= \mathcal{C}_{|\chi_4\rangle}(\{1\}) = \mathcal{C}_{|\chi_4\rangle}(\{2\}) \tag{3.115}$$

$$\mathcal{C}_{|\chi_4\rangle}(\{3,4\}) = \frac{1}{4}\sin^2(2\phi) \tag{3.116}$$

$$= \mathcal{C}_{|\chi_4\rangle}(\{3\}) = \mathcal{C}_{|\chi_4\rangle}(\{4\}) \tag{3.117}$$

$$\mathcal{C}_{|\chi_4\rangle}(\text{all other } s) = \frac{1}{4}\left(\sin^2(2\theta) + \sin^2(2\phi) - \frac{1}{4}\sin^2(2\theta)\sin^2(2\phi)\right) \tag{3.118}$$

$$= \mathcal{C}_{|\chi_4\rangle}(\{1,2\}) + \mathcal{C}_{|\chi_4\rangle}(\{3,4\}) - \mathcal{C}_{|\chi_4\rangle}(\{1,2\})\mathcal{C}_{|\chi_4\rangle}(\{3,4\}). \tag{3.119}$$

Firstly, we have the result $\mathcal{C}_{|\psi\rangle}(S = s_1 \cup s_2) = \mathcal{C}_{|\psi\rangle}(s_1) + \mathcal{C}_{|\psi\rangle}(s_2) - \mathcal{C}_{|\psi\rangle}(s_1)\mathcal{C}_{|\psi\rangle}(s_2)$, exemplifying the sub-additivity of CE (see [25]). Secondly, it is not simple to see that this state is partially seperable, from these results, as $\mathcal{C}_{|\chi_4\rangle}(\{1,3\}) \neq 0$ etc. This is because while $P(|1010\rangle_C) = 0$, $P(|1111\rangle_C) \geq 0$. The individual probabilities, not the sub-system CE, must be used to construct the entanglement structure.

There is a second way to recover this information: let us instead consider a modified version of the c-SWAP test applied to grouped qubits within the input state. For example, let us apply a c-SWAP test with a two-qubit control state, such that the first control qubit controls the qubits in set s_1 and the second controls the qubits in s_2, where $s_1 \cup s_2 = S$.

Applying this version of the test to

$$|\psi\rangle = |\phi\rangle_{12} \otimes |\phi\rangle_{34} \tag{3.120}$$

$$= \left(\cos\left(\frac{\pi}{4} + \delta\right)|00\rangle + \sin\left(\frac{\pi}{4} + \delta\right)|11\rangle\right)_{12} \tag{3.121}$$

$$\otimes \left(\cos\left(\frac{\pi}{4} + \delta\right)|00\rangle + \sin\left(\frac{\pi}{4} + \delta\right)|11\rangle\right)_{34} \tag{3.122}$$

where the total CE of the bipartite system is $\mathcal{C}_{|\phi\rangle}(S) = \mathcal{C}_{|\phi\rangle} = \cos^2\theta\sin^2\theta$. The total CE of $|\psi\rangle$ is then $\mathcal{C}_{|\psi\rangle}(S) = 2\mathcal{C}_{|\phi\rangle} - \mathcal{C}^2_{|\phi\rangle}$. The subsystem CEs of all possible subsets s_1 and s_2 using both methods are shown in Table 3.1. As expected, the CE between the two different pairs is zero. The other results are explained by CE being subadditive. This

formalism more straightforwardly describes the entanglement structure of the input state.

s	$\mathcal{C}_{\lvert\psi\rangle}(s)$	$\mathcal{C}_{\lvert\psi\rangle}(s,\bar{s})$
$\{1\}$	$\mathcal{C}_{\lvert\phi\rangle}$	$\mathcal{C}_{\lvert\phi\rangle}$
$\{1,2\}$	$\mathcal{C}_{\lvert\phi\rangle}$	0
$\{1,3\}$	$2\mathcal{C}_{\lvert\phi\rangle} - \mathcal{C}^2_{\lvert\phi\rangle}$	$2\mathcal{C}_{\lvert\phi\rangle} - 2\mathcal{C}^2_{\lvert\phi\rangle}$

Table 3.1: CE across a bipartite cut $\mathcal{C}_{|\psi\rangle}(s,\bar{s})$ and sub-system CE $\mathcal{C}_{|\psi\rangle}(s)$ for $|\psi\rangle = |\phi\rangle_{12} \otimes |\phi\rangle_{34}$ where $\mathcal{C}_{|\phi\rangle} = \cos^2\theta \sin^2\theta$.

3.6 Summary

Let M rounds of the c-SWAP entanglement test as described in Section 2.6, with error-less operations, be applied to an ensemble of state ρ. If all three output qubits were to be measured, not just the control state, the resulting probabilities correlate with

$$P\left(|1\rangle_{C_k}\right) = P\left(\left|\Psi^-\right\rangle_{A_kB_k}\right) \tag{3.123}$$

$$P\left(|1\rangle_{C_j} \otimes |1\rangle_{C_k}\right) = P\left(\left|\Psi^-\right\rangle_{A_jB_j} \otimes \left|\Psi^-\right\rangle_{A_kB_k}\right). \tag{3.124}$$

If $|1\rangle_C$ is measured at the k-th qubit, this corresponds to a Bell state between ρ_k and ${\rho'}_k$ after the c-SWAP test. In essence, the entanglement within ρ and within ρ' is transformed into pairwise entanglement between ρ and ρ' by the c-SWAP test. However, as we will see in the next section, one $|1\rangle_C$ alone does not evidence entanglement in the initial ρ. Only even numbers of $|1\rangle_C$s, which corresponds to pairs of singlet Bell states between states A and B, evidence entanglement.

Labelling each qubit in ρ with $S = \{1, 2, ..., n\}$, the control state output probabilities are

$$P(\text{odd no. of } |1\rangle_C \text{ s}) \approx \frac{1}{2}\left(1 - \text{tr}\left[\rho^2\right]\right) \tag{3.125}$$

which for pure ρ equals zero, and

$$P(\text{non-zero even no. of } |1\rangle_C \text{ s}) \approx \frac{1}{2}\left(1 + \text{tr}\left[\rho^2\right]\right) - \frac{1}{2^n}\sum_{\alpha\in\mathcal{P}(S)} \text{tr}\left[\rho_\alpha^2\right] \tag{3.126}$$

where $\mathcal{P}(S)$ is the power set of S, $\rho_\alpha = \mathrm{Tr}_{S/\alpha}[\rho]$, and $\mathrm{tr}\left[\rho_\emptyset^2\right] = 1$. The approximates become equalities if all elements of the ensemble are identical to one another.

We have defined the concentratable entanglement (CE) as

$$\hat{\mathcal{C}}_\rho = \frac{1}{2}\left(1 + \mathrm{tr}\left[\rho^2\right]\right) - \frac{1}{2^n}\sum_{\alpha\in\mathcal{P}(S)} \mathrm{tr}\left[\rho_\alpha^2\right] \tag{3.127}$$

$$\approx P(\text{non-zero even no. of } |1\rangle_C \text{ s}) \tag{3.128}$$

which therefore increases with increased purity of the whole state and decreased purity of the subsystem states. If the ensemble elements are not all identical to one another and the state ρ is mixed then the CE is rigorously bounded by

$$\mathcal{C}_\rho^u = 1 - \frac{1}{2^n}\sum_{\alpha\in\mathcal{P}(S)} \mathrm{tr}\left[\rho_\alpha^2\right] \tag{3.129}$$

$$\approx P(\text{even no. of } |1\rangle_C \text{ s}) + P(\text{odd no. of } |1\rangle_C \text{ s}) \tag{3.130}$$

$$\mathcal{C}_\rho^l = \frac{1}{2^n} + \left(1 - \frac{1}{2^n}\right)\mathrm{tr}\left[\rho^2\right] - \frac{1}{2^n}\sum_{\alpha\in\mathcal{P}(S)} \mathrm{tr}\left[\rho_\alpha^2\right] \tag{3.131}$$

$$\approx P(\text{even no. of } |1\rangle_C \text{ s}) - \left(1 - \frac{2}{2^n}\right)P(\text{odd no. of } |1\rangle_C \text{ s}) \tag{3.132}$$

and the purity of ρ is

$$\gamma \approx 1 - 2P(\text{odd no. } |1\rangle_C \text{ s}) \tag{3.133}$$

where P are the probability results from the c-SWAP test on an ensemble described by ρ.

To conclude: previously presented entanglement measures the generalised concurrence and the n-tangle can be recovered from Concentratable Entanglement (CE), but CE has a simpler form and is directly derived from experiment. Individual output probabilities describe the entanglement structure of the input state. Variations of order δ in the input states give variations of order δ^2 in the probability outputs and therefore the CE, suggesting the test is robust to these kinds of errors and can be reliably used in experimental settings. This squaring of variations obscures errors, which decreases the relative error on the CE but reduces the likelihood of identifying error in the test state.

Chapter 4

The concentratable entanglement test for higher dimensional states

We are interested in extending both the c-SWAP test and concentratable entanglement to higher dimensional states, specifically qudit states and coherent states. Therefore we repeat much of the analysis in Chapter 3 with these states. Specifically, we expect the CE to behave in ways found by previous entanglement measures. Work in this chapter was produced with Oliver Prove (OP).

4.1 Qudit states

Higher dimensions allow the possibility for richer simulation of multi-level systems [74], reducing gate number in quantum circuits [75, 76], and reduction of fractional phase rotations from C_kNOT gates [76].

Let $\rho = \rho' = |\psi\rangle\langle\psi|$ where $|\psi\rangle$ is a $D > 2$ dimensional qudit state. Although the twin input states are qudits, the control state remains a qubit ($D = 2$); therefore the entanglement test's operation is unchanged, although the composite gate structure must be modified to achieve a SWAP operation on qudit states [77]. The following is my own work unless otherwise specified.

Recall the concurrence of a pure 2-qubit state $|\psi\rangle_{AB}$ is $c_2(|\psi\rangle) = \sqrt{2(1 - \mathrm{Tr}\rho_A^2)}$ from

equation (2.36), and that this gives $\mathcal{C}_{|\psi\rangle_{AB}} = \frac{1}{4}c_2^2$ shown in equation (3.10). Concurrence can be extended to generalized concurrence [43], which for bipartite pure states is $E_A(|\psi\rangle_{AB}) = \sqrt{2(1 - \mathrm{Tr}\rho_A^2)}$. Therefore:

$$\mathcal{C}_{|\psi\rangle} = P(|11\rangle_C) \tag{4.1}$$
$$= 1 - \frac{1}{4}\left(2 + 2\,\mathrm{tr}[\rho_A^2]\right) \tag{4.2}$$
$$= \frac{1}{2}\left(1 - \mathrm{tr}[\rho_A^2]\right) \tag{4.3}$$
$$= \frac{1}{4}E_A^2 \tag{4.4}$$

where we have used the definition in equation (3.127) where $n = 2$, $\mathrm{tr}[\rho_{AB}^2] = 1$, and $\mathrm{tr}[\rho_A^2] = \mathrm{tr}[\rho_B^2]$.

Let us define a GHZ-like n-qudit state $|\psi\rangle = \sum_{j=0}^{D-1} A_j\,|j\rangle^n$, which gives

$$\mathcal{C}_{|\psi\rangle} = P(\text{even no. of } |1\rangle\text{ s}) = 4\left(\frac{1}{2} - \frac{1}{2^n}\right)\sum_{j=0}^{D-1}\sum_{k>j}^{D-1}|A_j^2 A_k^2| \tag{4.5}$$

Figure 4.1 shows the CE for maximally entangled 2-qudit states of dimension D ($\mathcal{C}_{|\psi\rangle} = \frac{1}{2} - \frac{1}{2D}$) along with those for maximally GHZ-entangled n-qubit states ($\mathcal{C}_{|\psi\rangle} = \frac{1}{2} - \frac{1}{2^n}$)

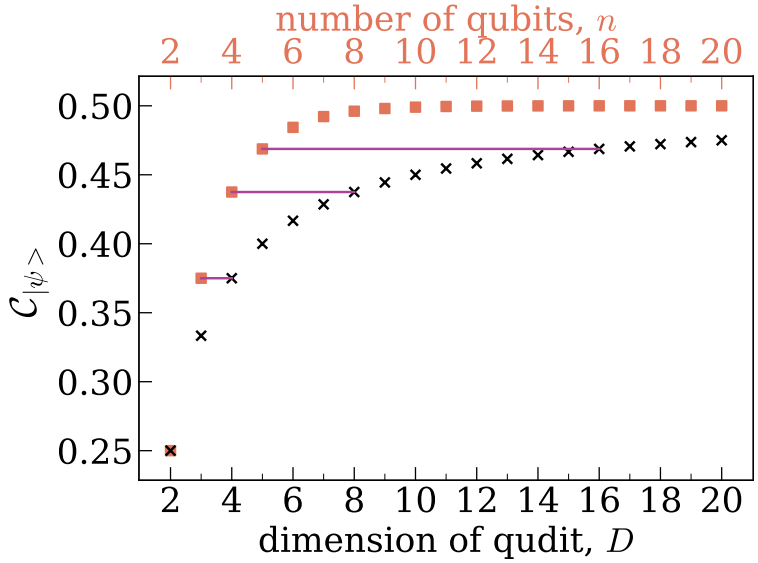

Figure 4.1: The total CE, $\mathcal{C}_{|\psi\rangle}$, given by the test for entanglement in maximally entangled 2-qudit input states $|\psi\rangle = \frac{1}{\sqrt{D}}\sum_{k=0}^{D-1}|k\rangle^n$ for various dimensions D (black crosses). For comparison, the CE for maximally entangled n-qubit GHZ states are shown in orange squares. The horizontal purple lines show that the 2-qudit CE is related to the n-qubit CE with $\mathcal{C}_{|\psi\rangle}(n = n', D = 2) = \mathcal{C}_{|\psi\rangle}(n = 2, D = 2^{n'-1})$.

for comparison. Both increase with D and n respectively and tend to $\frac{1}{2}$; increasing n however has a greater effect on CE than increasing D. Increasing n however has a greater effect on CE than increasing D, and in fact they are related by $\mathcal{C}_{|\psi\rangle}(n = n', D = 2) = \mathcal{C}_{|\psi\rangle}(n = 2, D = 2^{n'-1})$.

Now let the input states be different to represent variations in the ensemble as described in section 3.4, such that $\rho = |\psi\rangle\langle\psi|$ and $\rho' = |\phi\rangle\langle\phi|$. I therefore make use of the expressions found in section 3.5:

$$\mathcal{C}^u_{|\psi\rangle,|\phi\rangle} = P(\text{even no. of } |1\rangle_C \text{ s}) + P(\text{odd no. of } |1\rangle_C \text{ s}) \tag{4.6}$$

$$\mathcal{C}^l_{|\psi\rangle,|\phi\rangle} = P(\text{even no. of } |1\rangle_C \text{ s}) - \left(1 - \frac{2}{2^n}\right) P(\text{odd no. of } |1\rangle_C \text{ s}). \tag{4.7}$$

Let one input state be the maximally GHZ-entangled n-qudit state $|\psi\rangle = \frac{1}{\sqrt{D}} \sum_{k=0}^{D-1} |k\rangle^n$, and the other input state be some similar state $|\phi\rangle = \sum_{k=0}^{D-1} A_k |k\rangle^n$. When D is even we define

$$|\Phi^{\text{even}}(\delta)\rangle = \sqrt{\frac{2}{D}}\Big[\cos(\frac{\pi}{4} + \delta) \sum_{j=0}^{\frac{D}{2}-1} |j\rangle^n + \sin(\frac{\pi}{4} + \delta) \sum_{j=\frac{D}{2}}^{D-1} |j\rangle^n \Big] \tag{4.8}$$

so that all amplitudes are governed by δ, and $|\Phi^{\text{even}}(\delta = 0)\rangle = \frac{1}{\sqrt{D}} \sum_{k=0}^{D-1} |k\rangle^n$. Using $|\psi\rangle = |\Phi^{\text{even}}(\delta = 0)\rangle$ and $|\phi\rangle = |\Phi^{\text{even}}(\delta)\rangle$, fidelity $F = \cos^2\delta$ and:

$$P(\text{odd no. of} |1\rangle_C \text{ s}) = \frac{1}{2}\sin^2\delta \tag{4.9}$$

$$P(\text{even no. of} |1\rangle_C \text{ s}) = 4\Big(\frac{1}{2} - \frac{1}{2^n}\Big)\Big(\frac{1}{2} - \frac{1}{2D}\Big) - \Big(\frac{1}{2} - \frac{1}{2^n}\Big)\sin^2\delta \tag{4.10}$$

therefore

$$\mathcal{C}^u_{|\psi\rangle,|\phi\rangle} = 4\Big(\frac{1}{2} - \frac{1}{2^n}\Big)\Big(\frac{1}{2} - \frac{1}{2D}\Big) + \frac{1}{2^n}\sin^2\delta \tag{4.11}$$

$$\mathcal{C}^l_{|\psi\rangle,|\phi\rangle} = 4\Big(\frac{1}{2} - \frac{1}{2^n}\Big)\Big(\frac{1}{2} - \frac{1}{2D}\Big) - \left(1 - \frac{2}{2^n}\right)\sin^2\delta. \tag{4.12}$$

Here, the δ-dependant terms are not dependant on D. Consider instead that D is odd and define similarly

$$\begin{aligned}\Big|\Phi^{\text{odd}}(\delta)\Big\rangle = \sqrt{\frac{2}{D}}\Big[\cos(\frac{\pi}{4} + \delta) \sum_{j=0}^{\frac{D-1}{2}-1} |j\rangle^n + \frac{1}{\sqrt{2}}\left|\frac{D-1}{2}\right\rangle^n \\ + \sin(\frac{\pi}{4} + \delta) \sum_{j=\frac{D-1}{2}+1}^{D-1} |j\rangle^n \Big]\end{aligned} \tag{4.13}$$

where $|\psi\rangle = \left|\Phi^{\text{odd}}(\delta = 0)\right\rangle$ and $|\phi\rangle = \left|\Phi^{\text{odd}}(\delta)\right\rangle$, and again fidelity $F = \cos^2\delta$:

$$P(\text{odd no. of } |1\rangle_C \text{ s}) = \frac{1}{2}\frac{D-1}{D}\sin^2\delta \tag{4.14}$$

$$P(\text{even no. of } |1\rangle_C \text{ s}) = 4\Big(\frac{1}{2} - \frac{1}{2^n}\Big)\Big(\frac{1}{2} - \frac{1}{2D}\Big) - \Big(\frac{1}{2} - \frac{1}{2^n}\Big)\frac{D-1}{D}\sin^2\delta \tag{4.15}$$

As always, non-identical input states can be evidenced and tolerance-bounded by measurements of odd no. of $|1\rangle_C$ s, the difference being that the greater D the greater $P(\text{odd no. of } |1\rangle_C \text{ s})$. Since the even version had no such dependence, this suggests that the dependence on D is related to how many amplitudes are divergent between $|\psi\rangle$ and $|\phi\rangle$.

It also follows

$$\mathcal{C}^u_{|\psi\rangle,|\phi\rangle} = 4\Big(\frac{1}{2} - \frac{1}{2^n}\Big)\Big(\frac{1}{2} - \frac{1}{2D}\Big) + \frac{1}{2^n}\frac{D-1}{D}\sin^2\delta \tag{4.16}$$

$$\mathcal{C}^l_{|\psi\rangle,|\phi\rangle} = 4\Big(\frac{1}{2} - \frac{1}{2^n}\Big)\Big(\frac{1}{2} - \frac{1}{2D}\Big) - \Big(1 - \frac{2}{2^n}\Big)\frac{D-1}{D}\sin^2\delta \tag{4.17}$$

which has a slightly tighter bound range than the even-D version since one of the basis state's amplitudes does not vary, but otherwise behaves the same. The results for both even and odd D-dimensional non-identical states are shown in Figure 4.2.

It can be seen therefore that qudit state CE behaves similarly to qubit state CE, with the addition that the greater D the greater the CE and the bound range for non-identical states. This follows from the idea that there is a higher level of possible entanglement as the qudit dimension increases [30].

4.2 Entangled coherent states

We now consider how the c-SWAP test and concentratable entanglement can be applied to coherent states. Let $\rho = \rho' = |\psi\rangle\langle\psi|$ and therefore $P(|11\rangle_C) = 1 - P(|00\rangle_C)$. Our (OP, VK, SF) proposed optical set up to perfom the c-SWAP test is shown in Figure 4.3. The circuit is applied to the k-th mode in each of the input states ρ and ρ'. This pair enters the circuit on spatial paths A and B respectively, and the control state is

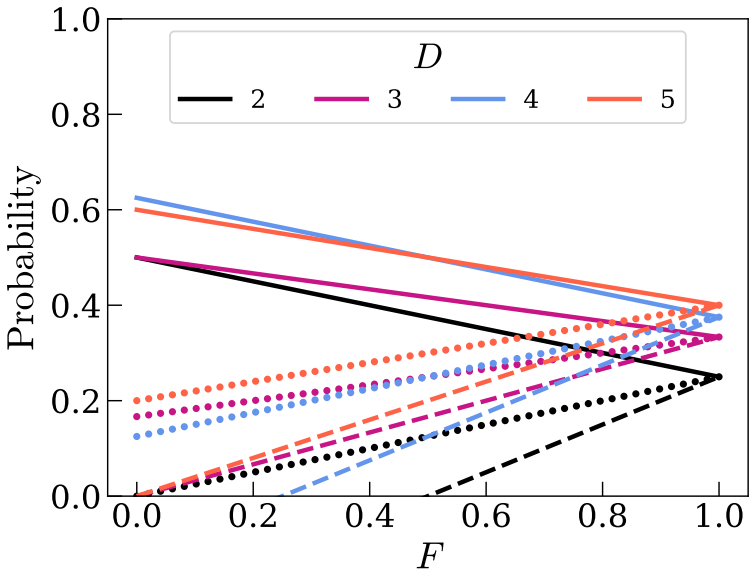

Figure 4.2: C-SWAP test probability results against fidelity F for input states $|\psi\rangle = |\Phi(\delta = 0)\rangle$ and $|\phi\rangle = |\Phi(\delta)\rangle$ where $n = 2$. The effect of δ on $|\phi\rangle$ is slightly different for even and odd D. The continuous lines are $\mathcal{C}^u_{|\psi\rangle,|\phi\rangle}$, the dotted lines are $P(\text{even no. of } |1\rangle_C \text{ s})$, and the dashed lines are $\mathcal{C}^l_{|\psi\rangle,|\phi\rangle}$.

encoded in their polarisations. As with the qubit/qudit state test, the circuit is applied to each of the n modes in ρ, M times (in parallel).

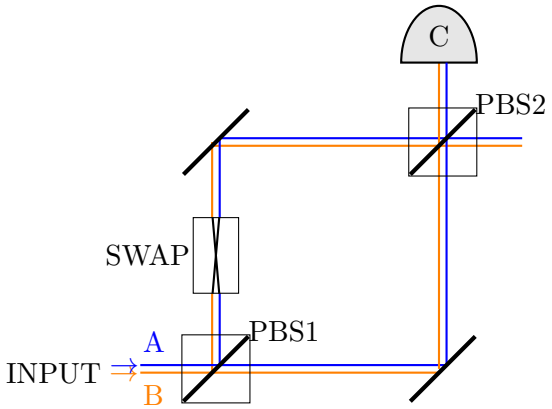

Figure 4.3: A proposed circuit, to be applied to each k-th mode, for implementing the c-SWAP test on optical states. The k-th mode of the input states $|\psi\rangle$ and $|\phi\rangle$ each enter the circuit on a different spatial path A (blue) and B (orange). PBS1 and PBS2 are polarizing beam splitters, with the transmitted polarization corresponding to control state $|0\rangle_C$ and the reflected polarization to $|1\rangle_C$. The SWAP operation crosses the two paths, such that $|\psi\rangle_A |\phi\rangle_B \to |\phi\rangle_A |\psi\rangle_B$. A detector is placed at C.

In this set-up, the individual modes must be able to be swapped; therefore we restrict

our investigation to coherent state superpositions of the form

$$|\psi\rangle = \mathcal{N} \sum_{o \in O_n} A_o |o\rangle \tag{4.18}$$

where $O_n = \{\alpha, \beta\}^n$ is the set of all configurations of two coherent states α and β from equation (2.16) on modes $\{1, 2, \ldots, n\}$, $\mathcal{N}$ is a normalisation constant, and $P(|o\rangle) = |\mathcal{N} A_o|^2$. Some states of this form can be implemented through parametric amplification and photodetection [39].

First, we compare the CE and entropy of entanglement of one such state. For ease we choose a 2-mode entangled coherent state $|\psi\rangle = (|\alpha\alpha\rangle + |\beta\beta\rangle) / \sqrt{1 + \langle\alpha|\beta\rangle^2}$, the CE of which is

$$\mathcal{C}_{|\psi\rangle} = P(|11\rangle_C) = \frac{1}{4} \frac{(1 - \langle\alpha|\beta\rangle^2)^2}{(1 + \langle\alpha|\beta\rangle^2)^2} \tag{4.19}$$

and the entropy of entanglement from equation (2.48) [51] is

$$S_A(\rho_A) = \log(2) + \log\left(1 + \langle\alpha|\beta\rangle^2\right) \tag{4.20}$$

$$- \frac{(1 - \langle\alpha|\beta\rangle)^2}{1 + \langle\alpha|\beta\rangle^2} \log\left(1 - \langle\alpha|\beta\rangle\right) \tag{4.21}$$

$$- \frac{(1 + \langle\alpha|\beta\rangle)^2}{1 + \langle\alpha|\beta\rangle^2} \log\left(1 + \langle\alpha|\beta\rangle\right). \tag{4.22}$$

Figure 4.4 shows $\mathcal{C}_{|\psi\rangle}$ and $S_A(\rho_A)/4\log 2$ (so that the two agree when $\langle\alpha|\beta\rangle = 0$) as a function of $\langle\alpha|\beta\rangle$. The shape of the two functions are very similar however $\mathcal{C}_{|\psi\rangle} < S_V(\rho_A)/4\log 2$ for all $\langle\alpha|\beta\rangle$.

Let us consider the more general 2-mode entangled coherent state

$$|\psi\rangle = \mathcal{N}(A_{\alpha\alpha} |\alpha\rangle |\alpha\rangle + A_{\alpha\beta} |\alpha\rangle |\beta\rangle + A_{\beta\alpha} |\beta\rangle |\alpha\rangle + A_{\beta\beta} |\beta\rangle |\beta\rangle). \tag{4.23}$$

The CE of this state is

$$\mathcal{C}_{|\psi\rangle} = P(|11\rangle_C) = \frac{1}{4} C_2'^2 \left(1 - \langle\alpha|\beta\rangle^2\right)^2 \tag{4.24}$$

where

$$C_2' = 2\mathcal{N}^2 |A_{\alpha\alpha} A_{\beta\beta} - A_{\alpha\beta} A_{\beta\alpha}| \tag{4.25}$$

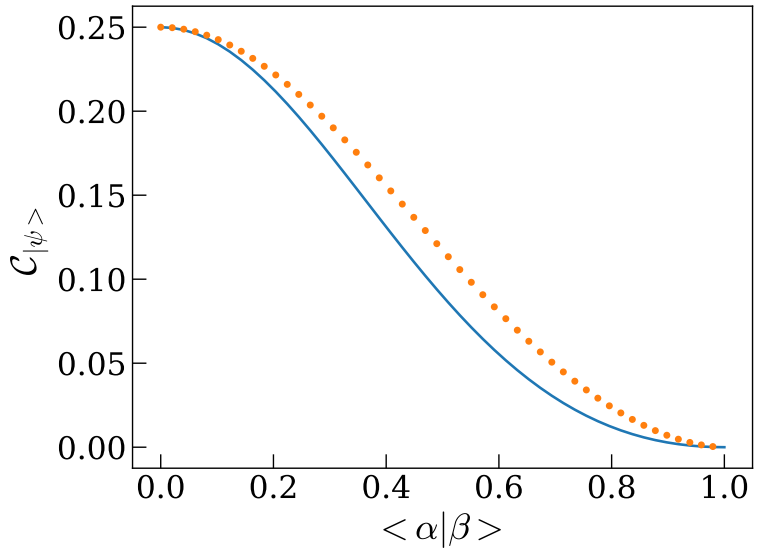

Figure 4.4: Graph showing the C.E. (blue solid line) and the normalised entanglement entropy (orange dotted line) of entangled coherent state $|\psi\rangle = (|\alpha\alpha\rangle + |\beta\beta\rangle)/\sqrt{1+\langle\alpha|\beta\rangle^2}$ for various $\langle\alpha|\beta\rangle$.

as an analogue to pure qubit state concurrence in equation (2.37). Note that unlike this value is not invariant under linear optics. The specific case $|\beta\rangle = |-\alpha\rangle$ is shown in shown in Figure 4.5. The C.E. increases with α until $0.75 < \alpha < 1.5$ where it plateaus to the qubit state CE. The α at which C.E. plateaus increases with C_2'.

Finally consider n-mode entangled coherent states such as the GHZ-like ECS $|\psi\rangle = \mathcal{N}(A_{n\alpha}|\alpha\rangle^n + A_{n\beta}|\beta\rangle^n)$, which gives CE

$$\mathcal{C}_{|\psi\rangle} = \mathcal{N}^4\left(1-\langle\alpha|\beta\rangle^2\right)^n\left(\frac{1}{2}-\frac{1}{2^n}\right)4|A_{n\alpha}^2A_{n\beta}^2| \tag{4.26}$$

and W-like ECSs $|\psi\rangle = \mathcal{N}\sum_{i=1}^n A_i|\beta\rangle^{i-1}|\alpha_i\rangle|\beta\rangle^{n-i}$ which give

$$\mathcal{C}_{|\psi\rangle} = \mathcal{N}^4\left(1-\langle\alpha|\beta\rangle^2\right)^2\sum_{i=1}^n\sum_{j>i}^n|A_i^2A_j^2|. \tag{4.27}$$

From results (4.19), (4.24), (7.6), and (4.27) we conjecture that the CE of an entangled coherent state of the form equation (4.18) can be obtained from the corresponding n-qubit results – i.e. let $\langle\alpha|\beta\rangle = 0$ then renormalise – multiplied by $\mathcal{N}^4(1-\langle\alpha|\beta\rangle^2)^{x\leq n}$, where x is the number of qubit swaps the state has undergone during the c-SWAP test to give the amplitude in the final expression.

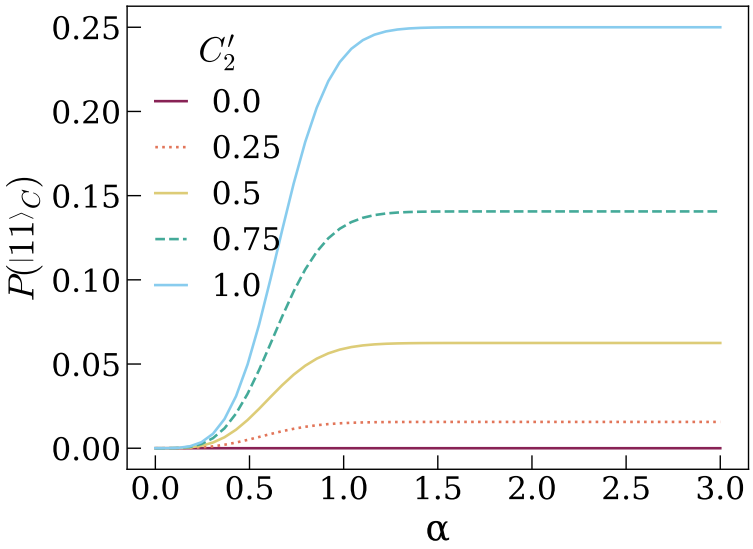

Figure 4.5: Graph showing the probability of observing the entanglement signature $|11\rangle_C$ after the c-SWAP test applied to state $|\psi\rangle = |\text{ECS}\rangle = \mathcal{N}(A_{++}|\alpha\rangle|\alpha\rangle + A_{+-}|\alpha\rangle|-\alpha\rangle + A_{-+}|-\alpha\rangle|\alpha\rangle + A_{--}|-\alpha\rangle|-\alpha\rangle)$, plotted against coherent state amplitude α for various values of C_2' as defined in equation (4.25).

Further work is needed to discoverer how this extends to entangled coherent states (ECS) with more than two distinct coherent states, and therefore $D > 2$ dimensions in the corresponding n-qudit state.

4.3 Coherent states as high dimensional qudits

As seen from the set-up in section 4.2, the c-SWAP test requires swapable modes. An alternative method for other coherent states is to approximate them with high dimensional qudits, with the D-dimensional approximation:

$$|\alpha_{\text{qudit}}\rangle = e^{-\frac{|\alpha|^2}{2}} \sum_{j=0}^{D-1} \frac{\alpha^j}{\sqrt{j!}} |j\rangle . \tag{4.28}$$

First, to test the accuracy of this approximation for the c-SWAP test and concentratable entanglement, we recall an entangled coherent state from section 4.2 that the c-SWAP test can directly be applied to for comparison.

Consider the simple entangled coherent state (ECS)

$$|\psi_\alpha\rangle = \mathcal{N}\left(|\alpha\rangle|\alpha\rangle + |-\alpha\rangle|-\alpha\rangle\right) \tag{4.29}$$

which can be approximated by

$$|\psi_{\text{qudit}}\rangle = e^{-|\alpha|^2} \sum_{j,k=0}^{14} (1 + (-1)^{j+k}) \frac{\alpha^j}{\sqrt{j!}} \frac{\alpha^k}{\sqrt{k!}} |j\rangle |k\rangle \tag{4.30}$$

where we have chosen $D = 15$ so that $|\psi_{\text{qudit}}\rangle$ is approximately normalised in the range $0 < \alpha < 3$ – see Figure 4.6. The c-SWAP test output probabilities against α for this state are shown in Figure 4.7, calculated by OP. In the same plot are the results for $|\psi_\alpha\rangle$ for comparison.

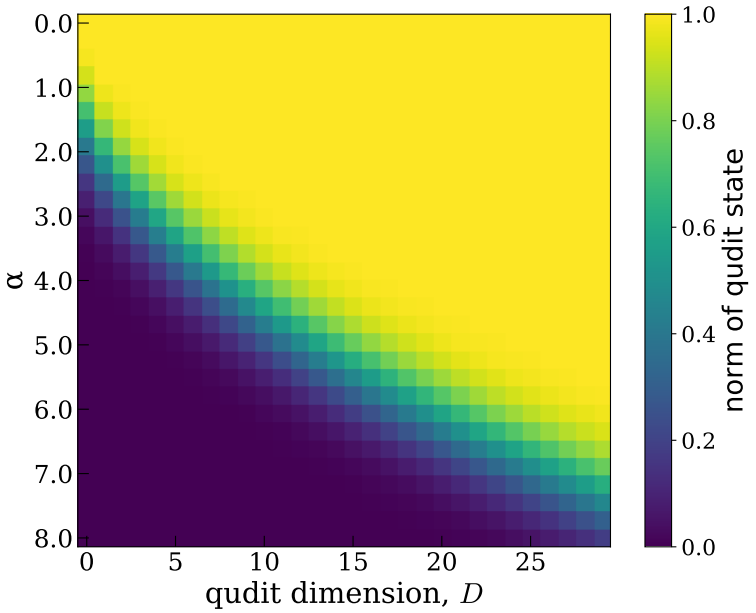

Figure 4.6: The norm of the qudit approximated ECS, equation (4.30), as a heatmap across different qudit dimensions and coherent state amplitudes. This was used to determine a value of D for which the qudit state accurately models the ECS, equation (4.29), across the coherent state amplitude α range considered.

The behaviour of $P(|11\rangle_C)$ for each state are very similar, tending to the same value, but the qudit approximation overestimates in the region of $0 < \alpha < 1.8$.

Now consider a coherent state that the c-SWAP test cannot be trivally applied to: the two-mode squeezed vacuum state $|\text{TMSV}_\alpha\rangle = S_2(\xi)\,|0,0\rangle$, where $S_2(\xi)$ is the two-mode squeeze operator defined in equation (2.24). These states have been used to demonstrate the EPR paradox experiment with continuous position and momentum

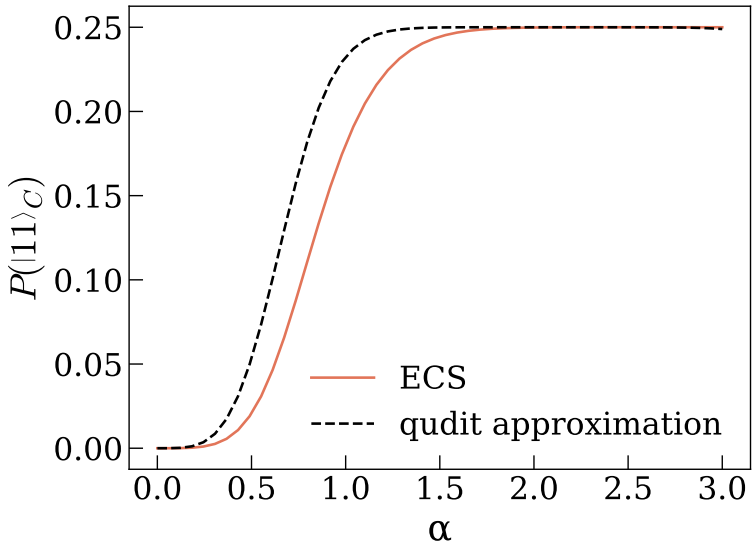

Figure 4.7: A comparison of $P(|11\rangle_C)$ for ECS equation (4.29) and a qudit approximation ECS equation (4.30) against coherent state amplitude α.

variables [78]. The qudit approximation of a TMSV state is [79]

$$|\text{TMSV}_{\text{qudit}}\rangle = \frac{\mathcal{N}}{\cosh r} \sum_{j=0}^{14} (-e^{i\theta} \tanh r)^j \, |jj\rangle \, . \tag{4.31}$$

The c-SWAP probability result is then

$$P(|11\rangle_C) = \frac{\mathcal{N}^4}{2\cosh^4 r} \sum_{j=0}^{14} \sum_{k=0, k\neq j}^{14} (\tanh r)^{2(j+k)}. \tag{4.32}$$

This is shown in Figure 4.8, alongside the normalised entanglement entropy $\frac{7}{15}\frac{S_A(\rho_A)(r)}{S_A(\rho_A)(r=2.5)}$ where $S_A(\rho_A)(r) = \cosh^2 r \log\cosh^2 r - \sinh^2 r \log\sinh^2 r$ [36]. Unfortunately, $\mathcal{C}_{|\text{TMSV}_{\text{qudit}}\rangle}$ does not seem to be a good estimation of $\mathcal{C}_{|\text{TMSV}_\alpha\rangle}$. The entanglement entropy increases with r linearly and indefinitely, however the C.E. of the qudit approximation has a maximum at $r \approx 2.5$ where it plateaus with $\mathcal{C}_{|\psi\rangle} = \frac{7}{15}$. It is unclear whether the c-SWAP test cannot be applied to squeezed states or simply that the qudit approximation cannot be used for states with indefinitely increasing CE.

4.4 Summary

The c-SWAP test and therefore Concentratable Entanglements can be trivially applied to higher dimensional states so long as the substates are swappable in an experimental

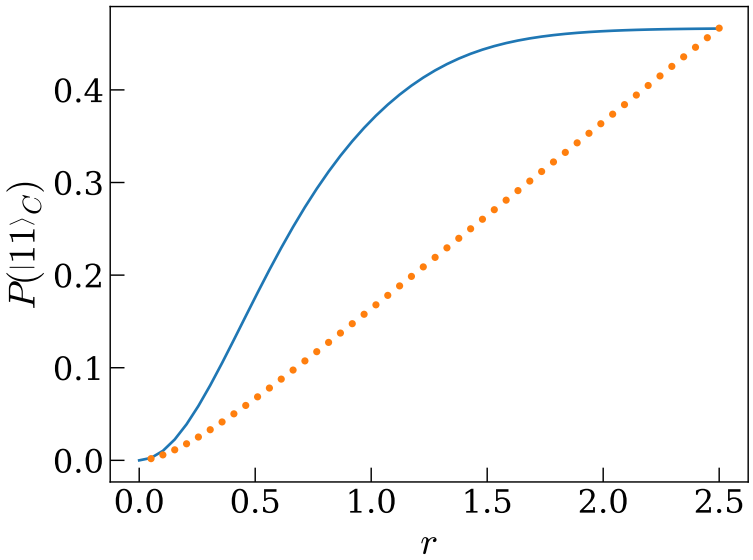

Figure 4.8: The probability results for a two mode squeezed vacuum (TMSV) state approximated by a $D = 15$ qudit state from equation 4.31 (solid blue line) alongside $frac715\frac{S_A(\rho_A)(r)}{S_A(\rho_A)(r=2.5)}$ of the TMSV state (dotted orange line).

setting. CE increases with dimension D, coherent amplitude α, and squeeze parameter r strengthening it as a multidimensional entanglement measure.

Chapter 5

Experimental implementation

Once we are convinced that Concentratable Entanglement (CE) is a good measure of entanglement, we turn to how it might be estimated in experiment. First, we present a second CE test, then we compare the two by numerically simulating each with a Rydberg setting. Work presented in sections 5.1 and 5.2 was produced with Jacob Beckey (JB), Gerard Pelegrí (GP), and Natalie L. Pearson (NP). Finally in section 5.3 I review the less resource intensive case of evidencing non-zero CE.

5.1 Bell-basis measurement test for entanglement

The Bell-basis test is an alternative method for obtaining c-SWAP test measurement data, proposed in [27] by JB, GP, SF, and NP. As with the c-SWAP test, the Bell-basis test requires $2M$ copies of the n-qubit input state ρ. The c-SWAP test applies $M \cdot n$ one-qubit measurements whereas the Bell-basis test applies $2M \cdot n$. However, the Bell-basis test does not require ancilla qubits or three-qubit gates.

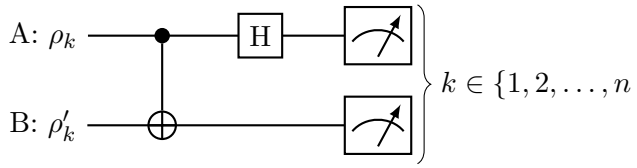

Figure 5.1: One round m of the Bell-basis test for entanglement on input states ρ and ρ'. H is a Hadamard gate and the two-qubit gate is a CNOT gate.

During each round $m \in \{1, \ldots, M\}$, the circuit in Figure.5.1 is applied to the k-th qubits in ρ and its pair ρ', for each qubit $k \in \{1, \ldots, n\}$. Then all qubits are measured, in order to calculate the probability of measuring each possible $2n$-state output $(\rho\rho')_1 \ldots (\rho\rho')_n$.

During any one round, a measurement of an even number of $|11\rangle_k$s evidences entanglement. Therefore, for example, any non-zero $P(|\ldots(11)_i \ldots (11)_j \ldots\rangle)$ evidences entanglement in ρ. Additionally, an odd number of $|11\rangle_k$s in one round evidences that ρ and ρ' are not equivalent. This sounds very familiar! If you map $|11\rangle$ to $|1\rangle_C$, these statements hold for the c-SWAP test outputs.

Consider a one-qubit pure state $|\psi\rangle = A_0 |0\rangle + A_1 |1\rangle$ and its pair $|\phi\rangle = B_0 |0\rangle + B_1 |1\rangle$. Applying the c-SWAP test for equivalence from Chapter 2 to these states gives

$$P(|0\rangle_C) = \frac{1}{2} + \frac{1}{2}|\langle\psi|\phi\rangle|^2 \tag{5.1}$$

$$P(|1\rangle_C) = \frac{1}{2} - \frac{1}{2}|\langle\psi|\phi\rangle|^2 \tag{5.2}$$

Applying the Bell-basis test as described above gives

$$P(|00\rangle) = \frac{1}{2} - \frac{1}{2}(A_0B_1 - A_1B_0)^2 \tag{5.3}$$

$$P(|01\rangle) = \frac{1}{2} - \frac{1}{2}(A_0B_0 - A_1B_1)^2 \tag{5.4}$$

$$P(|10\rangle) = \frac{1}{2} - \frac{1}{2}(A_0B_1 + A_1B_0)^2 \tag{5.5}$$

$$P(|11\rangle) = \frac{1}{2} - \frac{1}{2}(A_0B_0 + A_1B_1)^2 \tag{5.6}$$

$$= \frac{1}{2} - \frac{1}{2}|\langle\psi|\phi\rangle|^2 \tag{5.7}$$

therefore $P(|1\rangle_C)_{\text{c-SWAP test}} = P(|11\rangle)_{\text{Bell-basis test}}$. As seen from a broader proof in [27], this is true for mixed states of any n. The Bell-basis test results correspond to

$$\mathcal{C}_{|\psi\rangle} = 1 - \frac{1}{2^n} \sum_{\alpha \in \mathcal{P}(S)} \text{tr}\left[\rho_\alpha^2\right] \tag{5.8}$$

$$= P(\text{even no. of } |11\rangle \text{ s}) \tag{5.9}$$

$$\mathcal{C}_\rho^u = 1 - \frac{1}{2^n} \sum_{\alpha \in \mathcal{P}(S)} \text{tr}\left[\rho_\alpha^2\right] \tag{5.10}$$

$$= P(\text{even no. of } |11\rangle \text{ s}) + P(\text{odd no. of } |11\rangle \text{ s}) \tag{5.11}$$

and so any results from the c-SWAP test can be exactly recovered by the Bell basis test.

To explain the link between these two circuits, recall the Bell basis states in Equation (2.31). The triplet states $\left|\Phi^{+}\right\rangle, \left|\Psi^{+}\right\rangle, \left|\Phi^{-}\right\rangle$ are evidenced after a Bell-basis measurement of $\left|00\right\rangle, \left|01\right\rangle, \left|10\right\rangle$ respectively, and the singlet state $\left|\Psi^{-}\right\rangle$ corresponds to $\left|11\right\rangle$. Therefore the Bell basis test is in fact detecting singlet states between qubits in ρ and qubits in ρ'. This is very similar in concept to the c-SWAP test, which is redistributing the entanglement in the input states into singlet states across ρ and ρ'.

5.2 Concentratable entanglement tests on a neutral atom platform

To compare the c-SWAP test and Bell basis test we numerically simulate each with noisy gates [27]. We chose the neutral atom platform as single species atoms are inherently identical, and to spotlight its programmable layout and non-local interactions.

In this setting $CNOT$ gates and $CCNOT$ gates are replaced by CZ and CCZ gates respectively with the addition of a Hadamard gate on the target qubit before and after the CZ/CCZ gate. The gate circuits in this formalism are shown in Figure 5.2 for the c-SWAP test and Figure 5.3 for the Bell-basis test. For the c-SWAP tests, each trio of atomic qubits $\{\rho_k, \rho'_k, C_k\}$ in one round m are arranged in an equilateral triangle such that each atom i is separated from atom j by d_{ij}. Similarly for the Bell-basis test each pair of atomic qubits $\{\rho_k, \rho'_k\}$ are nearest-neighbours with separation d_{ij}.

As seen in GP *et al.* [80, 27], CZ and CCZ gates can be realised using adiabatic rapid passage (ARP) techniques to control population dynamics [81]. States $|0\rangle$ and $|1\rangle$ are encoded in two long-lived hyperfine ground states. The required atom groups ($\{\rho_k, \rho'_k\}$ for CZ and $\{\rho_k, \rho'_k, C_k\}$ for CCZ) are globally illuminated with laser pulses such that each state $|1\rangle$ is coupled to a Rydberg state $|r\rangle$ with Rabi frequency Ω_R and detuning δ_R, via a two-photon transition through an far-detuned intermediate excited state $|e\rangle$

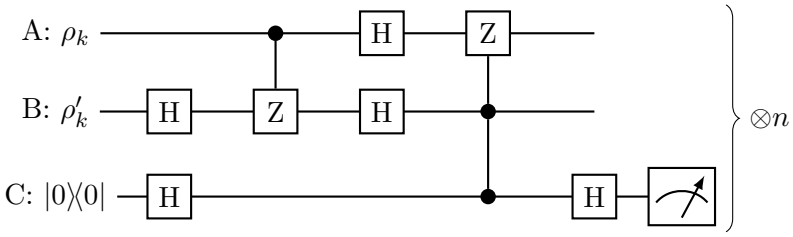

Figure 5.2: Gate circuit for one round m of the c-SWAP test suitable for the ARP technique. The two-qubit gate is a CZ gate from equation (2.14) and the three-qubit gate is a CCZ gate from equation (2.15).

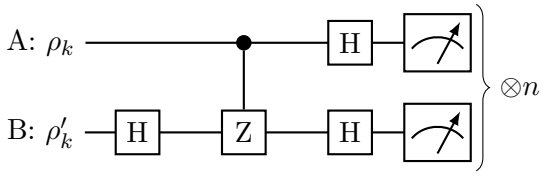

Figure 5.3: Gate circuit for one round m of the Bell-basis test suitable for the ARP technique. The two-qubit gate is a CZ gate from equation (2.14).

[80, 27]. The Rydberg blockade effect is such that when $|V_{rr}^{ij} \ll \Omega_R|$ where the pairwise Rydberg interaction strength V_{rr}^{ij} is determined by separation d_{ij}, only one qubit can be in state $|r\rangle$. The laser pulses therefore drive the transitions [80]

$$(|0\rangle)\,|01\rangle \leftrightarrow (|0\rangle)\,|0r\rangle \tag{5.12}$$

$$(|0\rangle)\,|11\rangle \leftrightarrow \frac{1}{\sqrt{2}}(|0\rangle)\,(|1r\rangle + |r1\rangle) \tag{5.13}$$

$$|111\rangle \leftrightarrow \frac{1}{\sqrt{3}}\,(|11r\rangle + |1r1\rangle + |r11\rangle) \tag{5.14}$$

with detuning $\delta_R(t)$ and Rabi frequencies Ω_R, $\sqrt{2}\Omega_R$, and $\sqrt{3}\Omega_R$ respectively. To achieve a CZ or CCZ gate two consecutive ARP pulses are applied, such that $\delta_R(t) > 0$ during the first pulse and $\delta_R(t) < 0$ during the second, resulting in the required phase flip [81].

A numerical simulation of each test was performed by GP, modelled with the above architecture, Cs atoms, and currently available laser specifications [27]. CZ and CCZ gates are simulated with non-unitary matrices; this simulates loss of population outside of the computational basis during the excitation process due to the finite linewidths Γ_e and Γ_r of the states $|e\rangle$ and $|r\rangle$. The noise associated with the one-qubit Hadamard gates is considered negligible. The effective matrices for the CZ and CCZ gates are

therefore

$$\begin{aligned} U_{CZ} = &|00\rangle\langle 00| + 0.9990e^{i0.9906\pi}(|01\rangle\langle 01| + |10\rangle\langle 10|) \\ &+ 0.9986e^{i1.000\pi}|11\rangle\langle 11| \end{aligned} \tag{5.15}$$

$$\begin{aligned} U_{CCZ} = &|000\rangle\langle 000| + 0.9981e^{i0.9845\pi}(|001\rangle\langle 001| + |010\rangle\langle 010| + |100\rangle\langle 100|) \\ &+ 0.9973e^{i0.9934\pi}(|110\rangle\langle 110| + |101\rangle\langle 101| + |011\rangle\langle 011|) \\ &+ 0.9963e^{i0.9911\pi}|111\rangle\langle 111|. \end{aligned} \tag{5.16}$$

Since population leakage can be detected in experiment [82] and therefore discarded in post-processing, after the effective matrices are applied we re-normalize the system's state. The loss of norm during numerical simulation is recorded and used to estimate the number of rounds M required to estimate the CE within ϵ. A comparison of the recorded loss of norm for the c-SWAP test and Bell basis test for n-qubit GHZ states is shown in Figure 5.4(b), calculated by JB.

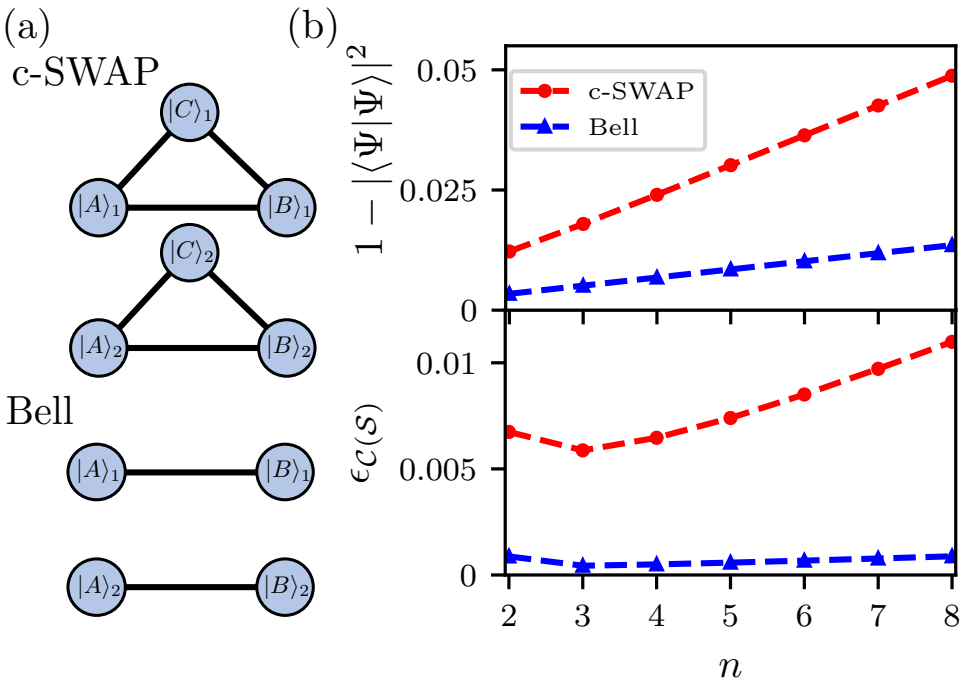

Figure 5.4: Image taken from [27]. a) Atom architecture for the c-SWAP test and the Bell-basis test respectively. b) Comparison of c-SWAP and Bell basis tests on n-qubit GHZ state $|\text{GHZ}_n\rangle = \frac{1}{\sqrt{2}}(|0\rangle^n + |1\rangle^n)$. The top panel shows the loss of norm due to noisy Rydberg pulses. The bottom panel shows the error that this results in in the estimation of the CE. For both we see the Bell-basis test outperforms the c-SWAP test.

The loss of norm is less for the Bell-basis test than for the c-SWAP test for all n considered ($2 \leq n \geq 8$). Therefore the required experimental data can be obtained with fewer copies of ρ and fewer total gates with the Bell basis method. Since the implementation of three-qubit gates on other platforms have achieved worse or similar fidelities to those on Rydberg platforms [83], we conclude that on current and near-term platforms the Bell basis test is the more viable method to estimate concentratable entanglements.

Let us investigate the effects of loss of norm during the estimation of CE of other entangled states. Figure 5.5(a) shows the total CE $\mathcal{C}(S)$ of pure n-qubit Line, GHZ, and W states as calculated by the noisy numerical simulation as well as the error between this and the analytical results found in Chapter 3. For $3 \leq n \leq 15$ the error $\epsilon_{\mathcal{C}(S)} < 2 \times 10^{-3}$ for all states. Unlike GHZ and W states, the error on the CE of Line states *decreases* with larger n with $\epsilon_{\mathcal{C}(S)} < 0.5 \times 10^{-3}$. Figure 5.5(b) shows the number of rounds M of the Bell-basis test on an n-qubit Line state required to achieve a 95% confidence interval (CI) of size K, calculated from the Clopper-Pearson (CP) method and Hoeffding's equality from Equations (2.58) and (2.59) by JB. The CP method predicts less required measurements than Hoeffding's equality even for $n = 12$. We consider the CP method to be more accurate since it exploits the underlying binomial probability distribution of pure CE. A 95% CI of size 10^{-2} can be achieved with $M = \Theta(10^3)$ rounds.

Also shown in Figure 5.5(b) is the loss of norm calculated by the numerical simulation, which for $n \leq 15$ is $1 - |\langle\psi|\psi\rangle|^2 < 0.03$ and increases linearly with n. Therefore a correction to the number of measurements M is at most $1.03M$.

5.3 Evidencing non-zero Concentratable Entanglement

The last two sections calculate CE in its entirety – however one function of the Bell-basis test is that non-zero values of CE can be evidenced with just one measurement

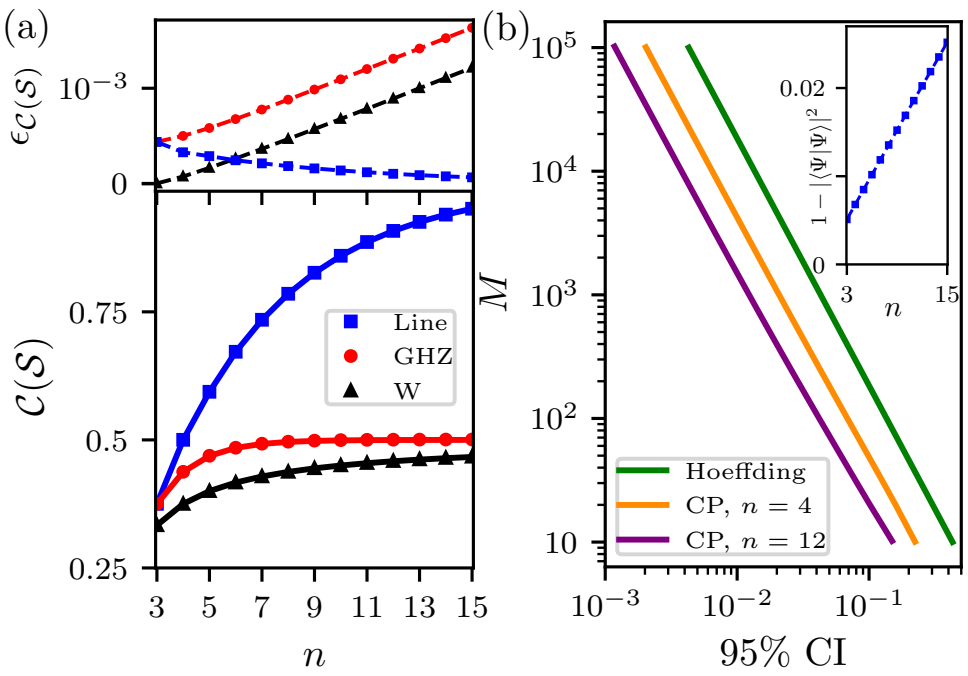

Figure 5.5: Image taken from [27]. a) The bottom panel shows the total CE of pure n-qubit Line, GHZ, and W states as calculated by a noisy numerical simulation (dots) alongside the analytical results (solid lines), and the upper plot shows the error $\epsilon_{\mathcal{C}}$ between the two. b) the number of rounds M of the Bell-basis test on an n-qubit Line state required to achieve a 95% CI of size K, calculated using Clopper-Pearson (CP) or Hoeffding's equality. The inset shows the loss of norm.

of $P(\text{even no. of } |11\rangle \text{ s})$. I investigate how many iterations of the test, and therefore number of copies of ρ are required to evidence non-zero CE.

I model the expected number of copies with simply

$$E(\text{no. of copies}) = \frac{2}{P(\text{even no. of } |11\rangle \text{ s})} \tag{5.17}$$

$$= \frac{2}{\mathcal{C}_\rho^{\text{estimate}}} \tag{5.18}$$

since two copies are required per iteration. The more entangled the state, the fewer number of copies required. Therefore, the less entangled the state, the lower the entanglement signature probability, and the higher the number of measurements required. Shown in Figure 5.6 is this scaling relation. Vertical line segments indicate results for various GHZ-like pure states, and then for comparison these same states with the minimun expected number of copies required for quantum state tomography (QST) found

in [55]. For $n \geq 3$ pure states of CE $\mathcal{C} > 0.05$ the Bell-basis test evidences entanglement with less copy states than QST. This highlights the Bell-basis test's suitability for larger multipartite states.

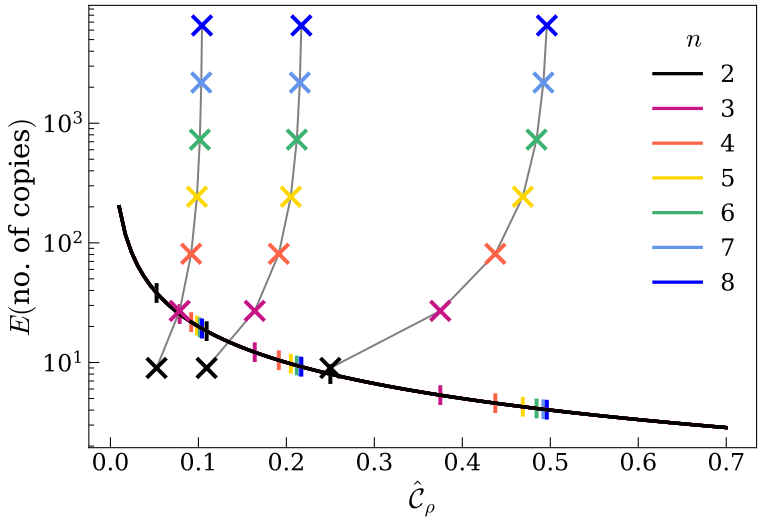

Figure 5.6: The expected number of copies against CE to evidence non-zero CE. The vertical line segments and crosses show the results for GHZ-like states from equation (3.29) with $\alpha_0 = \frac{1}{\sqrt{2}}, \frac{1}{2\sqrt{2}}, \frac{1}{3\sqrt{2}}$ from right to left. The vertical lines and continuous thick black line show the scaling for the Bell-basis test and the crosses and thin grey lines show the scaling for quantum state tomography (QST).

5.4 Summary

Complement to equations (6.1) and (3.133), for any subset $s \in S$ where $S = \{1, 2, ..., n\}$ is the set of labels for each qubit in ρ, the CE of ρ is

$$\mathcal{C}_\rho^{\text{estimate}}(s) = P(\text{even no. of } |11\rangle \text{ s on } s) \tag{5.19}$$

$$\mathcal{C}_\rho^{u}(s) = P(\text{even no. of } |11\rangle \text{ s on } s) + P(\text{odd no. of } |11\rangle \text{ s}) \tag{5.20}$$

$$\mathcal{C}_\rho^{l}(s) = P(\text{even no. of } |11\rangle \text{ s on } s) - \left(1 - \frac{2}{2^n}\right) P(\text{odd no. of } |11\rangle \text{ on } s) \tag{5.21}$$

and the purity of ρ is

$$\gamma_\rho^{\text{estimate}} = 1 - 2P(\text{odd no. of } |11\rangle_{AB} \text{ s}) \tag{5.22}$$

where P are the probability results from the Bell-basis test as described in section 5.1 on state ρ.

As these results are directly equivalent to those obtained by the c-SWAP test, all state error and entanglement structure analysis from Chapter 3 holds also for the Bell-basis test.

The Bell-basis test can be efficiently performed on Rydberg atom hardware with an order of $\Theta(10^3)$ rounds on a $n \leq 12$-qubit pure state, achieving a 95% confidence interval of size $\Theta(10^{-2})$. The Bell-basis test therefore outperforms the c-SWAP test on this platform and so we consider the Bell-basis test more suited to experimental estimation of CE. The Bell-basis test is particularly suited to larger multipartite states of $n > 3$ due to its favourable scaling in n.

Chapter 6

Conclusions and Further Work

While the c-SWAP test for entanglement can be used on any n-party state, we conclude that the Bell-basis measurement test for entanglement (as described in Chapter 5) is more efficient at estimating the multipartite entanglement measure Concentratable Entanglement (CE) of a qubit state as well as requiring fewer resources.

For the set of labels $S = \{1, 2, ..., n\}$ for each subsystem in input state ρ, the Concentratable Entanglement (CE) is

$$\begin{aligned}
\hat{\mathcal{C}}_\rho &= \frac{1}{2}\left(1 + \operatorname{tr}\left[\rho^2\right]\right) - \frac{1}{2^n}\sum_{\alpha\in\mathcal{P}(S)} \operatorname{tr}\left[\rho_\alpha^2\right] \\
&\approx P(\mathcal{Z}_1^{\text{even}}) \qquad (6.1) \\
\mathcal{C}_\rho^u &= 1 - \frac{1}{2^n}\sum_{\alpha\in\mathcal{P}(S)} \operatorname{tr}\left[\rho_\alpha^2\right] \\
&\approx P(\mathcal{Z}_1^{\text{even}}) + P(\mathcal{Z}_1^{\text{odd}}) \qquad (6.2) \\
\mathcal{C}_\rho^l &= \frac{1}{2^n} + \left(1 - \frac{1}{2^n}\right)\operatorname{tr}\left[\rho^2\right] - \frac{1}{2^n}\sum_{\alpha\in\mathcal{P}(S)} \operatorname{tr}\left[\rho_\alpha^2\right] \\
&\approx P(\mathcal{Z}_1^{\text{even}}) - \left(1 - \frac{2}{2^n}\right)P(\mathcal{Z}_1^{\text{odd}}) \qquad (6.3)
\end{aligned}$$

and purity

$$\begin{aligned}
\gamma &= \operatorname{tr}\left[\rho^2\right] \qquad (6.4) \\
&\approx 1 - 2P(\mathcal{Z}_1^{\text{odd}}) \qquad (6.5)
\end{aligned}$$

where $\mathcal{Z}_1^{\text{even(odd)}}$ is the set of all bit strings with an even(odd) number of 1's or 11's outputted by one round of the c-SWAP test and Bell-basis measurement test respectively (where even does not include zero). The probability P is obtained with M repeats of the test on an ensemble of state ρ of size $2M$. $\mathcal{P}(s)$ is the power set of s, $\rho_\alpha = \text{Tr}_{s\setminus\alpha}[\rho]$, and $\text{tr}\,[\rho_\emptyset] = 1$. These values of $\hat{\mathcal{C}}_\rho$, ${\mathcal{C}^u}_\rho$, and ${\mathcal{C}^l}_\rho$ converge when ρ is pure and the ensemble elements are identical. These results are robust to small variations in the input states.

The Bell-basis test can be achieved experimentally with current hardware. It requires $2M$ copies of ρ, $M \cdot n$ two-partite operations, and $2M \cdot n$ measurements. For pure states, M is at maximum of the order

$$M = \Theta\left(\frac{\ln(1/\delta)}{\epsilon^2}\right) \tag{6.6}$$

where $1 - \delta \leq P(|\hat{\mathcal{C}}_{|\psi\rangle} - \mathcal{C}_{|\psi\rangle}| < \epsilon)$ and $\Theta(g(\delta, \epsilon))$ is the set bounded both above and below by g asymptotically.

Unlike many other multipartite measures, concentratable entanglement (CE) has a simple analytical form, can be directly estimated from experiment on arbitrary n-partite state ρ, and has favourable resource scaling in n. It is simpler to understand than generalised concurrence, easier to calculate than entropy of entanglement, and more encompassing than the n-tangle. Therefore, I argue that CE should be adopted as a standard entanglement measure for multipartite states.

Since the c-SWAP test for entanglement is composed of the c-SWAP test for state comparison applied to each subsystem, it is of interest to explore other tests for state comparison applied to each subsystem as a test for entanglement. Candidates include Barnett *et al.* and extensions [84, 85] which finds that the overlap between two states is given by the difference in probabilities between finding the systems in the symmetric and antisymmetric subspaces. A second avenue for further work it to increase the number of copies used in each round of the c-SWAP test [86], which may be more resource efficient.

Chapter 7

Appendices

Let $\rho = |\psi\rangle\langle\psi|$ and $\rho' = |\phi\rangle\langle\phi|$.

7.1 Two-qubit probability results

Let $|\psi\rangle = A_{00}|00\rangle + A_{01}|01\rangle + A_{01}|01\rangle + A_{11}|11\rangle$ and $|\phi\rangle = B_{00}|00\rangle + B_{01}|01\rangle + B_{01}|01\rangle + B_{11}|11\rangle$:

$$\begin{aligned}
P(|00\rangle_C) &= \frac{1}{4}[4({A_{00}}^2{B_{00}}^2 + {A_{01}}^2{B_{01}}^2 + {A_{10}}^2{B_{10}}^2 + {A_{11}}^2{B_{11}}^2) \\
&\quad + 2(A_{00}B_{01} + A_{01}B_{00})^2 + 2(A_{00}B_{10} + A_{10}B_{00})^2 \\
&\quad + 2(A_{01}B_{11} + A_{11}B_{01})^2 + 2(A_{10}B_{11} + A_{11}B_{10})^2 \\
&\quad + (A_{00}B_{11} + A_{01}B_{10} + A_{10}B_{01} + A_{11}B_{00})^2], \\
P(|01\rangle_C) &= \frac{1}{4}[2(A_{00}B_{01} - A_{01}B_{00})^2 + 2(A_{10}B_{11} - A_{11}B_{10})^2 \\
&\quad + (A_{00}B_{11} - A_{01}B_{10} + A_{10}B_{01} - A_{11}B_{00})^2], \\
P(|10\rangle_C) &= \frac{1}{4}[2(A_{00}B_{10} - A_{10}B_{00})^2 + 2(A_{01}B_{11} - A_{11}B_{01})^2 \\
&\quad + (A_{00}B_{11} + A_{01}B_{10} - A_{10}B_{01} - A_{11}B_{00})^2], \\
P(|11\rangle_C) &= \frac{1}{4}(A_{00}B_{11} - A_{01}B_{10} - A_{10}B_{01} + A_{11}B_{00})^2
\end{aligned} \tag{7.1}$$

If $|\psi\rangle = |\phi\rangle = A_{00}|00\rangle + A_{01}|01\rangle + A_{01}|01\rangle + A_{11}|11\rangle$:

$$\begin{aligned} P(|00\rangle_C) &= 1 - (A_{00}A_{11} - A_{01}A_{10})^2 \\ &= 1 - \frac{1}{4}c_2^2, \\ P(|01\rangle_C) &= 0, \\ P(|10\rangle_C) &= 0, \\ P(|11\rangle_C) &= (A_{00}A_{11} - A_{01}A_{10})^2 \\ &= \frac{1}{4}c_2^2 \end{aligned} \tag{7.2}$$

where c_2 is the concurrence.

7.2 Three-qubit probability results

Let $|\psi\rangle = |\phi\rangle = \sum A_{ijk}|ijk\rangle$:

$$\begin{aligned} P(|000\rangle_C) = \frac{1}{2}[&2({A_{000}}^4 + {A_{001}}^4 + {A_{010}}^4 + {A_{011}}^4 \\ &+ {A_{100}}^4 + {A_{101}}^4 + {A_{110}}^4 + {A_{111}}^4) \\ &+ 4{A_{000}}^2({A_{001}}^2 + {A_{010}}^2 + {A_{100}}^2) \\ &+ 4{A_{011}}^2({A_{001}}^2 + {A_{010}}^2 + {A_{111}}^2) \\ &+ 4{A_{101}}^2({A_{001}}^2 + {A_{100}}^2 + {A_{111}}^2) \\ &+ 4{A_{110}}^2({A_{010}}^2 + {A_{100}}^2 + {A_{111}}^2) \\ &+ 2(A_{000}A_{011} + A_{001}A_{010})^2 \\ &+ 2(A_{000}A_{101} + A_{001}A_{100})^2 \\ &+ 2(A_{000}A_{110} + A_{010}A_{100})^2 \\ &+ 2(A_{001}A_{111} + A_{011}A_{101})^2 \\ &+ 2(A_{010}A_{111} + A_{011}A_{110})^2 \\ &+ 2(A_{100}A_{111} + A_{101}A_{110})^2 \\ &+ (A_{000}A_{111} + A_{001}A_{110} + A_{010}A_{101} + A_{011}A_{100})^2], \end{aligned}$$

$$
\begin{aligned}
P(|001\rangle_C) &= 0, \\
P(|010\rangle_C) &= 0, \\
P(|011\rangle_C) &= \frac{1}{2}[2(A_{000}A_{011} - A_{001}A_{010})^2 \\
&\quad + 2(A_{100}A_{111} - A_{101}A_{110})^2 \\
&\quad + (A_{000}A_{111} - A_{001}A_{110} - A_{010}A_{101} + A_{011}A_{100})^2], \\
P(|100\rangle_C) &= 0, \\
P(|101\rangle_C) &= \frac{1}{2}[2(A_{000}A_{101} - A_{001}A_{100})^2 \\
&\quad + 2(A_{010}A_{111} - A_{011}A_{110})^2 \\
&\quad + (A_{000}A_{111} - A_{001}A_{110} + A_{010}A_{101} - A_{011}A_{100})^2], \\
P(|110\rangle_C) &= \frac{1}{2}[2(A_{000}A_{110} - A_{010}A_{100})^2 \\
&\quad + 2(A_{001}A_{111} - A_{011}A_{101})^2 \\
&\quad + (A_{000}A_{111} + A_{001}A_{110} - A_{010}A_{101} - A_{011}A_{100})^2], \\
P(|111\rangle_C) &= 0
\end{aligned} \tag{7.3}
$$

For 3-qubit GHZ-like test states where $|\psi\rangle = A_{000}\,|000\rangle + A_{111}\,|111\rangle$ and $|\phi\rangle = B_{000}\,|000\rangle + |111\rangle\,B_{111}$:

$$
\begin{aligned}
P(|000\rangle_C) &= {A_{000}}^2{B_{000}}^2 + {A_{111}}^2{B_{111}}^2 \\
&\quad + \frac{1}{8}(A_{000}B_{111} + A_{111}B_{000})^2, \\
P(|001\rangle_C) &= \frac{1}{8}(A_{000}B_{111} - A_{111}B_{000})^2 \\
&= P(|010\rangle_C) = P(|100\rangle_C) = P(|111\rangle_C), \\
P(|011\rangle_C) &= \frac{1}{8}(A_{000}B_{111} + A_{111}B_{000})^2 \\
&= P(|101\rangle_C) = P(|110\rangle_C)
\end{aligned} \tag{7.4}
$$

For 3-qubit W-like test states where $|\psi\rangle = A_{001}|001\rangle + A_{010}|010\rangle + A_{100}|100\rangle$ and $|\phi\rangle = B_{001}|001\rangle + B_{010}|010\rangle + B_{100}|100\rangle$:

$$\begin{aligned}
P(|000\rangle_C) &= {A_{001}}^2{B_{001}}^2 + {A_{010}}^2{B_{010}}^2 + {A_{100}}^2{B_{100}}^2 \\
&\quad + \frac{1}{4}[(A_{001}B_{010} + A_{010}B_{001})^2 + (A_{001}B_{100} + A_{100}B_{001})^2 \\
&\quad + (A_{010}B_{100} + A_{100}B_{010})^2], \\
P(|001\rangle_C) &= \frac{1}{4}[(A_{001}B_{010} - A_{010}B_{001})^2 \\
&\quad + (A_{001}B_{100} - A_{100}B_{001})^2], \\
P(|010\rangle_C) &= \frac{1}{4}[(A_{001}B_{010} - A_{010}B_{001})^2 \\
&\quad + (A_{010}B_{100} - A_{100}B_{010})^2], \\
P(|011\rangle_C) &= \frac{1}{4}(A_{001}B_{010} + A_{010}B_{001})^2, \\
P(|100\rangle_C) &= \frac{1}{4}[(A_{001}B_{100} - A_{100}B_{001})^2 \\
&\quad + (A_{010}B_{100} - A_{100}B_{010})^2], \\
P(|101\rangle_C) &= \frac{1}{4}(A_{001}B_{100} + A_{100}B_{001})^2, \\
P(|110\rangle_C) &= \frac{1}{4}(A_{010}B_{100} + A_{100}B_{010})^2, \\
P(|111\rangle_C) &= 0.
\end{aligned} \tag{7.5}$$

7.3 n-qubit probability results

For n-qubit identical GHZ-like cases $|\psi\rangle = |\phi\rangle = \alpha_0|0\rangle^n + \alpha_1|1\rangle^n$:

$$\begin{aligned}
P(|0\rangle_C^n) &= 1 - \frac{2^{n-1}-1}{2^{n-2}}\alpha_0^2\alpha_1^2, \\
&= 1 - \frac{2^{n-1}-1}{2^{n-2}}\alpha_0^2(1-\alpha_0^2), \\
P(|\text{even no. of 1s}\rangle_C) &= \frac{2^{n-1}-1}{2^{n-2}}\alpha_0^2\alpha_1^2 \qquad (7.6) \\
&= \frac{2^{n-1}-1}{2^{n-2}}\alpha_0^2(1-\alpha_0^2). \qquad (7.7)
\end{aligned}$$

For n-qubit identical W-like cases $|\psi\rangle = |\phi\rangle = a_1 |00...1\rangle + a_2 \sum_{j=2}^{n} |0...1_j...0\rangle$:

$$P(|0\rangle_C^n) = 1 - (n-1)a_2^2 \left(a_1^2 + \frac{n-1}{2} a_2^2\right),$$
$$P(|\text{exactly two 1s}\rangle_C) = (n-1)a_2^2 \left(a_1^2 + \frac{n-1}{2} a_2^2\right). \tag{7.8}$$

For n-qubit identical W-like states where $|\psi\rangle = |\phi\rangle = \sum_{i=1}^{n} a_i |0...1_i...0\rangle$:

$$P(|0\rangle_C^n) = \sum_{i=1}^{n} a_i^2 \left(a_i^2 + \sum_{j>i}^{n} a_j^2\right), \tag{7.9}$$
$$P(|\text{exactly two 1s}\rangle_C) = \sum_{i=1}^{n} \sum_{j>i}^{n} a_i^2 a_j^2 \tag{7.10}$$
$$\tag{7.11}$$

For n-qubit GHZ-like states where $|\psi\rangle \neq |\phi\rangle$, $|\psi\rangle = \alpha_0 |0\rangle^n + \alpha_1 |1\rangle^n$ and $|\phi\rangle = \beta_0 |0\rangle^n + \beta_1 |1\rangle^n$:

$$P(|0\rangle_C^n) = \alpha_0^2\beta_0^2 + \alpha_1^2\beta_1^2 + \frac{1}{2^n}(\alpha_0\beta_1 + \alpha_1\beta_0)^2,$$
$$P(|\text{odd no. of 1s}\rangle_C) = \frac{1}{2} - \frac{1}{2}(\alpha_0\beta_0 + \alpha_1\beta_1)^2,$$
$$P(|\text{even no. of 1s}\rangle_C) = \frac{2^{n-1}-1}{2^n}(\alpha_0\beta_1 + \alpha_1\beta_0)^2. \tag{7.12}$$

For n-qubit W-like states where $|\psi\rangle = \sum_{i=1}^{n} a_i |0...1_i...0\rangle$, $|\phi\rangle = \sum_{j=1}^{n} b_j |0...1_j...0\rangle$:

$$P(|0\rangle_C^n) = \sum_{i=1}^{n} \left(a_i^2 b_i^2 + \frac{1}{4} \sum_{j>i}^{n} (a_i b_j + a_j b_i)^2\right) \tag{7.13}$$
$$P(|0...1_i...0\rangle_C) = \frac{1}{2} \sum_{j} (a_i b_j - a_j b_i)^2 \tag{7.14}$$
$$P(|0...1_i...1_j...0\rangle_C) = \frac{1}{4}(a_i b_j + a_j b_i)^2 \tag{7.15}$$

which total to

$$P(|\text{exactly one 1}\rangle_C) = \frac{1}{2} \sum_{i=1}^{n} \sum_{j>i}^{n} (a_i b_j - a_j b_i)^2$$
$$P(|\text{exactly two 1s}\rangle_C) = \frac{1}{4} \sum_{i=1}^{n} \sum_{j>i}^{n} (a_i b_j + a_j b_i)^2.$$

Bibliography

[1] S.J. Freedman. Experimental test of local hidden-variable theories. *Physical Review Letters*, 28(14):938–941, 1972.

[2] Alain Aspect, Philippe Grangier, and Gérard Roger. Experimental realization of einstein-podolsky-rosen-bohm gedankenexperiment: A new violation of bell's inequalities. *Phys. Rev. Lett.*, 49:91–94, Jul 1982.

[3] Wenjamin Rosenfeld, Daniel Burchardt, Robert Garthoff, Kai Redeker, Norbert Ortegel, Markus Rau, and Harald Weinfurter. Event-ready bell test using entangled atoms simultaneously closing detection and locality loopholes. *Phys. Rev. Lett.*, 119:010402, Jul 2017.

[4] Daniel Carney, Holger Müller, and Jacob M. Taylor. Using an atom interferometer to infer gravitational entanglement generation. *PRX Quantum*, 2:030330, Aug 2021.

[5] Vivien Kendon and William Munro. Entanglement and its role in shor's algorithm. *Quantum information & computation*, 6, 01 2005.

[6] Paul Benioff. The computer as a Phys. system: A microscopic quantum mechanical Hamiltonian model of computers as represented by Turing machines. *J. Stat. Phys.*, 22:563–591, 05 1980.

[7] Isaac L. Chuang, Neil Gershenfeld, and Mark Kubinec. Experimental implementation of fast quantum searching. *Phys. Rev. Lett.*, 80:3408–3411, Apr 1998.

[8] Arun K Pati and Samuel L Braunstein. Role of entanglement in quantum computation. *J. Indian I. Sci.*, 89(3):295–302, 2012.

[9] He-Liang Huang, Ashutosh K. Goswami, Wan-Su Bao, and Prasanta K. Panigrahi. Demonstration of essentiality of entanglement in a deutsch-like quantum algorithm. *Science China Physics, Mechanics & Astronomy*, 61:1869–1927, 03 2018.

[10] Artur K. Ekert. Quantum cryptography based on Bell's theorem. *Phys. Rev. Lett.*, 67:661–663, Aug 1991.

[11] K Shannon, E Towe, and O K Tonguz. On the use of quantum entanglement in secure communications: A survey. arXiv:2003.07907, 2020.

[12] Samuel L. Braunstein and Carlton M. Caves. Statistical distance and the geometry of quantum states. *Phys. Rev. Lett.*, 72:3439–3443, May 1994.

[13] Kunkun Wang, Xiaoping Wang, Xiang Zhan, Zhihao Bian, Jian Li, Barry C. Sanders, and Peng Xue. Entanglement-enhanced quantum metrology in a noisy environment. *Phys. Rev. A*, 97:042112, Apr 2018.

[14] Charles Bennett, Gilles Brassard, Claude Crépeau, Richard Jozsa, Asher Peres, and William Wootters. Teleporting an unknown quantum state via dual classical and Einstein-Podolsky-Rosen channels. *Phys. Rev. Lett.*, 70:1895–1899, 04 1993.

[15] Chenyu Zhang, J. F. Chen, Chaohan Cui, Jonathan P. Dowling, Z. Y. Ou, and Tim Byrnes. Quantum teleportation of photonic qudits using linear optics. *Phys. Rev. A*, 100:032330, Sep 2019.

[16] Wei-Bo Gao et al. Teleportation-based realization of an optical quantum two-qubit entangling gate. *Proc. Natl. Acad. Sci. U.S.A*, 107(49):20869–20874, 2010.

[17] Yong Wan et al. Quantum gate teleportation between separated qubits in a trapped-ion processor. *Science*, 364(6443):875–878, 2019.

[18] M. Barrett, J. Chiaverini, T. Schaetz, et al. Deterministic quantum teleportation of atomic qubits. *Nature*, 429:737–9, 07 2004.

[19] R F Werner. All teleportation and dense coding schemes. *J. Phys. A*, 34(35):7081–7094, Aug 2001.

[20] Tillmann Baumgratz, Alexander Nüßeler, Marcus Cramer, and M. Plenio. A scalable maximum likelihood method for quantum state tomography. *New J. Phys*, 15:125004, 08 2013.

[21] Otfried Gühne and Géza Tóth. Entanglement detection. *Phys. Rep.*, 474(1):1–75, 2009.

[22] Raymon G. Beausoleil, William J. Munro, Timothy P. Spiller, and Willem K. van Dam. Tests of quantum information. Patent Lens, April 2008. US Patent 7,559,101 B2.

[23] Gus Gutoski, Patrick Hayden, Kevin Milner, and Mark M. Wilde. Quantum interactive proofs and the complexity of separability testing. *Theory Comput.*, 11:59–103, 2015.

[24] Steph Foulds, Viv Kendon, and Tim Spiller. The controlled swap test for determining quantum entanglement. *Quantum Science and Technology*, 6(3):035002, 2021.

[25] Jacob L. Beckey, N. Gigena, Patrick J. Coles, and M. Cerezo. Computable and operationally meaningful multipartite entanglement measures. *Phys. Rev. Lett.*, 127:140501, Sep 2021.

[26] Oliver Prove, Steph Foulds, and Viv Kendon. Generalizing the controlled swap test for entanglement for practical applications: qudit, optical, and slightly mixed states. *arXiv preprint*, 2022. arXiv:2112.04333.

[27] Jacob L. Beckey, Gerard Pelegrí, Steph Foulds, and Natalie J. Pearson. Multipartite entanglement measures via bell-basis measurements. *Phys. Rev. A*, 107:062425, Jun 2023.

[28] M.A. Nielsen and I. L. Chuang. *Quantum Computation and Quantum Information: 10th Anniversary Edition*. Cambridge University Press, 2010.

[29] Nikola Šibalić and Charles S Adams. *Rydberg Physics*. 2399-2891. IOP Publishing, 2018.

[30] P Rungta, WJ Munro, K Nemoto, P Deuar, Gerard J Milburn, and CM Caves. Qudit entanglement. In *Directions in Quantum Optics*, pages 149–164. Springer, 2001.

[31] Timothy J Proctor. Quantum information with general quantum variables: a formalism encompassing qubits, qudits, and quantum continuous variables, 2019.

[32] Gregg Jaeger. *Quantum Information*. Springer Science & Business Media, 2007.

[33] Gerardo Adesso and Fabrizio Illuminati. Entanglement in continuous-variable systems: recent advances and current perspectives. *J. Phys. A*, 40(28):7821, 2007.

[34] Michael A Nielsen and Isaac Chuang. *Quantum computation and quantum information*. American Association of Physics Teachers, 2002.

[35] Christopher Gerry, Peter Knight, and Peter L Knight. *Introductory quantum optics*. Cambridge university press, 2005.

[36] Tohya Hiroshima. Decoherence and entanglement in two-mode squeezed vacuum states. *Phys. Rev. A*, 63(2):022305, 2001.

[37] C. Monroe, D. M. Meekhof, B. E. King, and D. J. Wineland. A "Schrödinger cat" superposition state of an atom. *Science*, 272(5265):1131–1136, 1996.

[38] Timothy C Ralph, Alexei Gilchrist, Gerard J Milburn, William J Munro, and Scott Glancy. Quantum computation with optical coherent states. *Phys. Rev. A*, 68(4):042319, 2003.

[39] Barry C Sanders. Review of entangled coherent states. *J. Phys. A*, 45(24):244002, 2012.

[40] Alexei Ourjoumtsev, Rosa Tualle-Brouri, Julien Laurat, and Philippe Grangier. Generating optical schrödinger kittens for quantum information processing. *Science*, 312(5770):83–86, 2006.

[41] Jaewoo Joo, William J Munro, and Timothy P Spiller. Quantum metrology with entangled coherent states. *Phys. Rev. Lett*, 107(8):083601, 2011.

[42] William K Wootters. Entanglement of formation and concurrence. *Quantum Inf. Comput.*, 1(1):27–44, 2001.

[43] V.S. Bhaskara and P.K. Panigrahi. Generalized concurrence measure for faithful quantification of multiparticle pure state entanglement using lagrange's identity and wedge product. *Quantum Inf. Process.*, 16(118), 2017.

[44] Yu Guo, Jinchuan Hou, and Yuncai Wang. Concurrence for infinite-dimensional quantum systems, 2012.

[45] Florian Mintert and Andreas Buchleitner. Observable entanglement measure for mixed quantum states. *Phys. Rev. Lett.*, 98:140505, Apr 2007.

[46] W. Dür, G. Vidal, and J. I. Cirac. Three qubits can be entangled in two inequivalent ways. *Phys. Rev. A*, 62:062314, Nov 2000.

[47] Adá n Cabello. Bell's theorem with and without inequalities for the three-qubit greenberger-horne-zeilinger and w states. *Physical Review A*, 65(3), feb 2002.

[48] Daniel M. Greenberger, Michael A. Horne, and Anton Zeilinger. *Going Beyond Bell's Theorem*, pages 69–72. Springer Netherlands, Dordrecht, 1989.

[49] Hans J. Briegel and Robert Raussendorf. Persistent entanglement in arrays of interacting particles. *Physical Review Letters*, 86(5):910–913, jan 2001.

[50] M. Walter, D. Gross, and J. Eisert. Multi-partite entanglement. arXiv:1612.02437v2, Feb 2017.

[51] Ryszard Horodecki, Paweł Horodecki, Michał Horodecki, and Karol Horodecki. Quantum entanglement. *Rev. Mod. Phys.*, 81:865–942, Jun 2009.

[52] Alexander Wong and Nelson Christensen. Potential multiparticle entanglement measure. *Physical Review A*, 63(4), mar 2001.

[53] Dafa Li. The n-tangle of odd n qubits. *Quantum Information Processing*, 11(2):481–492, jul 2011.

[54] Konrad Banaszek, Marcus Cramer, and David Gross. Focus on quantum tomography. *New J. Phys*, 15(12):125020, 2013.

[55] H. Häffner, W. Hänsel, C. F. Roos, J. Benhelm, D. Chek al kar, M. Chwalla, T. Körber, U. D. Rapol, M. Riebe, P. O. Schmidt, C. Becher, O. Gühne, W. Dür, and R. Blatt. Scalable multiparticle entanglement of trapped ions. *Nature*, 438(7068):643–646, dec 2005.

[56] Marcus Cramer, Martin B. Plenio, Steven T. Flammia, Rolando Somma, David Gross, Stephen D. Bartlett, Olivier Landon-Cardinal, David Poulin, and Yi-Kai Liu. Efficient quantum state tomography. *Nature Communications*, 1(1), dec 2010.

[57] Harry Buhrman, Richard Cleve, John Watrous, and Ronald de Wolf. Quantum fingerprinting. *Phys. Rev. Lett*, 87(16):167902, 2001.

[58] Raj B. Patel, Joseph Ho, Franck Ferreyrol, Timothy C. Ralph, and Geoff J. Pryde. A quantum fredkin gate. *Science Advances*, 2(3):1501531, 2016.

[59] Min-Sung Kang, Jino Heo, Seong-Gon Choi, Sung Moon, and Sang-Wook Han. Implementation of SWAP test for two unknown states in photons via cross-Kerr nonlinearities under decoherence effect. *Sci. Rep*, 9(1):1–14, 2019.

[60] Wassily Hoeffding. Probability inequalities for sums of bounded random variables. *Journal of the American Statistical Association*, 58(301):13–30, 1963.

[61] C. J. Clopper and E. S. Pearson. The use of confidence or fiducial limits illustrated in the case of the binomial. *Biometrika*, 26(4):404–413, 12 1934.

[62] Karen Wintersperger, Florian Dommert, Thomas Ehmer, Andrey Hoursanov, Johannes Klepsch, Wolfgang Mauerer, Georg Reuber, Thomas Strohm, Ming Yin, and Sebastian Luber. Neutral atom quantum computing hardware: performance and end-user perspective. *EPJ Quantum Technology*, 10(1), aug 2023.

[63] I. I. Beterov and M. Saffman. Rydberg blockade, förster resonances, and quantum state measurements with different atomic species. *Phys. Rev. A*, 92:042710, Oct 2015.

[64] Iris Cong, Harry Levine, Alexander Keesling, Dolev Bluvstein, Sheng-Tao Wang, and Mikhail D. Lukin. Hardware-efficient, fault-tolerant quantum computation with rydberg atoms. *Phys. Rev. X*, 12:021049, Jun 2022.

[65] Sepehr Ebadi, Tout T. Wang, Harry Levine, Alexander Keesling, Giulia Semeghini, Ahmed Omran, Dolev Bluvstein, Rhine Samajdar, Hannes Pichler, Wen Wei Ho, Soonwon Choi, Subir Sachdev, Markus Greiner, Vladan Vuletić, and Mikhail D. Lukin. Quantum phases of matter on a 256-atom programmable quantum simulator. *Nature*, 595(7866):227–232, jul 2021.

[66] F. Nogrette, H. Labuhn, S. Ravets, D. Barredo, L. Béguin, A. Vernier, T. Lahaye, and A. Browaeys. Single-atom trapping in holographic 2d arrays of microtraps with arbitrary geometries. *Phys. Rev. X*, 4:021034, May 2014.

[67] Dolev Bluvstein, Harry Levine, Giulia Semeghini, Tout T. Wang, Sepehr Ebadi, Marcin Kalinowski, Alexander Keesling, Nishad Maskara, Hannes Pichler, Markus Greiner, Vladan Vuletić, and Mikhail D. Lukin. A quantum processor based on coherent transport of entangled atom arrays. *Nature*, 604(7906):451–456, apr 2022.

[68] D. Bluvstein, A. Omran, H. Levine, A. Keesling, G. Semeghini, S. Ebadi, T. T. Wang, A. A. Michailidis, N. Maskara, W. W. Ho, S. Choi, M. Serbyn, M. Greiner, V. Vuletić, and M. D. Lukin. Controlling quantum many-body dynamics in driven rydberg atom arrays. *Science*, 371(6536):1355–1359, 2021.

[69] P. Huft, Y. Song, T. M. Graham, K. Jooya, S. Deshpande, C. Fang, M. Kats, and M. Saffman. Simple, passive design for large optical trap arrays for single atoms. *Phys. Rev. A*, 105:063111, Jun 2022.

[70] Simon J. Evered, Dolev Bluvstein, Marcin Kalinowski, Sepehr Ebadi, Tom Manovitz, Hengyun Zhou, Sophie H. Li, Alexandra A. Geim, Tout T. Wang, Nishad Maskara, Harry Levine, Giulia Semeghini, Markus Greiner, Vladan Vuletić, and Mikhail D. Lukin. High-fidelity parallel entangling gates on a neutral-atom quantum computer. *Nature*, 622(7982):268–272, oct 2023.

[71] Harry Levine, Alexander Keesling, Giulia Semeghini, Ahmed Omran, Tout T. Wang, Sepehr Ebadi, Hannes Bernien, Markus Greiner, Vladan Vuletić, Hannes Pichler, and Mikhail D. Lukin. Parallel Implementation of High-Fidelity Multiqubit Gates with Neutral Atoms. *Phys. Rev. Lett.*, 123:170503, 2019.

[72] B. Nikolov, E. Diamond-Hitchcock, J. Bass, N. L. R. Spong, and J. D. Pritchard. Randomized benchmarking using nondestructive readout in a two-dimensional atom array. *Phys. Rev. Lett.*, 131:030602, Jul 2023.

[73] Steph Foulds, Viv Kendon, and Tim Spiller. The controlled SWAP test for determining quantum entanglement. *Quantum Science and Technology*, 6(3):035002, apr 2021.

[74] Matthew Neeley, Markus Ansmann, Radoslaw C. Bialczak, Max Hofheinz, Erik Lucero, Aaron D. O'Connell, Daniel Sank, Haohua Wang, James Wenner, Andrew N. Cleland, Michael R. Geller, and John M. Martinis. Emulation of a quantum spin with a superconducting phase qudit. *Science*, 325(5941):722–725, 2009.

[75] Benjamin P. Lanyon, Marco Barbieri, Marcelo P. Almeida, Thomas Jennewein, Timothy C. Ralph, Kevin J. Resch, Geoff J. Pryde, Jeremy L. O'Brien, Alexei Gilchrist, and Andrew G. White. Simplifying quantum logic using higher-dimensional hilbert spaces. *Nature*, 5(2):134–140, 2009.

[76] Michael Hanks and M. S. Kim. Fault-tolerance in qudit circuit design, 2022.

[77] Kazuyuki Fujii. Exchange gate on the qudit space and Fock space. *J. Opt. B: Quantum Semiclass. Opt.*, 5(6):S613–S618, oct 2003.

[78] Z. Y. Ou, S. F. Pereira, H. J. Kimble, and K. C. Peng. Realization of the Einstein-Podolsky-Rosen paradox for continuous variables. *Phys. Rev. Lett.*, 68:3663–3666, Jun 1992.

[79] Bonny L. Schumaker and Carlton M. Caves. New formalism for two-photon quantum optics. II. Mathematical foundation and compact notation. *Phys. Rev. A*, 31:3093–3111, May 1985.

[80] G. Pelegrí, A. J. Daley, and J. D. Pritchard. High-fidelity multiqubit rydberg gates via two-photon adiabatic rapid passage. *Quantum Science and Technology*, 7(4):045020, 2022.

[81] I I Beterov, D B Tretyakov, V M Entin, E A Yakshina, I I Ryabtsev, M Saffman, and S Bergamini. Application of adiabatic passage in rydberg atomic ensembles for quantum information processing. *Journal of Physics B: Atomic, Molecular and Optical Physics*, 53(18):182001, jul 2020.

[82] Armands Strikis, Animesh Datta, and George C. Knee. Quantum leakage detection using a model-independent dimension witness. *Phys. Rev. A*, 99:032328, Mar 2019.

[83] Vivek V. Shende and Igor L. Markov. On the cnot-cost of toffoli gates. *Quantum Info. Comput.*, 9(5):461–486, may 2009.

[84] Stephen M. Barnett, Anthony Chefles, and Igor Jex. Comparison of two unknown pure quantum states. *Physics Letters A*, 307(4):189–195, feb 2003.

[85] M. Kleinmann, H. Kampermann, and D. Bruß. Generalization of quantum-state comparison. *Physical Review A*, 72(3), sep 2005.

[86] Xavier Gitiaux, Ian Morris, Maria Emelianenko, and Mingzhen Tian. Swap test for an arbitrary number of quantum states, 2021.

Colophon

This thesis is based on a template developed by Matthew Townson and Andrew Reeves. It was typeset with LaTeX 2_ε. It was created using the *memoir* package, maintained by Lars Madsen, with the *madsen* chapter style. The font used is Latin Modern, derived from fonts designed by Donald E. Kunith.